Investigating and Engineering Polymeric Interfaces: Elucidating the Swelling of Polyelectrolyte Brushes and Brush Bilayer Thin Films and the Development of Novel Electrospun Polymer Membranes for the Catalysis of Biodiesel

by

Nisha R. Hollingsworth

A dissertation submitted in partial fulfillment
of the requirements for the degree of
Doctor of Philosophy
(Macromolecular Science and Engineering)
in the University of Michigan
2020

Doctoral Committee:

Professor Ronald G. Larson, Chair
Professor Zhan Chen
Professor Jinsang Kim
Professor Nicholas A. Kotov

Nisha R. Hollingsworth

nrhollin@umich.edu

ORCID iD: 0000-0002-2152-0836

Dedication

For Mom, Dad, and Akhil

Acknowledgments

First and foremost, I would like to especially thank my thesis advisor, Professor Ronald G. Larson. When I joined the group in the fall of 2016 working on a project entirely unrelated to my thesis research, I couldn't have imagined how far I've come. His wisdom and mentorship and his ability to challenge me were invaluable as a doctoral student; I truly credit my thesis work and the tools and skills I have now to his advising, which pushed me to grow as a scholar. I'd also like to thank the other members of my committee—Prof. Zhan Chen, Prof. Jinsang Kim, and Prof. Nicholas Kotov—for their support and valuable advice. It was a pleasure to take specialized courses with them on their areas of expertise and to receive their valuable feedback throughout my doctoral journey.

Additionally, I would also like to thank the entire Larson Group. It has been an absolute joy to learn and grow with everyone in the group, with so many different backgrounds and areas of expertise. I will sincerely miss working with so many brilliant, curious people every day and our office dynamic—especially eating group lunches and taking afternoon breaks for "emergency" chocolate. I'd also like to give a special thanks to my collaborator (see Chapter 4) Dr. Sabina Wilkanowicz, who taught me electrospinning and the Polish alphabet.

I would also like to my entire program, University of Michigan Macromolecular Science and Engineering. Macro has truly been a wonderful program to be a part of, and oftentimes feels more like a close-knit family than an affiliation. I'd like to especially thank our coordinator Julie Pollak and our program directors and faculty past and present for being so supportive and engaging. I am so happy to have been a part of such an incredible polymers program and to join

so many impressive alumni, and although I'm a little biased, I can honestly say that Macro truly is the best program (and perhaps the best kept secret) in the College of Engineering.

I would also like to thank my financial support for my graduate studies. The National Science Foundation (NSF) for funding the polyelectrolyte work, and the U-M Dow Sustainability Seed Grant for funding the biodiesel membrane collaboration. I'd like to thank Rackham Graduate School for supporting me financially through the Rackham Merit Fellowship (RMF), as well as by recognizing me through the Edward A. Bouchet Graduate Honors Society. I'd also like to thank my awesome team at Intel Corporation in Rio Rancho, New Mexico for providing me with the opportunity to conduct a remote summer internship during my final summer.

To say that 2020 has been totally unprecedented is an understatement. So, last but not least, I'd like to thank my close friends and family for not only making me laugh but truly supporting and motivating me throughout it all. I was fortune that the University of Michigan is only an hour away from my family's home in Haslett, Michigan. This made all the difference. I'd like thank my little brother, Akhil, for being the most even-keeled, positive, and caring person I know, and of course, my parents (both chemistry professors) for always encouraging me to pursue knowledge and to enjoy science, but never actually pushing me directly towards academia. My mom, Saleela, for taking care of me in every way possible, and especially for always making Indian food for me and my coworkers. Finally, I'd especially like to thank my dad, Rawle, who is truly my inspiration as a scientist and who passed away before he saw me graduate from college to pursue my doctorate. Hopefully, he's proud of me.

Table of Contents

Dedication ii

Acknowledgements iii

List of Tables vii

List of Figures viii

Abstract xii

Chapter 1: Introduction 1

1.i Introduction to Polymer Thin Films 1
1.ii Introduction to Polymer Membranes 9
1.iii References 12

Chapter 2: Salt- and pH-Induced Swelling of a Poly(Acrylic Acid) Brush via Quartz Crystal Microbalance w/ Dissipation (QCM-D) 18

2.i Abstract 18
2.ii Introduction 18
2.iii Materials & Methods 22
2.iv Results 30
2.v Conclusions and Discussion 47
2.vi References 49
2.a Appendix A 52
2.b Appendix B 54

Chapter 3: Swelling Hysteresis with Changes in pH or Salt Concentration in Weak Polyelectrolyte Brushes and Bilayer Films 58

3.i Abstract 58
3.ii Introduction 58
3.iii Materials and Methods 61
3.iv Results 65
3.v Discussion and Summary 80
3.vi References 83

Chapter 4: Immobilization of Calcium Oxide onto Polyacrylonitrile (PAN) Fibers as a Heterogeneous Catalyst for Biodiesel Production 86

4.i Abstract 86
4.ii Introduction 86
4.iii Materials and Methods 92
4.iv Results and Discussion 97
4.v Conclusions and Perspective 113
4.vi References 116

Chapter 5: Conclusions 121
5.i Overview 121
5.ii Polymer Thin Films 121
5.iii Polymer Membranes 123
5.iv References 125

List of Tables

Table 2.i: PAA brush thicknesses *d* and grafting densities, σ for the chain lengths studied……32

Table 3.i: VASE results for the dry thicknesses of the PAA brushes and (PAA/PEI) bilayers investigated in this work…….....66

Table 3.ii: Summary of experimental findings for PAA brushes & LbL bilayers (PAA/PEI) for various chain lengths and grafting densities……..……..…75

Table 4.i. Electro-hydrodynamic processing parameters of polymeric solutions of PAN, PAN-CaO and their physical properties. …….....99

Table 4.ii. Process production and biodiesel physical properties of samples made using KOH, CaO, PAN-CaO and PAN-DOPA-CaO catalysts. All measurements were taken at 20℃. Literature data for kinematic viscosity and density measured at 20℃ are: 74.2 mm^2/s and 0.9145 kg/dm^3 for Canola oil and 3.5-8.2 mm^2/s and 0.82-0.9 kg/dm^3 for biodiesel. …….……...106

Table 4.iii. Kinematic viscosity of biodiesel samples made via Canola oil transesterification with different means of deploying of the catalyst: unbound CaO (CaO), CaO immobilized mechanically on PAN fibers (PAN-CaO) and CaO immobilized chemically on PAN fibers (PAN-DOPA-CaO). Reactions were repeated up to 8 times using the same catalyst……...….113

List of Figures

Figure 1.i: Cartoon representations of the mushroom regime (left) versus the brush regime (right) depicting the coil radius R_{coil}, interchain distance D, and brush height H……..3

Figure 1.ii: Cartoon representations of the fabrication technique of "grafting from" (left) where the dashed chain and arrow indicates the growing chain end, and the technique of "grafting to" (right), where the arrow indicates where the chain attaches. ……..4

Figure 1.iii: A schematic of an LbL multilayer with oppositely charged polyelectrolytes on a negatively charged substrate. ……..…6

Figure 1.iv: Cartoon depicting the experimental setup described in Chapter 2 of a gold-coated QCM-D chip with a self-assembled monolayer (SAM) of poly(acrylic acid) (PAA) tethered via a thiol-gold linkage. ……..…8

Figure 1.v: Cartoon depicting the experimental setup described in Chapter 3 of a gold-coated QCM-D chip with a brush-bilayer composed of a self-assembled monolayer (SAM) of poly(acrylic acid) (PAA) with complementary adsorbed poly(ethylene imine) (PEI). ……..…9

Figure 1.vi: Schematic depiction of the electrospinning setup to draw fibers of polyacrylonitrile (PAN) into a nonwoven membrane for subsequent functionalization. …….12

Figure 2.i (A-C): Dependence of %Swelling and $\Delta Dissipation_{Swelling}$ on concentration of KCl at various values of pH for short-chain (M_n= 2,000 g/mol) PAA brush grafted to a gold crystal at various grafting densities, σ (chains/nm^2). (A) σ = 0.87, (B) σ = 1.04, & (C) σ = 2.15. Note: due to the logarithmic axes, in both this and subsequent figures the values of %Swelling and $\Delta Dissipation_{Swelling}$ at 10^{-1} mM represent the value at 0 mM salt for pH 3 (green circles). For pH 7 (purple squares) & pH 9 (blue triangles), the values at 10^{-1} mM are indistinguishable from the values at 0 mM salt. ……..…33

Figure 2.ii- Dependence of %Swelling and $\Delta D_{Swelling}$ on concentration of KCl at pH 7 for short-chain (M_n= 2,000 g/mol) PAA brush grafted to a gold crystal at low grafting densities, σ (chains/nm^2) σ = 0.12 & σ = 0.30. ……37

Figure 2.iii (A-C) Dependence of %Swelling and $\Delta Dissipation_{Swelling}$ of short-chain (M_n= 2,000 g/mol) at its highest grafting density and long-chain PAA (M_n= 39,000 g/mol) to KCl concentration at (A) pH 9, (B) pH 7, and (C) pH 3. …….39

Figure 2.iv (A-B). Brush height vs. PAA chain length, N at various KCl concentrations in the (A) OB regime and (B) SB regime, both at pH 7. The grafting densities are 2 kDa (σ=0.30 chains/nm^2), 14 KDa (σ=0.38 chains/nm^2), and 39 kDa (σ=0.45 chains/nm^2). ……41

Figure 2.v. Short-chain (Mn=2 kDa) PAA brush height vs. KCl Concentration (mM) at various grafting densities σ (chains/nm^2) in the OB regime and SB regime at pH 7. ……..43

Figure 2.vi(A-B). Short-chain (Mn=2 kDa) PAA brush height vs. grafting density at various KCl concentrations in the (A) OB regime and (B) SB regime, both at pH 7. ……44

Figure 2.A (A-D). (A) Change in dissipation $\Delta D(bare\ crystal) = \Delta D_{Solvent}$ as a function of salt concentration for various salts on a blank gold crystal from our measurements and $\Delta D(polymer\ coated)$ on a PMPC-grafted brush on a gold crystal (the latter from Zhang et al.). Note that some data points are obscured by overlap, such as the open square covered by a filled square at the highest salt concentration. (B) Corresponding $\Delta D_{Solvent}$ data for a blank gold crystal, compared to $\Delta D(polymer\ coated)$ data from our study for the densely PAA-grafted surfaced (σ=2.15). Note the difference in scale on the x- and y-axes, relative to (A). (C) Densities of KCl solutions at pH 7 obtained gravimetrically. (D) Change in dissipation $\Delta D(bare\ crystal) = (\Delta D_{Solvent})$ as a function of salt concentration for a blank crystal and $\Delta D(polymer\ coated)$ for various grafting densities σ of PAA (Mn= 2,000 g/mol) at pH 7. Error bars are comparable in size to the symbols and are therefore not shown on these or following graphs. ……..……..54

Figure 2.B.i %Change in Swelling (as defined by Wu et al.[1]) vs. grafting density for our short-chain (Mn= 2 kDa) PAA at various KCl concentrations in the OB regime at pH 7……56

Figure 2.B.ii. Brush height data reported by Wu et al.[1] replotted as %Change in Swelling for a nominally 4 kDa PAA brush at pH 5.8. ……57

Figure 3.i(A-D): A) Representative thickness responses to pH changes for a 2 kDa PAA brush with no PEI adsorbed, grafting density σ =0.87 in 100 mM KCl with pH varied as shown, with effect of overlying solvent subtracted, as discussed at the end of the methods section. B) Time-averaged thickness response vs. pH obtained from A), with numbers indicating the order in which the pH scans occurred. Error bars in B) and D) represent the standard deviation for N=3, but are invisible since they are smaller than the symbols. C) Representative thickness response for a (PAA/PEI) bilayer with a 2 kDa PAA brush underlayer, grafting density σ =0.87 in 100 mM KCl and 2.5 kDa PEI adsorbed overlayer, with solvent subtracted. D) Time-averaged thickness response vs. pH obtained from C). The dashed line represents a connecting segment that falls on top of another segment. ……68

Figure 3.ii(A-D): The same as in Fig. 3.i except for a 39 kDa PAA brush, grafting density σ =0.45, again in 100 mM KCl and in C) and (D) the overlayer is a 25 kDa PEI. Error bars represent the standard deviation for N=3 and if they are not visible, they are smaller than the symbols. The dashed line represents a connecting segment that falls on top of another segment. …….70

Figure 3.iii(A-D): The same as in Figure 3.i, except for a grafting density σ =0.023 in 100 mM KCl……72

Figure 3.iv(A-D): The same as Figure 3.ii, except for a 14 kDa PAA brush, and 10 kDa PEI in C) and D) at grafting density σ =0.06 in 100 mM KCl. Error bars represent the standard deviation for N=3. ……...74

Figure 3.v(A-D): A) Representative swelling response for a 2 kDa PAA brush, grafting density σ =0.87 at fixed, neutral pH with varying KCl concentration in mM (values given in plots). B) Average swelling vs. KCl concentration. C) Representative swelling response for a 39 kDa PAA brush, grafting density σ =0.023 at fixed, neutral pH with varying KCl concentration in mM (values given in plots). D) Average swelling vs. KCl concentration. Note that in C) and D), that the first and final salt concentration are the same and lie near the middle of the x axis at 100 mM. ……..76

Figure 3.vi. Height (i.e. Sauerbrey thickness) at various salt concentrations for a 39 kDa PAA brush at grafting density σ = 0.023 chains/nm^2 (red circles) and σ = 0.042 chains/nm^2 (green triangles) at pH 4.2, below the pKa (~5). Log-log fits demonstrate the scaling exponents for the Osmotic Brush (OB) regime (left slope) and Salted Brush (SB) regimes (right slope). ……80

Figure 4.i. Chemical immobilization of CaO onto PAN fibers that had been previously activated with Pinner reaction. ……..…99

Figure 4.ii (A-C)(i&ii). Top: Scanning Electron Microscopy of PAN nanofibers (A(i)), PAN fibers with CaO mechanically immobilized onto them (B(i)) and PAN fibers with chemically immobilized CaO catalyst onto the fibers (C(i)). Green arrows indicate CaO beads presence along the PAN fibers in both materials, where the catalyst was immobilized. Bottom: Fiber size diameter distribution of PAN, PAN with CaO mechanically immobilized onto the fibers and PAN with CaO particles chemically immobilized on the fibers (A(ii), B(ii) and C(ii) respectively). ……100

Figure 4.iii(A-C)(i&ii). Scanning Electron Microscopy (i) and Scanning Transmission Electron Microscopy (ii) of PAN nanofibers (A), PAN fibers with CaO mechanically immobilized onto them (B) and PAN fibers with CaO catalyst chemically immobilized onto the fibers (C). Red arrows indicate CaO particles. ……102

Figure 4.iv(A&B). Scanning Transmission Electron Microscopy (STEM) of PAN fibers with CaO mechanically immobilized (A) and chemically immobilized (B) after have been used in biodiesel production. Red arrows indicate CaO particles still stuck to the PAN fibers after a transesterification reaction repeated 8 (A) and 2 (B) times. ……103

Figure 4.v (A-D). FTIR spectra of CaO powder (A), PAN nanofibers (B), PAN nanofibers with mechanically immobilized CaO – PAN-CaO (C) and PAN nanofibers with chemically immobilized CaO – PAN-DOPA-CaO (D). ……104

Figure 4.vi. FTIR spectra of Canola oil, standard sample of FAME and biodiesel samples made using of different catalysts: KOH, CaO, PAN-CaO and PAN-DOPA-CaO, the first of which was

dissolved in the reaction mixture and the second one was free flowing. Arrows highlight peak changes in samples before and after transesterification reaction. ……107

Figure 4.vii. Enlarged versions of important region of FTIR spectra of biodiesel samples made with different CaO catalyst linkages, including free-flowing CaO at different times after start of the reaction. …….108

Figure 4.viii. Kinematic viscosity during biodiesel conversion as a function of time of samples made by using CaO catalyst (CaO, solid line), CaO catalyst immobilized mechanically in PAN nanofibers (PAN-CaO, dashed line) and CaO catalyst immobilized chemically in PAN nanofiber (PAN-DOPA-CaO, dotted line). ……..…109

Figure 4.ix (A&B). Left: FTIR spectra of peak at 3643 cm-1 for biodiesel samples with different CaO concentrations (from 200 mg to 3.125mg in 1 ml of FAME sample) and biodiesel samples made with different forms of CaO, namely – unbound CaO (CaO), CaO mechanically immobilized on PAN nanofibers (PAN-CaO) and CaO chemically immobilized onto PAN fibers with DOPA link (PAN-DOPA-CaO). Right: peaks of maximum absorbances from curves on the left as a function of CaO concentration in biodiesel samples. ……...111

Abstract

In this thesis, we examine a variety of engineered interfaces: polymer thin films—in the morphologies of brushes and LbL bilayers—and polymer membranes.

First, this work investigates the swelling/de-swelling behavior of polyelectrolyte brushes of length 2 kDa–39 kDa of the weakly ionizable polyanion, poly(acrylic acid) (PAA) in the presence of KCl at concentrations from 0.1–1000 mM, at pH = 3, 7, and 9, and at grafting densities σ = 0.12–2.15 chains/nm^2 using a Quartz Crystal Microbalance with Dissipation (QCM-D). After correcting our data for the effect of the solvent, we find that at pH 7 (above the pKa), at low and moderate grafting densities, our results in the high-salt "salted brush" (SB) regime (C_s > 10 mM salt) agree with the predicted scaling $H \sim N\sigma^{+1/3}C_s^{-1/3}$, where H is the brush height.[1,2] In the low-salt "osmotic brush" (OB) regime (Cs <10 mM salt), we find $H \sim N\sigma^{+1/3}C_s^{+0.28\text{-}0.38}$, where the dependence on C_s agrees with scaling theory for a weakly charged brush, which predicts a +1/3 power,[1] but the dependence on σ strongly disagrees with this theory, which predicts a -1/3 power. The predicted linearity in the degree of polymerization N is confirmed in both the OB and SB regimes.[1,2]

Next, these PAA brushes are complexed with a polyelectrolyte of the opposite charge poly(ethylene imine) (PEI) to form LbL bilayers with a brush underlayer for investigation by QCM-D. We find that both brush and bilayer structures may or

may not exhibit history-dependent swelling/de-swelling with respect to a pH cycle of pH 7-4-1-4-7 at fixed salt concentration, depending on their chain length and grafting density. We investigate chain lengths of 2 kDa–39 kDa, and use brush grafting densities of 0.023–0.87 chains/nm^2. We find that at a low grafting density of 0.45 chains/nm^2 and a high PAA molecular weight of 39 kDa, we see hysteresis in swelling over timescales of many minutes. For higher grafting densities (>0.45 chains/nm^2) and in short chains (2 kDa), we see little or no hysteresis, and at an intermediate chain length (14 kDa) and grafting density (0.06 chains/nm^2), hysteresis is observed at short timescales but is greatly reduced at longer timescales. We also observe hysteresis in swelling with a KCl cycle of 100-20-100-1000-100 mM at fixed pH=7 for a long chain brush (39 kDa) at low grafting density (0.023 chains/nm^2), but not for a short chain brush (2 kDa) at a high grafting density (0.86 chains/nm^2). We also revisit the discrepancies between our previous findings and scaling predictions[1] for brush height with respect to grafting density. We find that for a standalone PAA brush of sufficient chain length at a pH value at which it is partially charged (4.2), the brush height decreases with increased grafting density in the OB regime in agreement with theoretical predictions.[1]

Finally, this work describes the development of electrospun polyacrylonitrile (PAN) membranes featuring novel chemistry to immobilize the heterogenous alkaline catalyst CaO onto the membrane fibers using dopamine-catalyst coordination. The resultant membranes were found to successfully achieve biodiesel when used in the transesterification of crude canola oil.

References

1 Zhulina, E. B.; Birshtein, T. M.; Borisov, O. V. Theory of Ionizable Polymer Brushes. *Macromolecules* **1995**, *28*, 1491–1499 DOI: 10.1021/ma00109a021.

2 Israels, R.; Leermakers, J. F. A. M.; Fleer, J.; Zhulina, E. B. Charged Polymeric Brushes: Structure and Scaling Relations. *Macromolecules* **1994**, *27*, 3249–3261.

Chapter 1

Introduction

1.i Introduction to Polymer Thin Films

Since their introduction, polymers have a wide variety of uses and applications in areas including but not limited to energy, consumer goods, sensing, and biomedicine. [1–3] As materials, polymers are ideal for their light weight and flexibility.[4,5] Additionally, they are manufactured for far less cost than traditional inorganic materials. Polymers are also desirable as they can be synthesized to fit specific characteristics. For example, in the field of organic photovoltaics, a specific chemistry results in the desired energetic band gap and allows the overall efficiency of the system to be tuned.[3,4] Strategies such as polymer blends and copolymerization enable materials with diverse properties.[6] Polymers can also be introduced into inorganic materials in the form of composite materials,[7–9] which have a higher durability and stiffness to withstand greater loads, making them ideal for applications in the civil and transportation sectors.[10,11]

Of the various polymer morphologies, one of the most influential is the polymer thin film. Polymer thin films have tremendous important in industries such as coatings, adhesives, and electronics.[12–14] A polymer thin film is defined as a layer of polymeric material on the order of nanometers to <5 microns.[15] At this small length scale, polymer thin films often exhibit different properties than bulk polymeric materials as a result of differing interfacial energies, as well as differing entropic effects when chains are highly confined and more entangled than in the bulk.[16–20] This in turn affects the fundamental properties of glass transition temperature, viscosity, and the

specific volume.[17,21–24] The properties of polymer thin films can also be attributed to the thin film substrate, where closer to the substrate, polymer chains are affected directly by attractive and repulsive forces of the substrate itself.[15] Polymer thin films can take a variety of nanostructured architectures, including films of particles, block copolymer thin films, homopolymer brushes, mixed polymer brushes, and crosslinked elastomeric networks.[25] The polymers used within these films can vary to include neutral polymers, hydrophobic polymers, block copolymers, or ion-containing polymers (or polyelectrolytes).[25] Another exciting architecture is the layer-by-layer film, which has gained increased popularity over the past decades for its versatility and ease of manufacture.[26,27] In this work, we will focus specifically on the areas of polyelectrolyte homopolymer brushes and layer-by-layer films.

1.i.a Introduction to Polymeric Brushes

Polymer brushes are an extremely versatile and exciting area of polymer thin films, with a range of applications in areas such as lubrication, separations, colloidal stabilization, drug delivery, adhesion, and sensing.[28–31] Since the 1940s, polymer brushes have been studied and described in great detail through experiments, simulations, and numerical theory.[29,32–40] Polymer brushes may exist with a variety of substrate geometries, including planar substrates or particles.[41–43]

The physics governing the conformation of polymer brushes is a delicate balance of forces. When polymer chains are grafted onto a surface in the form of a polymer brush, chain monomer units experience steric repulsive forces from being closely confined, and to maximize their translational entropy, they extend away from the substrate. In good solvent, at low grafting density, individual adjacent polymer chains form solution-like islands at an interchain distance D larger than the coil size (R_{coil}). This is known as the "mushroom regime" (Figure 1.i).[40] As chains are grafted, again, as a result of monomer repulsion and elasticity from being end-tethered, this

mushroom regime gives rise to a "brush regime" (see Figure 1.i),[40] where chains extend away from the substrate to a height H and the distance between chains D is now smaller than R_{coil}. Of course, in the case of polyelectrolytes, electrostatics are important in dictating polymer grafting as well, where electrostatic repulsion between adjacent chains is also at play.[41]

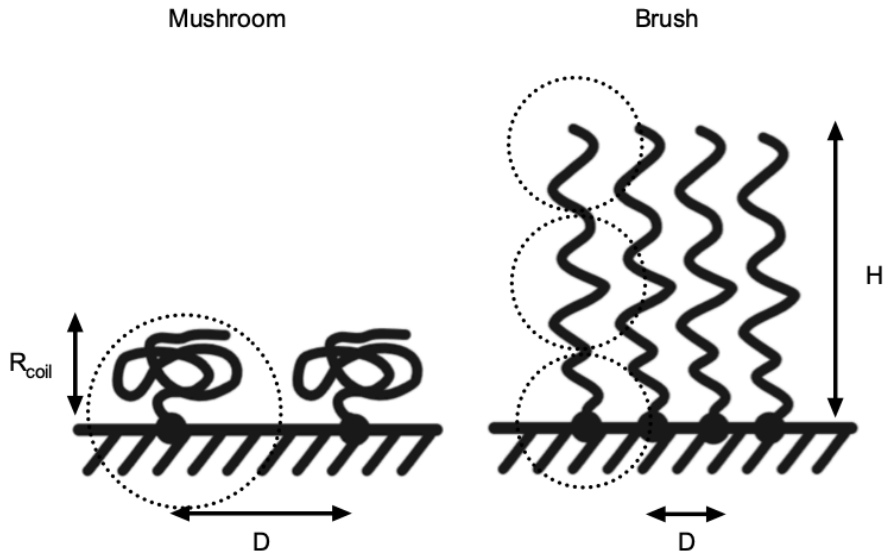

Figure 1.i: Cartoon representations of the mushroom regime (left) versus the brush regime (right) depicting the coil radius R_{coil}, interchain distance D, and brush height H

Polymer brushes are traditionally fabricated using two main types of fabrication strategies that are generally described as either "grafting from", where the polymer chain growth initiates on the substrate, and the chains continue to grow away from it, or "grafting to", where the entire polymer chain is end-functionalized onto the substrate (Figure 1.ii).[15,42,44,45] "Grafting from" *in situ* techniques include variations of surface-initiated atom-transfer radical polymerization (SI-ATRP), which can often incorporate "grafting from" strategies to the growing chain as well.[28,45,46] Other strategies include anionic, cationic, and free radical polymerization. The self-initiated photo grafting and photopolymerization (SIPGP) of polymer brushes has also been reported.[47] "Grafting from" techniques involve strategies including click chemistry and self-assembled monolayers.[48–

[50] A limitation of "grafting from" techniques is that they are limited in density due to the elasticity and steric repulsion of already-tethered chains. In order to overcome this energetic barrier, the strategy of self-assembled monolayers involves a highly efficient, stable linkage which results in spontaneous tethering of a dilute polymer solution.[51] In this work, we will use the technique of self-assembled monolayers to assemble brushes of polyelectrolytes onto a gold substrate through non-labile, gold-thiol interactions.

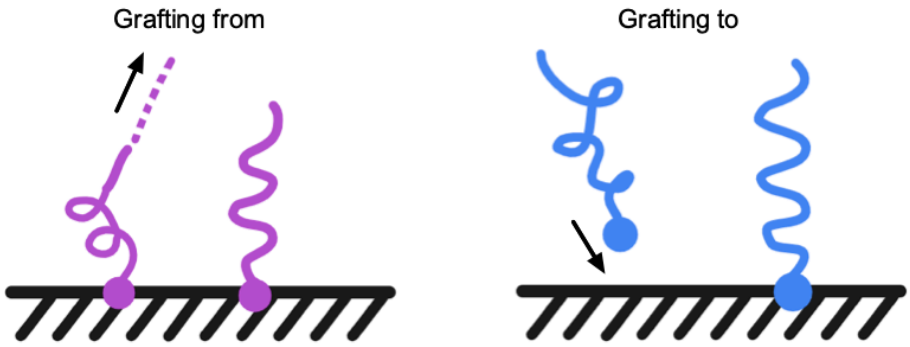

Figure 1.ii: Cartoon representations of the fabrication technique of "grafting from" (left) where the dashed chain and arrow indicates the growing chain end, and the technique of "grafting to" (right), where the arrow indicates where the chain attaches.

1.i.b Introduction to Polyelectrolytes: Brushes and Layer-by-Layer (LbL) films

Polyelectrolytes, or ion-containing polymers, are an extremely exciting for their dynamic nature and responsiveness, where the presence of ionizable charged monomers makes them extremely unique in their physical behavior, allowing them to complex with a polyelectrolyte of the opposite charge. In aqueous solution, polyelectrolytes exhibit acid-base behavior. They are able to dissociate as simple electrolytes do into a charged polymer molecule, where charge is balanced by the dissociated counterions, which in turn, provide chain electroneutrality.[38,52,53]

Whereas a strongly charged polyanion (a polyacid) dissociates fully in solution, weakly charged polyanions do not dissociate, and thus are only partially ionized (Equation 1.1), where HA is the protonated weak acid, and A^- is the deprotonated conjugate base.

$$HA + H_2O \Longleftrightarrow A^- + H_3O^+ \quad [1.1]$$

Unlike simple acids whose ionization constant, or pKa, is expressed by a simple relationship based on the Henderson-Hasselbach equation,[54] the ionization constant of a polyacid monomer is expressed better as an effective dissociation constant pKa^{eff} (Equation 1.2), where α_A is the extent of ionization.

$$pK_A^{eff} = pH + \log\frac{1-\alpha_A}{\alpha_A} \quad [1.2]$$

Polyelectrolyte brushes are an important class of polymer brushes with applications in areas from water purification to drug delivery carriers, colloidal stabilizers and deposition chemistry, and antifouling.[41,46,55,56]. Polyelectrolyte brushes involve end-tethered polyelectrolyte chains versus charge neutral ones. A great deal of experimental and theoretical work exists to predict the equilibrium thickness of polyelectrolyte brushes and provide scaling relationships to predict their behavior.[37–39,57,58]

Polyelectrolytes in solution may complex with polyelectrolytes of the opposite charge to form polyelectrolyte complexes, which have proven to be extremely useful in a variety of applications. Our group has done considerable work in the area of polyelectrolyte complexes in not only describing their equilibrium through numerical theory and simulations, but also

characterizing their chemical composition and rheology.[59–61] Polyelectrolyte complexation is harnessed as a strategy in the technique of layer-by-layer (LbL) self-assembly.[26,27]

LbL self-assembly describes the technique of building a multilayer polymer film architecture using complementary interactions, usually of oppositely-charged polyelectrolytes (Figure 1.iii). While LbL films are traditionally known to utilize electrostatic interaction to grow the architectures, other interactions may be used, including weak dipole-dipole, hydrophobic, hydrogen bonding, and host-guest interactions.[26,44] This allows LbL films to feature a variety of materials, including small molecule drugs to dyes for applications in biomedicine and sensing. The techniques to fabricate and deposit LbL films vary greatly, and can include techniques such as dip coating, spray coating, and spin coating.[26,27] In this work, we will investigate the fabrication technique of Quartz Crystal Microbalance w/ Dissipation (QCM-D), which is also a powerful analytical tool to measure bulk film properties.[21,62–64]

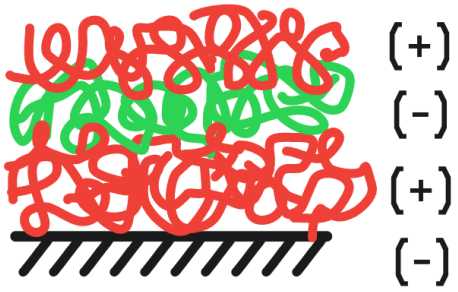

Figure 1.iii: A schematic of an LbL multilayer with oppositely charged polyelectrolytes on a negatively charged substrate.

The assembly of LbL films occurs in aqueous solution, which sets it apart from other polymer thin film fabrication techniques. At each growth step, complementary polyelectrolytes are allowed to equilibrium to irreversibly form a new layer. At each adsorption step, a rinse step occurs which

prevents the adsorption of aspecifically-adsorbed polymer and anneals the layer for the subsequent layer. LbL films can also grow from brushes to form polyelectrolyte brush-bilayers.[15,65]

In Chapters 2 and 3, we will examine both polyelectrolyte brushes and brush-bilayers of polyelectrolyte brushes in an effort to understand their fundamental equilibrium in order to develop a fundamental understanding and to provide a comprehensive data set for testing future theories and for comparison against other polyelectrolyte brush and multilayer systems.me

1.i.c Motivation and Objectives

Polyelectrolyte brushes are used in a variety of industries for a variety of different applications. Their dynamic nature as ionizable materials allows them to possess different characteristics depending on their environment, which can be harnessed for applications such as sensing or drug delivery. While many applications exist for polyelectrolyte brushes, and a wealth of experimental and theoretical work has been done in this area, their fundamental equilibrium behavior is still not fully known, which makes it difficult to use them in applications where specific characteristics are desired, or environments are required. Understanding the equilibrium response of polyelectrolyte brushes to changes in pH, salt, and grafting density is extremely critical to predicting their behavior. Thus, the focus of this thesis work was to understand as well as possible the fundamental equilibrium of these polyelectrolyte brushes and brush-bilayers. In the case of the polyelectrolyte brushes, this involved investigation of the swelling behavior PE brushes using Quartz Crystal Microbalance with Dissipation, or QCM-D, where the QCM-D is able to provide the swollen thicknesses (modeled from the changes in Frequency) and a qualitative description of the viscoelasticity of the material as a function of the Dissipation.[63,64]

In Chapter 2, we will examine the effect of the swelling/de-swelling behavior of weak polyelectrolyte brushes of short- (2 KDa), medium- (14 kDa), and long-chain (39 KDa) a weakly ionizable polyanion, poly(acrylic acid) (PAA), in the presence of KCl at various pH values, and at grafting densities from 0.12 to 2.15 chains/nm^2 using QCM-D. The brushes were created using a thiol-gold linkages[50,51,66,67] to form a polymer self-assembled monolayer (SAM) directly on the gold-coated QCM-D crystal sensor (Figure 1.iv) rather than a traditional surface-initiated polymerization method, which allows for control of the molecular weight of the brush by avoiding synthesis of the brush layer *in situ*. Finally, we compare our results for swollen equilibrium height to scaling predictions from self-consistent field theory for both weakly- and strongly- ionizable brushes with respect to salt concentration, chain length, and grafting density.[37,39]

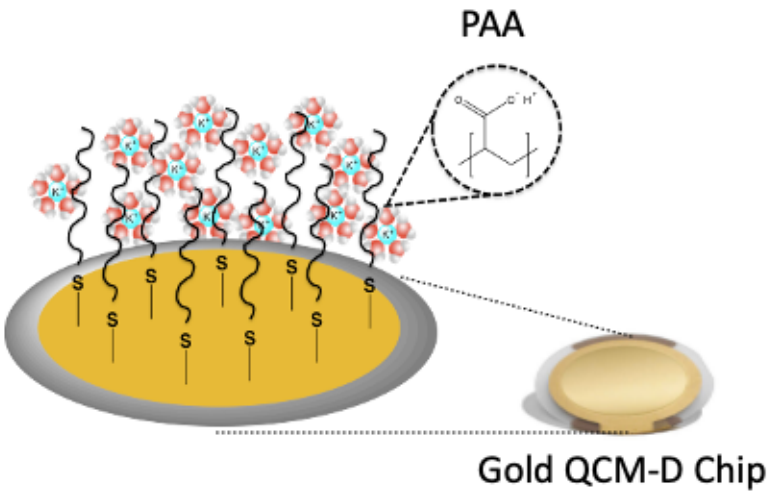

Figure 1.iv: Cartoon depicting the experimental setup described in Chapter 2 of a gold-coated QCM-D chip with a self-assembled monolayer (SAM) of poly(acrylic acid) (PAA) tethered via a thiol-gold linkage.

In Chapter 3, we will go a step further in understanding the swelling equilibriums to investigate the history dependence of these systems. Here, we will investigate both a polyelectrolyte brush monolayer as well as an LbL bilayer: a complementary polyelectrolyte layer

adsorbed onto a polyelectrolyte brush underlayer. To do this, we take the same PAA brush system used in Chapter 2 and adsorb a complementary polycation of poly(ethylene imine) (PEI), which forms a brush-bilayer, *in situ* using the QCM-D (Figure 1.v). In this work, we will investigate the history dependence as a function of the brush underlayer grafting density as well as the chain length, where both KCl concentration is fixed and pH is cycled, and where pH is fixed and KCl concentration is cycled. Finally, using the intermediate collapse observed in our pH cycle for an elastic (long change, sparsely-grafted) brush, we will revisit the scaling observations from Chapter 2 to rectify our disagreements in scaling with the predictions of Zhulina et al.[39] for a weakly-ionizable brush with a more suitable (i.e. more Gaussian) experimental brush model system.

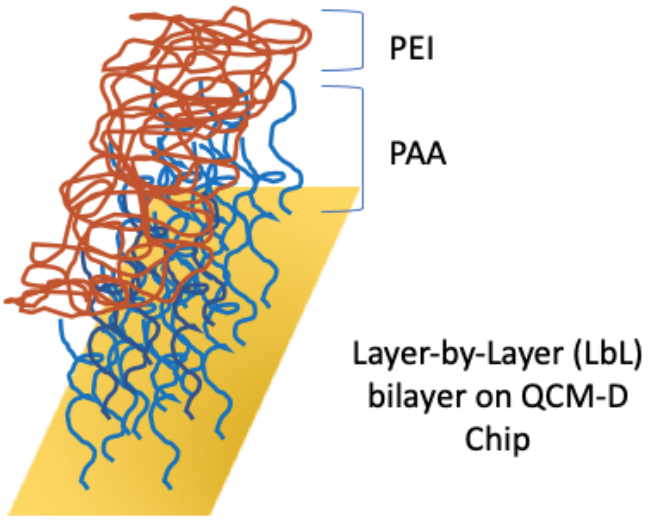

Figure 1.v: Cartoon depicting the experimental setup described in Chapter 3 of a gold-coated QCM-D chip with a brush-bilayer composed of a self-assembled monolayer (SAM) of poly(acrylic acid) (PAA) with complementary adsorbed poly(ethylene imine) (PEI).

1.ii Introduction to Polymer Membranes

Polymer membranes are used in a variety of applications; however, most notably, it is used in the physical filtration of mixtures, the purification of water, and the separation of gas-phase mixtures.[12,68–70] Polymer membranes are typically nonwoven, and generated through either fibers

of polymers or even on the nanoscale of polymer chains themselves.[71] The term "nonwoven" arises from how these materials were offered on the market as a low-cost substitute to textiles, which are typically made with dry fibers using traditional fiber processing equipment. Nonwovens, however, are often made through dry, wet, or even spinning methods. In contrast to a "woven textile", a nonwoven membrane is typically processed by laying down fibers onto a substrate in either a wet, powder, or molten state. The terms to describe these nonwoven membranes vary from webs to mats or woven sheets.[72] They can be on the order of thin films (nanometers), microns or even hundreds of centimeters, and are used in industries from petroleum to biomedicine.[73] Generally speaking, the industrial membranes market is expected to grow to over $1.6B by 2025.[74]

1.ii.a Polymer Membranes for Biofuel Processing

Of the many applications for polymer membrane, one of the most popular is physical filtration. Filtration refers to the isolation of typically solid-phase particles from a mixture by passage of most of the fluid mixture through a septum or membrane that retains most of the solids on or within itself. Membranes may be functionalized for applications such as the filtration of monocolonal antibodies[75] or as catalytic reactors the processing of biofuel,[76] which is the focus of Chapter 4 of this thesis.

A catalytic membrane for biofuel processing can be described as a functional membrane that features reaction and separation together. By incorporating chemical catalyst, it allows crude oil to be passed through the membrane to undergo a transesterification reaction with the catalyst to form biodiesel. Catalytic membranes circumvent many of the major traditional problems with biofuels processing. One major problem with traditional biofuels processing is that catalysts need to be separated from the biodiesel. This results in expensive and time-consuming physical filtration

and chemical separation of the catalyst, depending on if it is homogenous or heterogenous in nature. Furthermore, residual catalyst is extremely dangerous to engines, and to the environment.[76]

1.ii.b Motivation and Objectives

Motivated by the large industry for biofuel membrane reactors and the desire to design a sustainable and effective material, Chapter 4 will describe the development of a catalytic membrane featuring electrospun fibers of the thermoplastic polymer polyacrylonitrile (PAN) (Figure 1.vi). We then describe a novel approach of chemically immobilizing an alkaline catalyst (CaO) using dopamine-metal coordination by functionalizing the PAN membranes with dopamine moieties. In doing so, we aimed to engineer a truly multifunctional material that circumvents many of the issues posed by traditional biofuel processing. More specifically, we avoid the leaching of toxic alkaline catalyst into the environment and we avoid leaching of the catalyst into the resultant fuel through chemical immobilization. This is more sustainable for the environment and will be more cost effective. In immobilizing the catalyst, we also create a membrane that is reusable; it can be wrung out and re-used, which is also more environmentally-friendly and more economical. Finally, in using a basic, heterogenous catalyst versus more popular acid, homogenous catalysts, we are able to take advantage of milder reaction conditions, which is more desirable for large-scale processing.

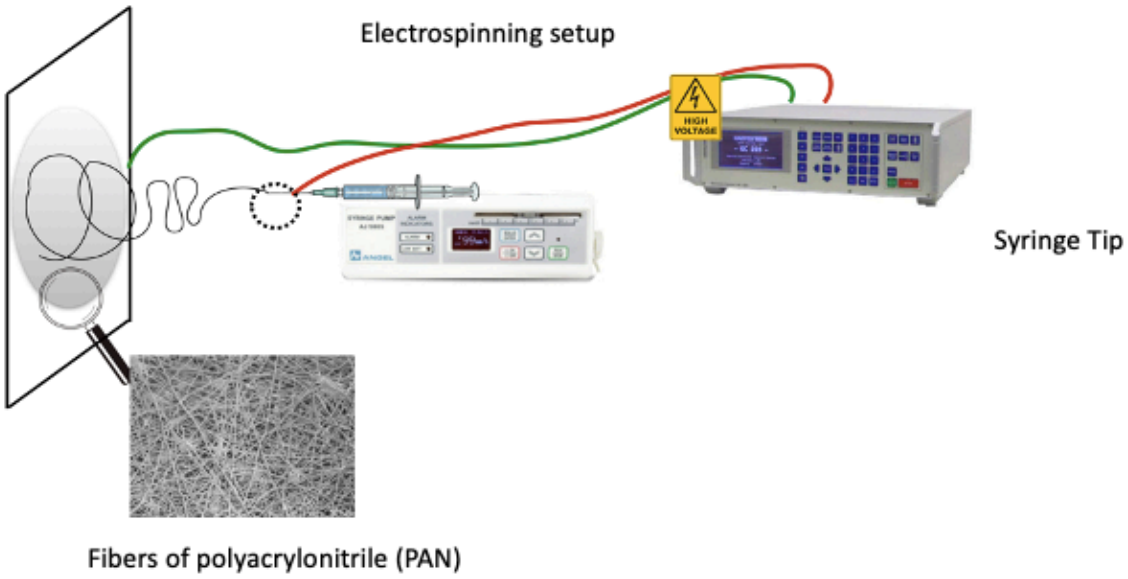

Figure 1.vi: Schematic depiction of the electrospinning setup to draw fibers of polyacrylonitrile (PAN) into a nonwoven membrane for subsequent functionalization.

The market for biodiesel is expected to be worth upwards $54.8B by 2025.[77] It is therefore our goal to design a unique and effective membrane capable to addressing the major biofuel processing concerns to provide a feasible solution that could potentially be scaled-up in industry.

1.iii References

1 Pucci, A. Smart and modern thermoplastic polymer materials. *Polymers*, 2018, *10*.
2 Jagur-Grodzinski, J. Polymeric materials for fuel cells: Concise review of recent studies. *Polymers for Advanced Technologies*, 2007, *18*, 785–799.
3 Hou, W.; Xiao, Y.; Han, G.; Lin, J. Y. The applications of polymers in solar cells: A review. *Polymers*, 2019, *11*.
4 Zhang, Z.; Li, X.; Guan, G.; Pan, S.; Zhu, Z.; Ren, D.; Peng, H. A Lightweight Polymer Solar Cell Textile that Functions when Illuminated from Either Side. *Angew. Chemie Int. Ed.* **2014**, *53*, 11571–11574 DOI: 10.1002/anie.201407688.
5 MacDiarmid, A. G. "Synthetic metals": A novel role for organic polymers (Nobel lecture). *Angewandte Chemie - International Edition*, 2001, *40*, 2581–2590.
6 Li, L.; Huang, W.; Wang, B.; Wei, W.; Gu, Q.; Chen, P. Properties and structure of polylactide/poly (3-hydroxybutyrate-co-3-hydroxyvalerate) (PLA/PHBV) blend fibers.

Polymer (Guildf). **2015**, *68*, 183–194 DOI: 10.1016/j.polymer.2015.05.024.
7 Sachs, E.; Cima, M.; Cornie, J.; Brancazio, D.; Bredt, J.; Curodeau, A.; Fan, T.; Khanuja, S.; Lauder, A.; Lee, J.; et al. Three-Dimensional Printing: The Physics and Implications of Additive Manufacturing. *CIRP Ann. - Manuf. Technol.* **1993**, *42*, 257–260 DOI: 10.1016/S0007-8506(07)62438-X.
8 Hsiao, C.-W.; Bai, M.-Y.; Chang, Y.; Chung, M.-F.; Lee, T.-Y.; Wu, C.-T.; Maiti, B.; Liao, Z.-X.; Li, R.-K.; Sung, H.-W. Electrical coupling of isolated cardiomyocyte clusters grown on aligned conductive nanofibrous meshes for their synchronized beating. *Biomaterials* **2013**, *34*, 1063–1072 DOI: 10.1016/j.biomaterials.2012.10.065.
9 Lee, S.-B.; González-Cabezas, C.; Kim, K.-M.; Kim, K.-N.; Kuroda, K. Catechol-Functionalized Synthetic Polymer as a Dental Adhesive to Contaminated Dentin Surface for a Composite Restoration. *Biomacromolecules* **2015**, *16*, 2265–2275 DOI: 10.1021/acs.biomac.5b00451.
10 Ramakrishna, S.; Mayer, J.; Wintermantel, E.; Leong, K. W. Biomedical applications of polymer-composite materials: A review. *Compos. Sci. Technol.* **2001**, *61*, 1189–1224 DOI: 10.1016/S0266-3538(00)00241-4.
11 Pendhari, S. S.; Kant, T.; Desai, Y. M. Application of polymer composites in civil construction: A general review. *Compos. Struct.* **2008**, *84*, 114–124 DOI: 10.1016/j.compstruct.2007.06.007.
12 Joseph, N.; Leuven, K. U.; Ahmadiannamini, P.; Richard, H.; Hoogenboom, R.; Vankelecom, I. F. J. Layer-by-layer preparation of polyelectrolyte multilayer membranes for separation. **2014** DOI: 10.1039/c3py01262j.
13 Shi, F. F. Recent advances in polymer thin films prepared by plasma polymerization Synthesis, structural characterization, properties and applications. *Surface and Coatings Technology*, 1996, *82*, 1–15.
14 Ozaydin-Ince, G.; Coclite, A. M.; Gleason, K. K. CVD of polymeric thin films: Applications in sensors, biotechnology, microelectronics/organic electronics, microfluidics, MEMS, composites and membranes. *Reports on Progress in Physics*, 2012, *75*, 016501.
15 Hashim, A. A. *Polymer Thin Films*; InTech, 2012.
16 Oyerokun, F. T.;Schweizer, K. S. Theory of Glassy Dynamics in Conformationally Anisotropic Polymer Systems. *J. Chem. Phys.* **2005**, 224901.
17 Keddie, J. L.; Jones, R. A. L.; Cory, R. A. Size-Dependent Depression of the Glass Transition Temperature in Polymer Films. *Eur. Lett.* **1994**, *27*.
18 Kalathi, J. T.; Yamamoto, U.; Schweizer, K. S.; Grest, G. S.; Kumar, S. K. Nanoparticle Diffusion in Polymer Nanocomposites. *Phys. Rev. Lett.* **2014**, 108301.
19 Kim, H.; Ruhm, A.; Lurio, L. B.; Basu, J. K.; Lal, J.; Lumma, D.; Mochrie, S. G. J.; Sinha, S. K. Surface Dynamics of Polymer Films. *Phys. Rev. Lett.* **2003**, *90*, 068302.
20 Jiang, Z.; Kim, H.; Mochrie, S. G. J.; Lurio, L. B.; Sinha, S. K. Surface and Interfacial Dynamics of Polymeric Bilayer Films. *Phys. Rev. E* **2006**, *74*, 011603.
21 Denolf, G. C.; Sturdy, L. F.; Shull, K. R. High-Frequency Rheological Characterization of Homogeneous Polymer Films with the Quartz Crystal Microbalance. *Langmuir* **2014**, *30*, 9731−9740 DOI: 10.1021/la502090a.
22 de Gennes, P. G. Glass Transitions in Thin Polymer Films. *Eur. Phys. J. E* **2000**, 201–203.
23 Yang, Z.; Clough, A.; Lam, C.-H.; Tsui, O. K. C. Glass Transition Dynamics and Surface Mobility of Entangled Polystyrene Films at Equilibrium. *Macromolecules* **2011**, *44*,

8294–8300.
24 Tress, M.; Erber, M.; Mapesa, E. U.; Huth, H.; Mueller, J.; Serghei, A.; Schick, C.; Eichhorn, K.-J.; Volt, B.; Kremer, F. Glassy Dynamics and Glass Transition in Nanometric Thin Layers of Polystyrene. *Macromolecules* **2010**, *43*, 9937–9944.
25 Tokarev, I.; Motornov, M.; Minko, S. Molecular-engineered stimuli-responsive thin polymer film: A platform for the development of integrated multifunctional intelligent materials. *J. Mater. Chem.* **2009**, *19*, 6932–6948 DOI: 10.1039/b906765e.
26 Hammond, P. T. Engineering Materials Layer-by-Layer: Challenges and Opportunities in Multilayer Assembly. **2011** DOI: 10.1002/aic.12769.
27 Alkekhia, D.; Hammond, P. T.; Shukla, A. Layer-by-Layer Biomaterials for Drug Delivery. *Annual Review of Biomedical Engineering*, 2020, *22*, 1–24.
28 Saleh, N.; Sarbu, T.; Sirk, K.; Lowry, G. V; Matyjaszewski, K.; Tilton, R. D. Oil-in-Water Emulsions Stabilized by Highly Charged Polyelectrolyte-Grafted Silica Nanoparticles. *Langmuir* **2005**, *21*, 9873–9878 DOI: 10.1021/la050654r.
29 Milner, S. T. Polymer brushes. *Science (80-.).* **1991**, *251*, 905–914 DOI: 10.1126/science.251.4996.905.
30 Azzaroni, O. Polymer brushes here, there, and everywhere: Recent advances in their practical applications and emerging opportunities in multiple research fields. *J. Polym. Sci. Part A Polym. Chem.* **2012**, *50*, 3225–3258 DOI: 10.1002/pola.26119.
31 Liu, G.; Cai, M.; Wang, X.; Zhou, F.; Liu, W. Core–Shell–Corona-Structured Polyelectrolyte Brushes-Grafting Magnetic Nanoparticles for Water Harvesting. *ACS Appl. Mater. Interfaces* **2014**, *6*, 11625–11632 DOI: 10.1021/am502351x.
32 Hehmeyer, O. J.; Arya, G.; Panagiotopoulos, A. Z.; Szleifer, I. Monte Carlo simulation and molecular theory of tethered polyelectrolytes. *J. Chem. Phys.* **2007**, *126*, 244902 DOI: 10.1063/1.2747600.
33 Nap, R. J.; Tagliazucchi, M.; Szleifer, I. Born energy, acid-base equilibrium, structure and interactions of end-grafted weak polyelectrolyte layers. *J. Chem. Phys.* **2014**, *140*, 024910 DOI: 10.1063/1.4861048.
34 Wu, T.; Gong, P.; Szleifer, I.; Vlček, P.; Šubr, V.; Genzer, J. Behavior of Surface-Anchored Poly(acrylic acid) Brushes with Grafting Density Gradients on Solid Substrates: 1. Experiment. *Macromolecules* **2007**, *40*, 8756–8764 DOI: 10.1021/ma0710176.
35 Morochnik, S.; Nap, R. J.; Ameer, G. A.; Szleifer, I. Structural behavior of competitive temperature and pH-responsive tethered polymer layers. *Soft Matter* **2017**, *13* DOI: 10.1039/c7sm01538k.
36 Gong, P.; Genzer, J.; Szleifer, I. Phase Behavior and Charge Regulation of Weak Polyelectrolyte Grafted Layers. *Phys. Rev. Lett.* **2007**, *98*, 018302 DOI: 10.1103/PhysRevLett.98.018302.
37 Israels, R.; Leermakers, J. F. A. M.; Fleer, J.; Zhulina, E. B. Charged Polymeric Brushes: Structure and Scaling Relations. *Macromolecules* **1994**, *27*, 3249–3261.
38 Pryamitsyn, V. A.; Leermakers, F. A. M.; Fleer, G. J.; Zhulina, E. B. *Theory of the Collapse of the Polyelectrolyte Brush*; 1996.
39 Zhulina, E. B.; Birshtein, T. M.; Borisov, O. V. Theory of Ionizable Polymer Brushes. *Macromolecules* **1995**, *28*, 1491–1499 DOI: 10.1021/ma00109a021.
40 de Gennes, P. G. Polymers at an interface; a simplified view. *Advances in Colloid and Interface Science*, 1987, *27*, 189–209.
41 Das, S.; Banik, M.; Chen, G.; Sinha, S.; Mukherjee, R. Polyelectrolyte brushes: Theory,

modelling, synthesis and applications. *Soft Matter*, 2015, *11*, 8550–8583.
42 Matthias Ballauff. Spherical Polyelectrolyte Brushes. In *Polymer Brushes*; Rigoberto C. Advincula, Ed.; WILEY-VCH Verlag GmbH & Co.: Weinheim, 2004; pp 231–248.
43 Advincula, R. C. Polymer Brushes. In *Encyclopedia of Polymer Science and Technology*; John Wiley & Sons, Inc.: Hoboken, NJ, USA, 2004.
44 Aulich, D.; Hoy, O.; Luzinov, I.; Brücher, M.; Hergenröder, R.; Bittrich, E.; Eichhorn, K.-J.; Uhlmann, P.; Stamm, M.; Esser, N.; et al. In Situ Studies on the Switching Behavior of Ultrathin Poly(acrylic acid) Polyelectrolyte Brushes in Different Aqueous Environments. *Langmuir* **2010**, *26*, 12926–12932 DOI: 10.1021/la101762f.
45 Polanowski, P.; Hałagan, K.; Pietrasik, J.; Jeszka, J. K.; Matyjaszewski, K. Growth of polymer brushes by "grafting from" via ATRP – Monte Carlo simulations. *Polymer (Guildf).* **2017**, *130*, 267–279 DOI: 10.1016/j.polymer.2017.10.011.
46 Kusumo, A.; Bombalski, L.; Lin, Q.; Matyjaszewski, K.; Schneider, J. W.; Tilton, R. D. High Capacity, Charge-Selective Protein Uptake by Polyelectrolyte Brushes. *Langmuir* **2007**, *23*, 4448–4454 DOI: 10.1021/LA063660B.
47 Steenackers, M.; Küller, A.; Stoycheva, S.; Grunze, M.; Jordan, R. Structured and gradient polymer brushes from biphenylthiol self-assembled monolayers by self-initiated photografting and photopolymerization (SIPGP). *Langmuir* **2009**, *25*, 2225–2231 DOI: 10.1021/la803386c.
48 Desai, R. M.; Koshy, S. T.; Hilderbrand, S. A.; Mooney, D. J.; Joshi, N. S. Versatile click alginate hydrogels crosslinked via tetrazine–norbornene chemistry. *Biomaterials* **2015**, *50*, 30–37 DOI: 10.1016/j.biomaterials.2015.01.048.
49 Albert, S. K.; Thelu, H. V. P.; Golla, M.; Krishnan, N.; Chaudhary, S.; Varghese, R. Self-Assembly of DNA-Oligo(p-phenylene-ethynylene) Hybrid Amphiphiles into Surface-Engineered Vesicles with Enhanced Emission. *Angew. Chem. Int. Ed. Engl.* **2014**, 8352–8357 DOI: 10.1002/anie.201403455.
50 Almeida, B.; Shukla, A. Degradation of alkanethiol self-assembled monolayers in mesenchymal stem cell culture. *J Biomed Mater Res Part A J Biomed Mater Res Part A* **2017**, *105A*, 464–474 DOI: 10.1002/jbm.a.35922.
51 Xue, Y.; Li, X.; Li, H.; Zhang, W. Quantifying thiol-gold interactions towards the efficient strength control. *Nat. Commun.* **2014**, *5*, 1–9 DOI: 10.1038/ncomms5348.
52 Sing, C. E.; Zwanikken, J. W.; Olvera de la Cruz, M. Effect of Ion–Ion Correlations on Polyelectrolyte Gel Collapse and Reentrant Swelling. *Macromolecules* **2013**, *46*, 5053–5065 DOI: 10.1021/ma400372p.
53 Fares, H. M.; Schlenoff, J. B. Diffusion of Sites versus Polymers in Polyelectrolyte Complexes and Multilayers. *J. Am. Chem. Soc.* **2017**, *139*, 14656–14667 DOI: 10.1021/jacs.7b07905.
54 Crea, F.; De Stefano, C.; Gianguzza, A.; Pettignano, A.; Piazzese, D.; Sammartano, S. Acid-base properties of synthetic and natural poly electrolytes: Experimental results and models for the dependence on different aqueous media. *J. Chem. Eng. Data* **2009**, *54*, 589–605 DOI: 10.1021/je800518j.
55 Motornov, M.; Tam, K.; Pita, M.; Tokarev, I.; Katz, E.; Minko, S. Switchable selectivity for gating ion transport with mixed polyelectrolyte brushes: approaching "smart" drug delivery systems. *IOP Publ. Nanotechnol. Nanotechnol.* **2009**, *20*, 434006–434016 DOI: 10.1088/0957-4484/20/43/434006.
56 Weir, M. P.; Parnell, A. J. Water Soluble Responsive Polymer Brushes. *Polymers (Basel).*

2011, *3*, 2107–2132 DOI: 10.3390/polym3042107.
57 Pincus, P. Colloid stabilization with grafted polyelectrolytes. *Macromolecules* **1991**, *24*, 2912–2919 DOI: 10.1021/ma00010a043.
58 Meka, V. S.; Sing, M. K. G.; Pichika, M. R.; Nali, S. R.; Kolapalli, V. R. M.; Kesharwani, P. A comprehensive review on polyelectrolyte complexes. *Drug Discovery Today*, 2017, *22*, 1697–1706.
59 Ghasemi, M.; Larson, R. G. Role of Electrostatic Interactions in Charge Regulation of Weakly Dissociating Polyacids. *Submitted to Macromolecules* **2020**.
60 Salehi, A.; Desai, P. S.; Li, J.; Steele, C. A.; Larson, R. G. Relationship between Polyelectrolyte Bulk Complexation and Kinetics of Their Layer-by-Layer Assembly. *Macromolecules* **2015**, *48*, 400–409 DOI: 10.1021/ma502273a.
61 Salehi, A.; Larson, R. G. A Molecular Thermodynamic Model of Complexation in Mixtures of Oppositely Charged Polyelectrolytes with Explicit Account of Charge Association/Dissociation. *Macromolecules* **2016**, *49*, 9706–9719 DOI: 10.1021/acs.macromol.6b01464.
62 Sadman, K.; Wiener, C. G.; Weiss, R. A.; White, C. C.; Shull, K. R.; Vogt, B. D. Quantitative Rheometry of Thin Soft Materials Using the Quartz Crystal Microbalance with Dissipation. *Anal. Chem.* **2018**, *90*, 4079−4088 DOI: 10.1021/acs.analchem.7b05423.
63 Höök, F.; Kasemo, B.; Nylander, T.; Fant, C.; Sott, K.; Elwing, H. Variations in coupled water, viscoelastic properties, and film thickness of a Mefp-1 protein film during adsorption and cross-linking: a quartz crystal microbalance with dissipation monitoring, ellipsometry, and surface plasmon resonance study. *Anal. Chem.* **2001**, *73*, 5796–5804.
64 Liu, G.; Zhang, G. Chapter 1: Basic Principles of QCM-D. In *QCM-D Studies on Polymer Behavior at Interfaces*; Springer Science & Business Media, 2013; pp 1–8.
65 Kreer, T. Polymer-brush lubrication: A review of recent theoretical advances. *Soft Matter*, 2016, *12*, 3479–3501.
66 Brust, M.; Walker, M.; Bethell, D.; Schiffrin, D. J.; Whyman, R. Synthesis of thiol-derivatised gold nanoparticles in a two-phase Liquid?Liquid system. *J. Chem. Soc. Chem. Commun.* **1994**, 801 DOI: 10.1039/c39940000801.
67 Liu, G.; Yan, L.; Chen, X.; Zhang, G. Study of the kinetics of mushroom-to-brush transition of charged polymer chains. *Polymer (Guildf).* **2006**, *47*, 3157–3163 DOI: 10.1016/j.polymer.2006.02.091.
68 Maier, G. Gas separation with polymer membranes. *Angewandte Chemie - International Edition*, 1998, *37*, 2960–2974.
69 Kang, Y.; Emdadi, L.; Lee, M. J.; Liu, D.; Mi, B. Layer-by-Layer Assembly of Zeolite/Polyelectrolyte Nanocomposite Membranes with High Zeolite Loading. *Environ. Sci. Technol. Lett.* **2014**, *1*, 504–509 DOI: 10.1021/ez500335q.
70 Tsai, H.-J.; Lee, Y.-L. Facile method to fabricate raspberry-like particulate films for superhydrophobic surfaces. *Langmuir* **2007**, *23*, 12687–12692 DOI: 10.1021/la702521u.
71 Scampicchio, M.; Bulbarello, A.; Arecchi, A.; Cosio, M. S.; Benedetti, S.; Mannino, S. Electrospun Nonwoven Nanofibrous Membranes for Sensors and Biosensors. *Electroanalysis* **2012**, *24*, 719–725 DOI: 10.1002/elan.201200005.
72 Wilson, A. The formation of dry, wet, spunlaid and other types of nonwovens. In *Applications of Nonwovens in Technical Textiles*; Elsevier, 2010; pp 3–17.
73 King, M. W.; Chung, S. Medical Fibers and Biotextiles. In *Biomaterials Science: An Introduction to Materials: Third Edition*; Elsevier Inc., 2013; pp 301–320.

74 Non-woven - Industrial Membrane Market Global Forecast to 2025 | MarketsandMarkets https://www.marketsandmarkets.com/Market-Reports/nonwoven-fabric-market-in-industrial-membrane-257165275.html (accessed Oct 26, 2020).
75 Okuno, Y.; Yamazaki, Y.; Fukutomi, H.; Kuno, S.; Yasutake, M.; Sugiura, M.; Kim, C. J.; Kimura, S.; Uji, H. A Novel Surface Modification and Immobilization Method of Anti-CD25 Antibody on Nonwoven Fabric Filter Removing Regulatory T Cells Selectively. *ACS Omega* **2019** DOI: 10.1021/ACSOMEGA.9B03494.
76 Hafeez, S.; Al-Salem, · S M; Manos, · George; Achilleas Constantinou, ·. Fuel production using membrane reactors: a review. **2020**, *18*, 1477–1490 DOI: 10.1007/s10311-020-01024-7.
77 Biodiesel Market Size Worth $54.8 Billion By 2025 | Growth Rate: 7.3% https://www.grandviewresearch.com/press-release/global-biodiesel-market (accessed Oct 26, 2020).

Chapter 2

Salt- and pH-Induced Swelling of a Poly(Acrylic Acid) Brush via Quartz Crystal Microbalance w/ Dissipation (QCM-D)

2.i Abstract

We infer the swelling/de-swelling behavior of weakly ionizable poly(acrylic acid) (PAA) brushes of 2-39 kDa molar mass in the presence of KCl concentrations from 0.1-1000 mM, pH = 3, 7, and 9, and grafting densities $\sigma = 0.12–2.15$ chains/nm^2 using a Quartz Crystal Microbalance with Dissipation (QCM-D), confirming and extending the work of Wu et al[1] to multiple chain lengths. At pH 7, at low and moderate grafting densities, our results in the high-salt "salted brush" regime (C_s > 10 mM salt) agree with the predicted scaling $H \sim N\sigma^{+1/3}C_s^{-1/3}$ of brush height H, [2,3] while in the low-salt "osmotic brush" regime (C_s <10 mM salt), we find $H \sim N\sigma^{+1/3}C_s^{+0.28-0.38}$, whose dependence on C_s agrees with scaling theory for this regime,[2,3] but the dependence on σ strongly disagrees with it. The predicted linearity in the degree of polymerization N is confirmed. [2,3] The new results partially confirm scaling theory and clarify where improved theories and additional data are needed.

2.ii Introduction

Polymer brushes have been studied extensively for many decades and have gained considerable attention for their applications in a variety of areas, including oil recovery, protein antifouling, aqueous lubrication, nanocomposite fabrication, water harvesting, flow-control valves, drug delivery, and rectifiers.[4-13] Brushes are defined as densely-packed polymer chains that

are tethered on one end onto an impermeable substrate and extend into solvent at the other end.[3,14] By definition, the grafting density of a polymer brush is high enough that the polymer chains are forced to extend away from the substrate, thus preventing the random-coil arrangement typical in solution, or on surfaces in the "mushroom" regime, where the grafting density is too low to form a brush.[11,15] Polyelectrolyte brushes in particular are desirable for their swelling characteristics in aqueous conditions, making them suitable as colloidal stabilizers, water-based lubricants, and biomaterials.[16,17]

Weak polyelectrolyte brushes, or annealed brushes, are modifiable as their charge density and resultant swelling behavior is altered by the environmental pH or ionic strength, which affect the extent of chain ionization.[18,19] Furthermore, the swelling or structural behavior of weak polyelectrolyte brushes has been shown to depend on a variety of factors, including the type of salt ion, the valence of salt ion, the hydrophobicity of the polyelectrolyte monomers, the temperature, and the brush grafting density.[18,20,21] This behavior has been demonstrated to have a significant influence on properties such as the coefficient of friction of the brush as well as the overall adhesion or wettability of the brush towards other surfaces.[22,23] Weak polyelectrolytes have also been demonstrated to exhibit pH-specific responses consistent with their pKa, which affects their overall extent of ionization.[24] Despite this general understanding, the pH dependence of brush properties is not well understood and while theories for the dependence of brush height on chain length, grafting density, and salt concentration have been available for more than 20 years, tests of these theories have so far been somewhat limited. The most complete of these are the studies of Tirrell and coworkers using sodium polystyrene sulfonate (NaPSS) brushes bound to mica substrates, whose heights were measured by a surface forces apparatus,[25] of Chu et al. for a series of strong polyelectrolyte brushes of sodium polystyrene sulfonate (NaPSS), poly([2-

(methacryloyloxy)ethyl] trimethylammonium chloride) (PMTAC), and potassium poly(3-sulfopropyl methacrylate) (PSPMA) of a variety of chain lengths studied on silicon and silica surfaces by ellipsometry and QCM-D,[21] and of Wu et al. for a weak polyacrylic acid (PAA) brush of a single chain length grown directly onto a gold substrate and studied by QCM-D.[1] The studies of Tirrell and coworkers covered a limited range of surface coverages and chain lengths and showed brush height to be independent of salt concentration below 0.01 M, followed by a region of decreasing height with increased salt concentration, in agreement with scaling theory, including that of Pincus[26] and of Israëls et al.[3] discussed below. The studies of Chu et al. and Wu et al. showed, instead of the low-salt region of constant height, a striking *non-monotonic* dependence of brush height on added *salt concentration*, with a pronounced maximum in height at a salt molarity of around 0.01 M (or 0.1−1.0 M in Wu et al.), for all of the polyelectrolytes listed above, for various values of their pKa (weak vs. strong polyelectrolyte), chain lengths (brush molecular weights from 12 to 235 kg/mol),[21] and grafting densities (0.06 to 0.25 chains/nm^2)[21] and (0.130-0.863 chains/nm^2).[1] Both of these latter two studies found a *monotonic* dependence of brush height on *grafting density* σ, as one might naively expect, based on chain-crowding effects, but in disagreement with the scaling theory that assumes that the effects of electrostatic and Gaussian chain elasticity dominate.

The theory for strong, permanently charged, polyelectrolytes of Israëls et al.[3] predicts a low-salt "Osmotic Brush" (OB) regime in which brush height H is independent of salt concentration C_s and grafting density σ, followed by a transition to a "Salted Brush" regime in which $H \sim N\sigma^{\frac{1}{3}}C_S^{-\frac{1}{3}}$; i.e., the brush height increases with grafting density and decreases with salt concentration. Zhulina and coworkers[2] extended this theory to weak polyelectrolytes in which the charge density on the polymer is regulated by, and changes with, the salt concentration. The

prediction of this theory in the SB regime, where the polymer charge saturates, is the same as for strong polyelectrolytes, but in the OB regime predicts the opposite dependencies on σ and C_s, namely $H \sim \sigma^{-\frac{1}{3}} C_s^{\frac{1}{3}}$, implying that the brush height H has a maximum in height with increased salt concentration and a minimum with increased grafting density, for a weak polyelectrolyte. The existence of the maximum in H with respect to salinity seen by Wu et al. for PAA brushes would seem to confirm this theory; however, they did not observe the predicted minimum in H with respect to σ. Moreover, the observed pronounced maximum in H at 0.01 M salt for multiple strong polyelectrolytes by Chu et al.[21] seems to throw into doubt the connection of this maximum to charge regulation as is assumed by the weak polyelectrolyte theory. Hence, more studies, both theoretical and experimental, are clearly needed to determine the behavior and establish correct theoretical predictions of these brushes under various conditions.

In our study, a PAA brush was deposited directly onto a gold-plated QCM-D electrode via end-thiol-terminated PAA, which forms a self-assembled monolayer. Our "grafting-to" approach using pre-selected thiol-terminated chains of well-defined lengths, allows us to better control the brush molecular weight relative to traditional surface-initiated polymerization techniques. Our study covers a range of chain lengths, (2-39 KDa), grafting densities (0.12–2.15 chains/nm^2), salt concentrations (0.1-1000 mM), and pH values (3-9), expanding significantly on previous work. We also avoid salt concentrations that are within the same order of magnitude as the ionic strength due to buffers used to control pH, as such data likely to be subject to considerable error, as we discuss below.

A popular instrument for studying the swelling behavior of polyelectrolyte brushes is a Quartz Crystal Microbalance with Dissipation (QCM-D), which can be used to measure subtle

changes in adsorbed mass and material viscoelasticity.[20,21,27,28] Here, we use QCM-D to evaluate the effects of pH, salt concentration, chain length, and grafting density on the swelling response to salt of a weakly ionizable polyelectrolyte brush of Poly(acrylic acid) (PAA), providing the first comprehensive study that spans all four of these parameters over a wide range. In QCM-D measurements, the flow medium has been shown to significantly affect the measurement of the material deposited onto the crystal.[20,29–31] We demonstrate that assessing the contribution of the flow medium to the QCM-D response is crucial for correct interpretation of results.[22] In our study, the dry thicknesses of the brushes were measured by variable angle spectroscopic ellipsometry (VASE).

QCM-D is an ideal technique for monitoring both the uptake of salt and hydration of the brush within aqueous, ionic environments without the need for intervening drying steps, and it is sensitive enough for measurements of ultra-short brushes; however, because of the weak signal, it is imperative to correct for the effect of salts on the QCM-D signal in the absence of adsorbed polymers, as we show below.

2.iii Materials and methods

α-thiol ω-bromo terminated poly(acrylic acid) samples (PAA-SH) (Short-chain: M_n=2,000 g/mol, M_w=2,600 g/mol, M_w/M_n: 1.3, -SH > 99%; Medium-chain: Mn=14,000 g/mol, Mw=18,200 g/mol, Mw/Mn: 1.3, -SH >99%; Long-chain: M_n= 39,000 g/mol, M_w=55,000 g/mol, M_w/M_n: 1.4, -SH > 99%) were obtained from Polymer Source Inc. (Quebec, Canada). Potassium chloride (KCl), sodium chloride (NaCl), lithium chloride (LiCl), and calcium chloride ($CaCl_2$) were purchased from Sigma Aldrich USA and used as received. Hydrogen peroxide (H_2O_2) solution (30 wt%), ammonium hydroxide (NH_4OH) solution (25 wt%), 2-mercaptoethanol, and absolute ethanol

(EtOH) were obtained from Fisher Scientific and were used as received. HPLC plus grade water (pH 7) (Sigma Aldrich USA) was used to prepare all salt solutions used in this work. Solutions at concentrations between 0.1 and 1000 mM were prepared. Solutions of KCl were found to be at pH 7 upon mixing without buffer, while pH 3 and pH 9 solutions of KCl were obtained upon the addition of roughly <3 mM hydrochloric acid (HCl) (Sigma Aldrich USA) or potassium hydroxide (KOH) solutions (Sigma Aldrich USA), respectively. The pH and ionic strengths were confirmed using the combination of conductivity (CON 6+ conductivity meter, Oakton) and a benchtop pH meter (Accumet AE150, Fisher scientific) versus reference standards.

Gold-coated silicon wafers (QSX 301, AT-cut, F_0/n =5 MHz) were purchased from Q-Sense by Biolin Scientific (New Jersey, USA). In preparation for the deposition of PAA, the sensors were cleaned thoroughly to remove any residual dirt and debris via a TL-1 base cleaning solution. Gold-coated QCM-D wafers were fully immersed into base-cleaning solution (mixture of 30% hydrogen peroxide and ammonium hydroxide in ultra-pure water at the ratio 1:1:5) and left for two hours at 65 °C. The crystals were then rinsed thoroughly with deionized water, followed by absolute ethanol, and gently dried under a stream of pure air. The last step of crystal preparation was 15 minutes of O_2- plasma treatment.

2.iii.a Preparation of short-chain PAA-SH brush

All gold-coated silicon wafers were plasma treated before use. Short-chain PAA-SH (M_n: 2,000 g/mol, M_w/M_n=1.3) was dissolved in absolute ethanol to the final concentration of 4 mM.[32] To vary the grafting density the 4 mM PAA solution was used both as is and after dilution by factors of 1:500, 1:1000, 1:5000, and 1:10000 by volume in either absolute ethanol or a 10:1 (wt%) mixture of absolute ethanol to 2-mercaptoethanol. Here, 2-mercaptoethanol acts as a competitive adsorber to compete with the PAA-SH in binding. After this, 40 μL of the appropriate PAA

solution was deposited onto the pure gold crystal and allowed to incubate for 18 h. Excess polymer solution was removed by rinsing the crystal repeatedly with absolute ethanol and gently drying under stream of pure air, making it ready for QCM-D analysis.

2.iii.b Preparation of medium-chain PAA-SH brush

Medium-chain PAA-SH (M_n: 14,000 g/mol, M_w/M_n=1.3) was dissolved in absolute ethanol to a final concentration of 4 mM. 40 μL was then deposited onto the gold crystal and allowed to incubate for 60 minutes, rather than the 18 h used for the short brush. Allowing the solution with the medium-length chain to incubate for longer than 60 min. led to the formation of a thick, heterogenous physical film due presumably to solvent evaporation. No sign of such a film was present when incubation was limited to 60 min., and reproducibility of results under this constraint was excellent. Excess polymer solution was removed by rinsing the crystal repeatedly with absolute ethanol and drying gently under pure air. To vary the grafting density, the 4 mM PAA solution was diluted by a factor of 1:10000 by volume in a 10:1 (wt%) mixture of absolute ethanol to 2-mercaptoethanol. Thereafter, the deposition process was repeated as described before.

2.iii.c Preparation of long-chain PAA-SH brush

Longer-chain PAA-SH (M_n: 39,000 g/mol, M_w/M_n=1.4) was, as with the other chains, dissolved in absolute ethanol to a final concentration of 4 mM. 40 μL was deposited onto the gold crystal and allowed to incubate for 20 minutes. Note that this is considerably less time than for the short-chain PAA due to the viscosity of the solution. Allowing the solution to incubate for longer than this led to the formation of a thick, heterogenous physical film. Excess polymer solution was removed by rinsing the crystal repeatedly with absolute ethanol and drying gently under pure air. This process (40 μL polymer deposition and subsequent repeated rinsing) was repeated 6 times. To vary the grafting density, the 4 mM polymer solution was diluted by 1:10000 in a 10:1 (wt%)

mixture of absolute ethanol to 2-mercaptoethanol. Thereafter, the deposition process was repeated as described before.

2.iii.d Variable Angle Spectroscopic Ellipsometry (VASE)

The thickness of the dry PAA-SH brush on the gold-coated QCM-D crystal was characterized by Variable Angle Spectroscopic Ellipsometry (VASE) (Woollam M-2000 Spectroscopic Ellipsometer, J. A. Woollam, USA) using parameters recommended in the literature for a PAA layer on bulk gold.[33] Measurements were carried out at angles of incidence (Φ_0) of 55°, 65°, and 75°. Woollam Complete EASE software was used to analyze the data obtained from ellipsometry that required more than one wavelength to perform fitting, so a central wavelength λ of 631.5 nm was chosen in addition to two wavelengths on either side of this (629.7 nm & 632.7nm). The optical relative phase shift, Δ, and relative amplitude ratio, tan(Ψ), measured by VASE, were modeled using two slabs: a bulk gold substrate overlaid by a uniform thin layer (brush). The underlying gold on the crystal was treated as a bulk (infinitely thick) substrate since its thickness is ~100 nm.

The fundamental equation of ellipsometry allows the monitoring of the complex reflectance ratio, given by the Fresnel reflection coefficients R_P (*p*-polarized electrical field) and R_S (*s*-polarized electrical field). The ratio of these two coefficients is a known, complicated, complex (i.e., not real) function[33,34] of the wavelength λ, the angle of incidence Φ_0, the optical constants (index of refraction, n, and absorption, k) of the substrate (n_{sub}, k_{sub}), and of the ambient medium (n_{amb}), and the film layer (n_{film}, k_{film}), in addition to the film layer thickness (*d*), as described in Equation 2.1 below.

$$\frac{R_P}{R_S} = tan(\Psi)e^{(i\Delta)} = f(\lambda, \Phi_0, n_{sub}, k_{sub}, n_{amb}, n_{film}, k_{film}, d) \qquad [2.1]$$

The PAA layer was assumed to be transparent ($k_{film}(\lambda)=0$) and homogenous, and with index of refraction (n_{PAA}) of 1.522 at λ=631.5 nm. The optical constant d in Eq. 2.1 was found as the value required to match the modeled to the measured values of Δ and Ψ, using a well-established method that is explained in great detail elsewhere.[34,35]

2.iii.e Quartz Crystal Microbalance with Dissipation (QCM-D)

All QCM-D analyses were performed using the Q-Sense E4 system (Q-Sense AB, Gothenburg, Sweden). Fundamental frequency signals were established on the prepared sensors in air. A baseline for each measurement was established by flowing ultra-pure water (pH 7) until a stable response was seen, followed by the appropriate KCl solution (pH 3,7, or 9) again until a stable response was seen. Solutions were driven through the device by an IPC high precision multichannel peristaltic pump (ISMATEC, IDEX, USA) at a constant flow rate of 0.100 mL/min. The experiments were performed at room temperature (~22°C).

We model the change in frequency using the Sauerbrey relation rather than a viscoelastic model, following the work of DeNolf et al.,[28] who demonstrated that the Sauerbrey relation holds when the film is either very thin and/or rigid, expressed by the dimensionless quantity d/λ_n, where d is the thickness of the film, and λ_n is the shear wavelength of the material. The latter is a function of the complex shear modulus, the frequency at the appropriate harmonic, the density, and the viscoelastic phase angle. DeNolf et al. give the Sauerbrey limit as valid when d/λ_n is no greater than 0.05, beyond which a viscoelastic model should be used.[27,28] In our experiments, we find that d/λ_n ranges between 0.004 to 0.020, where d/λ_n approaches higher values in a thicker (longer chain) brush. Since $d/\lambda_n<0.05$ in all our QCM-D experiments, we use the Sauerbrey model in all instances, since viscoelastic modeling would overestimate the amount of adsorbed mass.

In what follows, we use conventional interpretations of the QCM-D response to infer the swelling behavior of the brush, based on the change in QCM-D for the brush-adsorbed surface relative to the bare surface. While the validity of the Sauerbrey relation gives us a quantitative measure of the adsorbed mass and swelling through the measurement of ΔF_3 using Equation 2.2, this also means that the dissipation is too small to be interpreted quantitatively, since viscoelastic modeling fails in the Sauerbrey limit.[27] Hence, we can only interpret the ΔD_3 data qualitatively as a measure of dissipation.

Typically, in a QCM-D measurement, the fundamental frequency is first found for the sample in air. In our case, either a blank crystal or a chip coated with a thin polymer brush was loaded in air. The fundamental frequency of a blank quartz chip, $F_{0,}$ is 5 MHz,[36] so that the resonance at the third overtone (n=3) is 15 MHz. A brush-coated chip, however, will possess a slightly different baseline frequency. Once this frequency is found, the QCM-D measurement begins by measuring the change in frequency (ΔF) and the change in dissipation (ΔD) at the desired overtones which are reported by the instrument hundreds of times per second, where again, the ΔF and ΔD reported by the instrument are changes from the initial frequency and dissipation measurements of the loaded sample, either of the bare crystal or of the dried polymer on the crystal; in our case at the third overtone n=3, which is considered to be more reliable than the noisier first overtone.[37] Only one overtone is needed to interpret the Sauerbrey mass for a rigid film, while more than one is necessary for viscoelastic modeling.[36] The equivalent adsorbed mass change (Δm) can be calculated using the simple Sauerbrey relation for relatively rigid films where the change in dissipation (ΔD) is small, as discussed above.[38]

$$\Delta F = -\Delta m \left(\frac{2nF_0^2}{A\sqrt{\mu_q \rho_q}} \right) = -\frac{1}{C_f} \Delta m \qquad [2.2]$$

$$\Delta d = \frac{\Delta m}{\rho} \quad [2.3]$$

$$D = \frac{E_{lost,cycle}}{2\pi E_{stored,oscillator}} \quad [2.4]$$

Here, the crystal parameter (C_f) values are known and fixed; F_0 is the fundamental frequency (= 5 MHz), n is the overtone number (=3), Δm is the change in mass per unit area, ρ_q is the density of quartz (=2.648 g/cm^3), A is the crystal area (=1.54 cm^2), and μ_q is the shear modulus of quartz (=2.947 x 10^{11} g.cm^{-1}.s^{-2}), respectively.[39–41] Assuming a homogenous film, the Sauerbrey mass difference Δm can then be converted to a Sauerbrey thickness increment Δd (Equation 2.3) using the added-mass density ρ. The dissipation D (Eq. 2.4) is a measure of the dimensionless ratio of energy lost in an oscillation cycle $E_{lost,cycle}$, to the energy stored in the oscillator, $E_{stored,oscillator}$.[36,37] An increase in ΔD indicates an increased dissipation of the film, meaning that it is less rigid, thicker, or both. A decrease in ΔF (i.e., more negative ΔF) indicates that more mass is adsorbed.

The most accurate QCM-D measurements are obtained as the differences in mass produced upon adding solvent to a dried crystal that is either bare or has an adsorbed brush. We therefore obtain the mass of the adsorbed brush by ellipsometry and use QCM-D only to obtain changes in brush mass due to solvation of the brush. In Appendix 2.a, we show the importance of correcting QCM-D data obtained with a polymer brush by subtracting from these data the results obtained for a bare, polymer-free crystal. This subtraction removes the effect of the inertia and viscosity of the overlying solvent, which varies with salt concentration. Without this subtraction, salt-induced changes in the overlying solvent can be incorrectly attributed to the effect of salt on the behavior of the polymer brush, and this leads to huge errors for thin brush layers, as we show in Appendix 2.a.

To obtain our results, we assume an additive relationship between the effects of the polymer brush $\Delta F_{Polymer}$, the solvent swelling the brush $\Delta F_{Swelling}$, and the overlying solvent $\Delta F_{Solvent}$, described in detail by Chu et al.[21] The effect of adding a polymer layer and solvent to a bare crystal surface would give $\Delta F_{Total} = \Delta F_{Polymer} + \Delta F_{Solvent} + \Delta F_{Swelling}$. However, the most reliable measurement is the change in frequency upon adding solvent to a dry specimen, either a bare dry crystal, or a polymer-coated dry crystal. For the latter, the frequency change $\Delta F(polymer\ coated) = \Delta F_{Solvent} + \Delta F_{Swelling}$ is obtained by measuring the change in frequency that occurs when a dry polymer-coated crystal is exposed to solvent, while $\Delta F(bare\ crystal) = \Delta F_{Solvent}$ is the change in frequency when solvent is added to the bare crystal. Thus, the difference in these two measured quantities $\Delta F(polymer\ coated) - \Delta F(bare\ crystal) = \Delta F_{Swelling}$ is the frequency change due to solvent swelling the brush, where "solvent" here includes any dissolved salt. This $\Delta F_{Swelling}$ was then converted to a Sauerbrey mass increment using Equation 2, and then to a finite thickening distance $\Delta d_{Swelling}$, and the wet brush height $d_{wet\ brush}$ is found by adding this thickening $\Delta d_{Swelling}$ to the dry brush height $d_{brush,dry}$ (found from VASE) for a given brush grafting density, and this $d_{brush,wet} = \Delta d_{Swelling} + d_{brush,dry}$ is equivalent to the wet brush height (H) data plotted in all subsequent figures.

To find the % Swelling as described by Sadman et al.[27], the wet brush thickness was compared to that of the dry brush (found from VASE) as shown in Equation 2.5. To find the change in dissipation response due to swelling $\Delta D_{Swelling}$, the dissipation was calculated according to the same additive relationship used to calculate the change in frequency due to swelling, where for dissipation, $\Delta D_{Swelling} = \Delta D(polymer\ coated) - \Delta D(bare\ crystal)$, as given in Eq. 2.6. Again, the first term on the right-hand side of Equation 2.6 is calculated from the change in

dissipation (3rd harmonic) upon solvating the dried polymer on the chip, while the second term is from solvating the bare chip.

$$\% \text{ Swelling} = \frac{\Delta d_{Swelling}}{d_{\text{dry brush}}} x\ 100 \quad [2.5]$$

$$\Delta D_{Swelling} = \Delta D(polymer\ coated) - \Delta D(bare\ crystal) \quad [2.6]$$

Following every experiment, each crystal was cleaned with TL-1 solution and O_2-plasma treatment as described earlier. All measurements were repeated three times and the averages of each value are presented in what follows; error bars are comparable to the size of the symbols used.

2.iv Results

2.iv.a Variable Angle Spectroscopic Ellipsometry (VASE)

The VASE results for the dry PAA brush at various grafting densities σ are given in Table 1. To calculate the grafting density σ in chains/nm^2, the following formula was used,[42] where $d_{brush,dry}$ is the dry thickness in nm determined by VASE, ρ is the bulk density of PAA (=1.08 x 10^{-21} g/nm^3), N_A is Avogadro's number, and M_n is the number average molecular weight of PAA:

$$\sigma = \frac{d_{brush,dry}\rho N_A}{M_n} \quad [2.7]$$

It should be noted that σ~1 is considered to be highly grafted, and σ ~0.3 is considered to be a "moderate" grafting density in the literature.[43] While our shortest chains achieve a grafting density σ>2 (chains/nm^2), which is considered to be extremely highly grafted, a similar grafting density has been achieved in the past in a combination grafted-to/grafted-on fabrication method[42] for polymer chains three times as long as ours. We note that the brushes in our study are fabricated as self-assembled monolayers (SAMs), which are typically end-functionalized oligomers that self-assemble onto their substrate at high grafting densities to form a uniform, highly elongated, dense

monolayer. Values of grafting densities σ exceeding 3 chains/nm^2 for oligomers are typical for SAMs,[44] and we note that at these extremely high grafting densities the polymer chains are most likely already highly elongated even while dry due to steric repulsion, leaving them little room to swell. Depending on dilution during preparation, the short-chain PAA-SH solutions yielded very dense, dense, moderately dense, and low-density brushes with grafting densities up to 20 times lower than that achieved using the original 4 mM solution. The medium molecular weight brush yielded a moderately dense brush. The long-chain PAA-SH solution yielded a moderately dense brush. The brush densities are summarized in Table 1. Although we define density here based on the magnitude of the surface coverage σ, the response of the brush to solvent also depends on its molecular weight. For example, a long-chain brush with a "moderate" grafting density as defined above may be more resistant to stretching out fully in solvent than is a shorter brush at the same grafting density.

Table 2.i- P-AA brush thicknesses *d* and grafting densities, σ for the chain lengths studied here. ND indicates that the dry thickness is not detectable by VASE

Polymer MW (Mn)	PAA Brush Density	Dry Thickness, *d* (nm)	Grafting Density, σ (chains/nm^2)
2 kDa	Very High	6.60 ± 0.10 nm	2.15
	Very High	4.49± 0.21 nm	1.46
	High	3.21 ± 0.61 nm	1.04
	Moderate	2.66 ± 0.13 nm	0.87
	Moderate	0.923 ± 0.12 nm	0.30
	Low	0.369 ± 0.59 nm	0.12
14 kDa	Moderate	8.17 ± 0.92 nm	0.38
39 kDa	Moderate	27.0 ± 2.04 nm	0.45
None (Ethanol/ 2-Mercaptoethanol 1:10)	-	ND	-
None (Bare Au)	-	ND	-

2.iv.b Quartz Crystal Microbalance with Dissipation (QCM-D) – Solvent-Induced Changes in Swelling and Dissipation

At pH 9 (Figure 2.i(A-C), triangles), the brush should be virtually fully ionized, and we see that at each surface coverage, the brush swells/becomes more dissipative with increased salt concentration at low ionic strength, indicating the uptake of salt and water, and then de-swells/becomes more rigid as the ionic strength increases further as evidenced by the %Swelling and $\Delta D_{Swelling}$. (We note that the changes in %Swelling and $\Delta D_{swelling}$ are insignificant when the salt concentration is increased from zero to the lowest non-zero salt concentration of 0.1 mM for

all work shown here.) A similar maximum was seen for PAA brushes by others in the vicinity of 10 mM,[1,21,45] corresponding to the end of the low-salt "osmotic brush" regime.[1,2,46,47] We observe subsequent de-swelling as the salt concentration increases into the "salted brush" regime, apparently due to charge screening,[45,48] as expected. This trend is seen at all grafting densities investigated. It can be seen from %Swelling that at moderate grafting densities (σ=0.87 and σ=1.04 chains/nm^2) (Figure 2.i(A-B), triangles), that less dense brushes are able to take in more water at low salt concentrations than the highly grafted brush (σ=2.15 chains/nm^2) ((Figure 2.i(C), triangles), but expel this water once electrostatics are screened by counterions at high salt concentration.

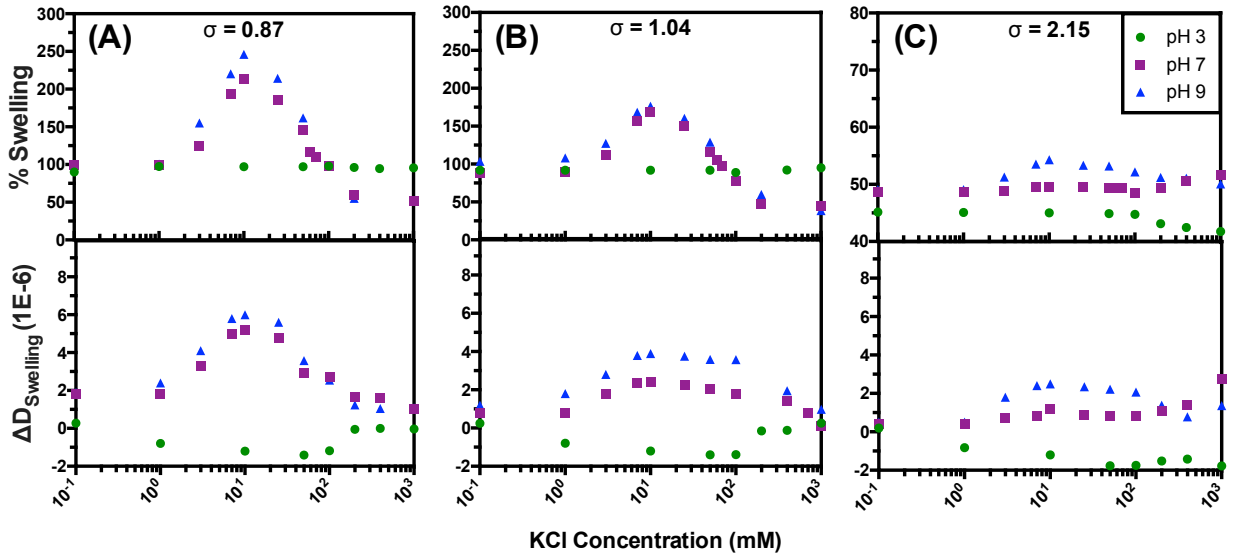

Figure 2.i (A-C)- Dependence of %Swelling and ΔDissipation$_{Swelling}$ on concentration of KCl at various values of pH for short-chain (M_n= 2,000 g/mol) PAA brush grafted to a gold crystal at various grafting densities, σ (chains/nm^2): (A) σ = 0.87, (B) σ = 1.04, & (C) σ = 2.15. Note: due to the logarithmic axes, in both this and subsequent figures the values of %Swelling and ΔDissipation$_{Swelling}$ at 10^{-1} mM represent the value at 0 mM salt for pH 3 (green circles). For pH 7 (purple squares) & pH 9 (blue triangles), the values at 10^{-1} mM are indistinguishable from the values at 0 mM salt.

The swelling is greater for the less dense brushes, evidently because there is more room for water, than at higher grafting densities. In a highly grafted brush (σ=2.15 chains/nm^2) (Figure

2.i(C), triangles) the %Swelling maximizes at 51% relative to a dry brush at low ionic strength. We note that at extremely high grafting densities and high salt concentrations, a polymer brush is expected to be dense enough that individual chains are almost fully elongated, to such an extent that the polyelectrolyte brush is only slightly solvated, and counterions should condense onto the polymer, making it less charged.[1,2,47] The attainment of high density and nearly full elongation is supported by VASE measurements, which yield a dry brush thickness of 6.6 nm at the highest grafting density (σ = 2.15 chains/nm^2), and the fully extended chain length is estimated to be roughly 7-9 nm,[49] where the upper and lower bounds of this range are, respectively, based on number and weight average molecular weights of the PAA used (M_w/M_n=1.3). Starting with a dry-brush thickness of 6 nm, the 51% peak in swelling exhibited by the highest grafting density (σ=2.15 chains/nm^2) corresponds to a thickness of ~10 nm. This shows that the brush is virtually fully extended at a salt concentration of 10 mM, and that the longer chains —within the polydispersity of the starting material— contribute to an effective thickness that is somewhat greater than that predicted by the average molecular weight.

At pH 7 (Figure 2.i(A-C), squares) the trend of increased swelling/increased dissipation at low salt concentration followed by decreased swelling/increased rigidity with increasing ionic strength is similar to that at pH 9, although to a somewhat lesser extent, as expected for the decreased ionization at pH 7, with one exception at the highest grafting density (σ=2.15 chains/nm^2). We note that this swelling at low ionic strengths again corresponds to the "osmotic brush" regime,[1,2,46,47] and that subsequent de-swelling as the salt concentration increases into the "salted brush" regime is presumably due to charge screening.[48] At lower grafting densities (σ=0.87 and σ=1.04 chains/nm^2) (Figure 2.i(A-B), squares) we again see a greater magnitude of swelling

than at the highest grafting density, presumably due to more space available.

At the highest grafting density (Figure 2.i(C), squares), we see that while the %Swelling at pH 7 does initially increase somewhat at low salt concentration and then decrease as expected, it eventually increases again at the highest ionic strengths. Correspondingly, the $\Delta D_{Swelling}$ at pH 7 (Figure 2.i(C), squares) continuously increases, indicating that the brush becomes more dissipative. It has been shown by Yu and colleagues that high grafting densities lead to the extension of the osmotic brush regime to higher ionic strengths as a result of the osmotic pressure of associated counterions.[50] We can hypothesize that this additional swelling at high ionic strengths, relative to pH 9, is due to incomplete ionization of the brush, but why this should lead to more swelling than at pH 9 at high salt concentration is mysterious. Looking closely at Fig. 8 of Wu et al., a similar increase in brush height at the highest salt concentration near 1 M can be seen for their short PAA brushes at pH 10 for the two lower grafting densities.[1] Thus, both our brush height and that of Wu et al. show a maximum, then deswelling, and finally again an increase in height with increasing salt. However, this final increase in height at ionic strength near 1 M occurs only for our densest brush (σ = 2.15 chains/nm^2) at pH 7, whereas it occurs only in their two lower-density brushes (σ = 0.130 and 0.404 chains/nm^2) at a pH of 10 (also well above the pKa), but is not evident in their highest density brush (σ = 0.863), and so the significance of upturn in height at high salt concentration in a few cases is not clear. We remark here that Wu et al. report wet brush thicknesses for their short (M_n= 4.10 kDa, M_w/M_n=1.29) brushes that are as high as 30 nm, which is higher than the fully extended length of PAA chains of this molecular weight, and so the actual molecular weight of their brush must be somewhat higher than they estimated. Adamcyzk et al.[49] estimated the contour length of PAA of molecular weight 12 kDa to be 40 nm, from which we can estimate that the brushes of Wu et al. must be around 9 kDa, at least. (This

difference from the reported value of Wu et al. is perhaps not too surprising, since the molecular weight of chemically grown PAA cannot be determined directly.)

Figure 2.ii shows the %Swelling and $\Delta D_{Swelling}$ for two additional grafting densities, σ=0.12 chains/nm^2 (diamonds) and σ=0.30 chains/nm^2 (crosses) at pH 7 only. These brushes swell considerably more than the denser brushes, as expected for their lower density, leaving them more room to swell, and become less rigid, as expected, since these brushes are more hydrated.

At pH 3, below the pKa (Figure 2.i(A-C), circles), our brush can be considered charge neutral and fully protonated. Accordingly, when KCl is added, the %Swelling decreases, indicating the loss of water which is presumably osmotically pulled out of the brush by the external solution, which has a higher KCl concentration than the brush because of excluded volume effects. (The decrease in swelling can be clearly seen in Fig. 2.i(C) but is too small to be evident in Fig. 2.i(A-B).) $\Delta D_{Swelling}$ supports this interpretation; as KCl is increased from zero concentration, the brush becomes less dissipative with increasing ionic strength, becoming negative, which implies that it is below the value for the hydrated blank crystal, indicating that the brush becomes more rigid due to dehydration as salt concentration increases.

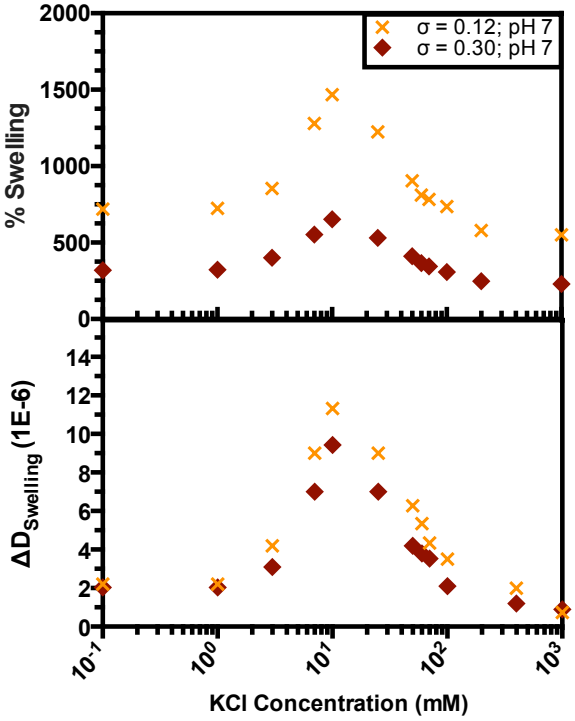

Figure 2.ii- Dependence of %Swelling and $\Delta D_{Swelling}$ on concentration of KCl at pH 7 for short-chain (M_n= 2,000 g/mol) PAA brush grafted to a gold crystal at low grafting densities, σ (chains/nm^2) σ = 0.12 & σ = 0.30.

The grafting density σ of the long-chain (M_n=39,000 g/mol) PAA brush deposited using the method described earlier was determined to be σ = 0.45 chains/nm^2 by VASE. While this grafting density might be considered "moderate" since it corresponds to fewer chains per unit area than the "moderately" dense short-chain brushes investigated (σ = 0.30 chains/nm^2; see Table 1), it can be considered very dense for a chain of this length (M_n=39 kDa). Thus, we compare in Figure 2.iii (A) %Swelling and (B) $\Delta D_{Swelling}$ for the long-chain brush of grafting density σ = 0.45 chains/nm^2 with the results for a short-chain brush of grafting density σ = 2.15 chains/nm^2 at pH 9, pH 7, and pH 3 (A-C, respectively). It can be seen from %Swelling (Figure 3(A-C)) that at every pH in the absence of salt (pure water), the long brush (squares) and the short brush (circles) swell to a similar extent (i.e., to within 10%), which is initially surprising, and is probably related to the dense grafting of both the long and short brushes. As we will discuss below, the swelling observed

in our short and long-chain brushes appears to be consistent with the scaling theory for the dependence of brush thickness on chain length at fixed grafting density.

At pH 9 (Figure 2.iii(A)), the brushes should be considered virtually fully ionized. As expected, in the low-salt regime, up to 10 mM KCl, the brush swells tremendously as exhibited by %Swelling (Figure 2.iii (A), top). At 50 mM, in the salted-brush regime, the %Swelling curves of the long and short chains intersect. The curves of $\Delta D_{Swelling}$ (Figure 3(A), bottom) intersect at a similar salt concentration, but are greater at lower ionic strengths in the long-chain brush than in the short-chain one, indicating more dissipation than for the nearly fully extended short chains. The decrease in $\Delta D_{Swelling}$ (Figure 2.iii (A), bottom, squares) indicates that the brush becomes more rigid as ionic strength increases. At pH 7 (Figure 2.iii (B)), this trend is seen again but to a slightly lesser extent as expected due to the lower ionization. Again, from the %Swelling, the long brush is seen to swell greatly at lower ionic strengths, then de-swell as the concentration of KCl increases, while the rise and fall of $\Delta D_{Swelling}$ also suggests that the brush takes up water at low ionic strengths and loses it due to counterion condensation as salt concentration increases. At pH 3, as evidenced by %Swelling (Figure 2.iii (C), top), both the long-chain and short-chain brushes de-swell slightly with increased KCl concentration, as water is driven out due to annealing from increased salt. Figure 2.iii (C), bottom, shows very little response overall in $\Delta D_{Swelling}$ for both brush lengths, suggesting that the loss of water in the brush has little effect on dissipation.

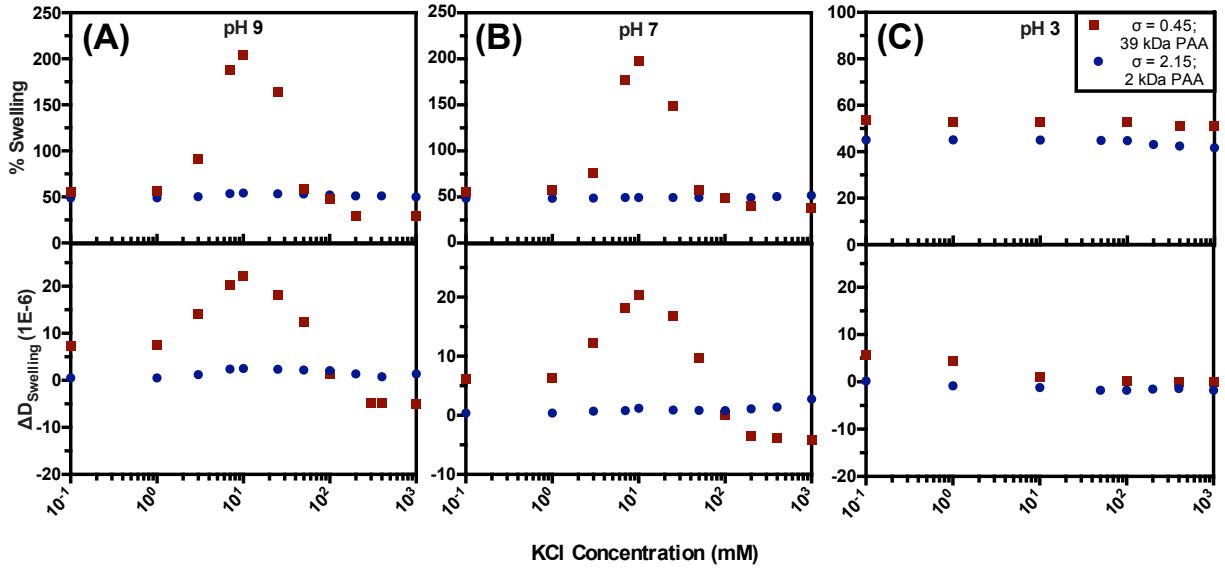

Figure 2.iii(A-C) Dependence of %Swelling and $\Delta Dissipation_{Swelling}$ of short-chain (M_n= 2,000 g/mol) at its highest grafting density and long-chain PAA (M_n= 39,000 g/mol) to KCl concentration at (A) pH 9, (B) pH 7, and (C) pH 3.

2.iv.c Comparison to Theory and Previous Work

While PAA is a "weakly" dissociating polymer, it is likely that it is highly ionized at pH 7 & 9, well above its pKa (~5). The similarity in the swelling and deswelling behavior seen at pH 7 and pH 9 in Figs. 2 and 4 also suggest that the polymer is sufficiently charged at pH 7 that the brush is essentially a "strong polyelectrolyte" at both these pH values. Oddly enough, however, Wu et al.[1] found similar salt dependence of PAA brush height, with a maximum at salt concentration ~ 0.1 M, for pH = 4, 5.8, and 10, which spans from below to above the pKa ~ 5, implying either that there is little change in the charge of the brush over this large range of pH, which seems unlikely, or that there is little effect of this change on the salt dependence of brush height. We have found that once pH is reduced to 3, the brush clearly loses its charge, as shown by the "neutral brush" behavior we observe in Figs. 2.ii and 2iv. The mean-field scaling theory of Israëls et al.[3] in the low-salt osmotic brush (OB) regime, predicts that the brush height (H)

follows the dependence given in Equation 2.8 where the chain length is measured in number of monomers (N), and α is the average fraction of charged monomers on the chain.

$$H \sim N\alpha^{1/2} \quad [2.8]$$

For a fully ionized PAA chain, for which α= 1, H is thus predicted to be independent of grafting density σ and salt concentration. In the salted brush (SB) regime, the theory of Israëls et al. predicts that the brush height scales according to the following Equation 2.9.

$$H \sim N\sigma^{\frac{1}{3}}C_s^{-\frac{1}{3}}\alpha^{2/3} \quad [2.9]$$

Israëls et al.[3] predict that when the brush is fully ionized ($\alpha = 1$), in both the OB regime (see Equation 2.8) and the SB regime (see Equation 2.9), the brush height should depend linearly on chain length, N, if grafting density, pH, and salt concentration are held fixed. Figure 2.iv (A-B) shows that this linear dependence is indeed obtained for our PAA brushes of chain length 2 kDa (σ=0.30 chains/nm^2), 14 KDa (σ=0.38 chains/nm^2), and 39 kDa (σ=0.45 chains/nm^2), in both the OB (Figure 2.iv (A)) and SB regimes (Figure 2.iv (B)) when grafting density is kept as constant as possible with our data sets.

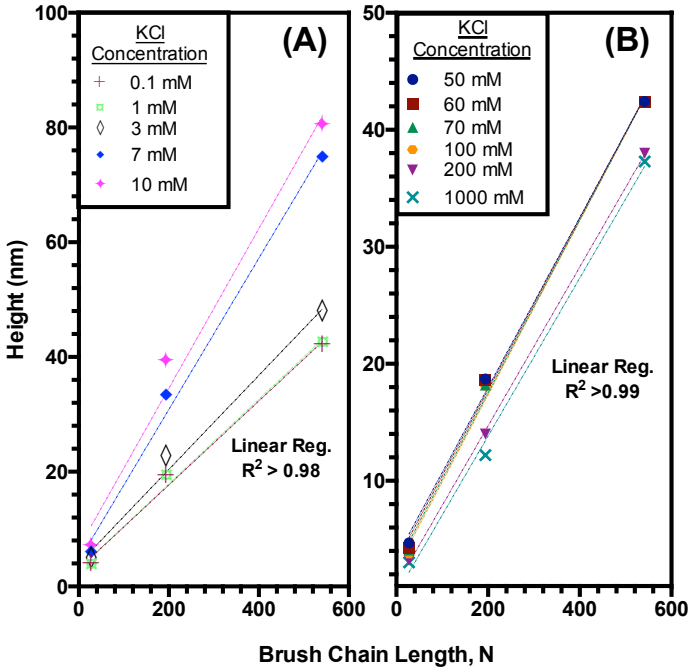

Figure 2.iv (A-B). Brush height vs. PAA chain length, N at various KCl concentrations in the (A) OB regime and (B) SB regime, both at pH 7. The grafting densities are 2 kDa (σ=0.30 chains/nm^2), 14 KDa (σ=0.38 chains/nm^2), and 39 kDa (σ=0.45 chains/nm^2).

As shown in Equations 2.8 and 2.9, Israëls et al.[3] predict that for a strong, fully charged, polyelectrolyte (i.e., α= 1), the brush height should be independent of salt concentration in the OB regime and should scale to the -1/3 power in the SB regime. In the weak polyelectrolyte regime, however, where $\alpha \ll 1$, Zhulina et al. predicted that in the OB regime the charge density α on the chains should vary with grafting density and salt concentration as

$$\alpha \sim [\sigma^{-1}([H^+] + C_s)]^{2/3} \qquad [10]$$

where the sum of the external proton concentration [H+] and the external salt concentration (C_s) is the total ionic strength of the solution. Combining this with Equation 8 yields the scaling for the OB regime for weak polyelectrolytes:

$$H \sim N\sigma^{-\frac{1}{3}}([H^+] + C_s)^{1/3} \qquad [11]$$

Figure 2.v shows our measured PAA brush height vs. salt concentration for the short-chain (2 kDa) PAA at pH 7. It shows an approximate power law with respect to salt concentration, with +0.28-0.38 exponent in the low-salt (presumably OB) regime spanning 1-10 mM salt concentration at every grafting density except at σ >1 chain/ nm^2, where the brush is nearly fully extended. While this 0.28-0.38 power-law scaling disagrees with the theoretical prediction for a strong polyelectrolyte in the osmotic brush (OB) regime, it agrees well with the theoretical prediction of Zhulina et al.,[2] given by Equation 11, for weakly dissociating polyelectrolytes, and with what has been observed by others for other weakly dissociating systems at low salt concentration.[1,25,51,52] As noted earlier, at the lowest salt concentration investigated (0.1 mM), the swelling at all grafting densities is similar to that seen in pure water. In the high salt SB region, the power law exponent is around -0.30, very close to the value of -1/3 predicted in both strong and weak polyelectrolyte theories in the SB regime. At the highest salt concentration (1000 mM), there is an apparent leveling off of the height of the brushes, which agrees with what has been observed experimentally by others,[1,21,45] and can be attributed to a transition to the "neutral brush" (NB) regime where polymer charge is nearly completely screened out. The long-chain brush (39 kDa), at the single grafting density (σ = 0.45 chains/nm^2) studied, shows a similar dependence on salt concentration as the short-chain brush, with a scaling exponent of 0.31 in the OB regime and -0.30 in the SB regime (data not shown).

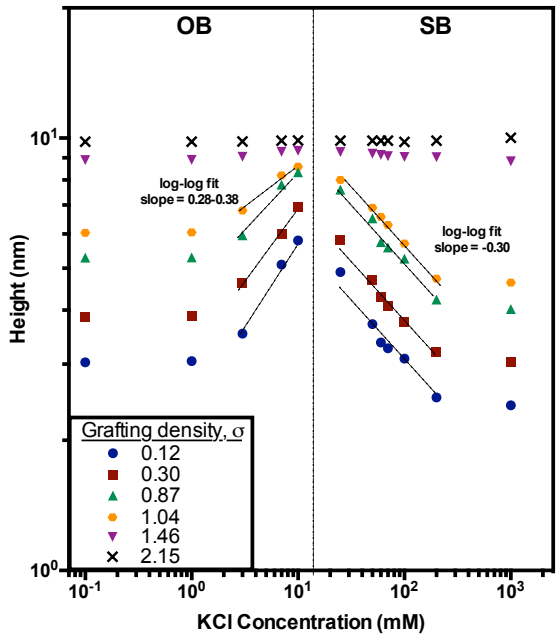

Figure 2.v. Short-chain (Mn=2 kDa) PAA brush height vs. KCl Concentration (mM) at various grafting densities σ (chains/nm^2) in the OB regime and SB regime at pH 7.

Figure 2.vi(A-B) shows our measured PAA brush height vs. grafting density for the short-chain PAA (2 kDa) at pH 7. In the SB regime, Figure 6(B) shows that the brush follows the predicted dependence on σ to the power +1/3 of Israëls et al., until σ >1 chains/nm^2, where the exponent shifts to around 0.21. The +0.33 scaling at the more modest grafting densities also has been predicted by Pincus and colleagues[26] and demonstrated experimentally numerous times.[25,51,52] In the low-salt, OB regime, Figure 2.vi (A) shows that at 10 mM, where maximal swelling is seen, the brush height scales weakly with σ to the 0.18 power, with this exponent shifting to 0.22 at 7 mM KCl, and to 0.31 at 0.1-3 mM KCl. While this disagrees with the theoretical prediction that the height should be either insensitive to σ in the OB regime for strongly ionized brushes (Equation 8), or should actually decrease with σ for weakly ionized brushes (Equation 11), our observation does agree with the +0.33 power-law scaling observed experimentally in the OB regime by Wu et al.[1] for a short PAA brush at pH 5.8 (slightly above the pKa). At this pH, close to the pKa (~ 5), the scaling of height with grafting density σ might be

expected to follow the prediction of Zhulina et al.[2] for a weak, only slightly charged polyelectrolyte, which yields a -1/3 power law dependence on σ in the OB regime, but this is clearly not observed. Possibly, our chains and/or those of Wu et al. are either too highly charged, or too short, for the applicability of the scaling theories, which require that the chains have a charge fraction much less than unity (for weak polyelectrolytes) and the chain elasticity be Gaussian. In particular, our PAA chains (Mn=2 kDa) in Fig. 2.vi (A) have heights ranging from 30% to 100% of maximum chain extension, which lies outside of the range of Gaussian elasticity.

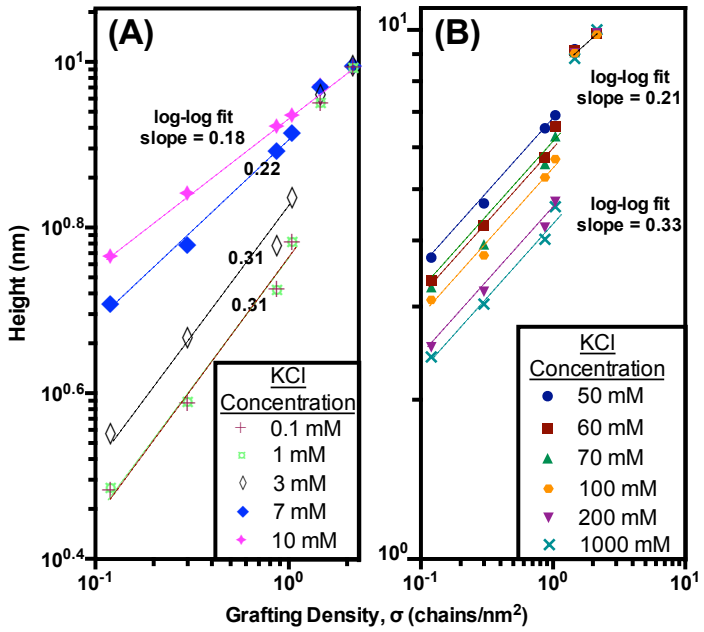

Figure 2.vi(A-B). Short-chain (Mn=2 kDa) PAA brush height vs. grafting density at various KCl concentrations in the (A) OB regime and (B) SB regime, both at pH 7

We also note also that the scaling theories predict that the transition from the OB to the SB regimes should occur at a salt concentration of around $C_s^* \sim \square\square^{1/2}/a$, where is the fraction of charged monomers and a is the monomer radius.[5] This implies that C_s^* should depend on grafting density, but in our work the maximum in brush height remains at nearly the same salt concentration of 10 mM, regardless of grafting density, which varied from 0.12 to 2.15 chains/nm^2. Wu et al.[1]

similarly found for PAA brushes little dependence of C_s^* on grafting density for pH = 4 or 5.8, but did see a roughly linear dependence on C_s at pH = 10, where the polyelectrolyte should be virtually completely charged, and hence act as a strong polyelectrolyte. Consistent with this, Yu et al. in the Tirrell group report that at high grafting density of the strong polyelectrolyte PSS, the osmotic brush regime is extended to as high as 1 M, while at much lower grafting densities (around 0.01 chains/nm^2) the transition from OB to SB regimes occurs at around 0.01 M.[50] Strangely, in the work of Wu et al., the maximum in brush height occurred at $C_s^* \sim 0.10$ M for pH = 4 and 5.8, while we find $C_s^* \sim 0.01$ M for the same polymer (PAA), similar range of PH, and molecular weights that encompass that used by Wu et al.

Thus, while the available scaling theories for weak polyelectrolytes do predict a non-monotonic dependence of brush height on salt concentration, they fail to account for numerous other features observed in our work and that of our predecessors. A more detailed self-consistent field theory of Willott et al.[53] which allows for charge regulation, also shows the non-monotonic dependence of height on salt concentration and finds that the maximum in height is sensitive to the hydrophobic or hydrophilic character of the polymers, as well as its charge. However, this method has not yet considered the effect of grafting density of chain length on brush height, and so cannot at present be compared with experimental results. Szleifer and coworkers derived a theory for the brush thermodynamics based on a free energy functional that includes excluded volume, Poisson-Boltzmann electrostatics, and acid-base equilibrium, all resolved spatially within the brush.[54] This theory provided semi-quantitative agreement with the measurements of brush height vs. salt concentration by Wu et al., but did not address the dependence of brush height on grafting density. The theory predicts that at pH = 10, the brush becomes fully charged, and the maximum in brush height at C_s^*, at the transition from OB to SB, therefore disappears. The brush

height is also predicted to be independent of salt concentration in the OB regime for strong polyelectrolytes by the density functional theory of Jiang and Wu.[55] This prediction disagrees with the experiments of Wu et al., who showed the retention of this maximum even at pH = 10, and of course our experiments also show this maximum at pH = 9. A subsequent Monte Carlo by Szleifer and coworkers[56] predicts such a decrease in brush height at low salt by allowing counterion condensation controlled by a Manning parameter; this helps neutralize the brush when the pH is too high for charge regulation to do so. However, this leaves unexplained why in the surface forces experiments of Tirrell and coworkers[5] the strong polyelectrolyte PSS, the brush height remains constant at low salt concentration. Perhaps the Manning parameter in this case is outside of the range for which counterion condensation becomes strong at low ionic strength.

We can summarize the comparison of our work with those of others and with available theory, and suggest where more work is needed, by posing the following questions:

1. Why do we not see a decrease in brush height with increasing grafting density σ in the OB regime, as predicted by weak-polyelectrolyte theory?
2. Why at high pH does the weak polyelectrolyte PAA still show a maximum in brush height with increasing salt concentration? Is it due to counterion condensation at low salt?
3. Why is the maximum seen in ellipsometry and QCM-D experiments for NaPSS[21] but not in the surface forces results of Tirrell and coworkers[51]?
4. Why does C_s^*, the transition salt concentration from OB to SB regimes, seem usually to be independent of grafting density in weak polyelectrolytes, in disagreement with theory?
5. Over what range of pH values does PAA function as a "weak" polyelectrolyte, for which charge regulation as a function of salt concentration and grafting density is important?

Finally, we note that the study by Wu et al.[1] of a nominally short-chain PAA brush (Mn = 4 kDa), presented brush height data at pH 5.8 (above the pKa) as a %Change in Swelling produced by the presence of salt water over that in pure water, as opposed to the %Swelling reported in our present work. Plotted as %Change in Swelling, Wu et al. observed a power law against grafting density σ with exponent -1/3. Since our data on brush height versus grafting density are qualitatively similar to theirs, we would expect to get a similar scaling law when our data are plotted in this same form, and, indeed, in Appendix 2.B, we show that such a power-law can be fit to our data. However, we show for both our set of data and that of Wu et al., the data are more accurately described as having two regimes, with a weak dependence on σ at small grafting densities σ, and a steep dependence at high σ.

2.v Conclusions and Discussion

Swelling/de-swelling of a weakly dissociating PAA polyelectrolyte brush as a function of ionic strength of KCl between 0.1-1000 mM, at different pH values (3, 7, and 9), chain grafting densities (from 0.45 to 2.15 chains/nm^2), and chain molar masses (from M_n = 2 KDa to 39 KDa), was investigated using QCM-D, the results of which are summarized in Figures 2 & 3. The PAA brush was deposited directly onto a gold QCM-D sensor via self-assembly using thiol-gold interaction. The brushes are thin enough that the Sauerbrey thickness can be extracted from ΔFrequency and expressed as %Swelling relative to the dry brush.

In all highly ionized brushes above the pKa (pH 7 & 9), swelling is seen upon addition of low KCl concentrations with a maximum swelling at 10 mM, in the so-called osmotic brush (OB) regime,[1,2,46,47] followed by de-swelling with increased salt concentration, where the latter is a well-known result of charge screening predicted in the literature for the salted brush (SB) regime.[21,48,57,58] As expected, swelling at low ionic strength is greater in looser, less-dense brushes

(σ = 0.12, 0.30, 0.87, 1.04) than in a very dense brush (σ = 1.46 & 2.15 chains/nm^2). We find maximum swelling for all chain lengths and grafting densities at around 10 mM salt, consistent with the work of Chu et al.,[21] Zhang and Rühe,[58] and Wu et al.,[1] all of whom found maximum swelling at around 10 mM for a strong polyelectrolyte brush of poly(sodium 4-styrenesulfonate) (NaPSS),[21] a "weak" polyelectrolyte brush of poly(methacrylic acid) (PMAA),[58] and a "weak" brush of PAA,[3] respectively. Oddly, in similar work by Wu et al. on PAA brushes, the maximum appeared at 100 mM for pH = 4 and 5.8, and at even higher salt concentrations at pH = 10. An insensitivity to grafting density of the salt concentration at which this apparent transition from OB to SB behavior occurs is not in accord with theory, which predicts a transition at a salt concentration that increases with grafting density.

We find that at pH 7, in the low-salt osmotic brush regime, the brush height scales with a +0.33 power at lower grafting densities with respect to grafting density. This disagrees strongly with the -1/3 power in the OB regime scaling theory of Zhulina et al. for weakly dissociating polyelectrolytes.[2] Noting that since the pKa of PAA is around 5, our brush at pH 7 and 9 is likely strongly ionized and hence effectively a "strong" polyelectrolyte, for which the theory of Zhulina et al. may not be applicable, since it assumes polyelectrolyte charge fractions << 1. For strongly dissociating polyelectrolytes, Israëls et al. predicted that the brush height in the OB regime should be independent of grafting density, which is closer to, but still in disagreement with, our exponent of 0.28-0.38. However, the theory for strongly dissociating polyelectrolytes predicts that brush height should be independent of salt concentration in the OB regime, contrary to our observation of a decrease in brush height with decreasing salt concentration in this regime. It is noteworthy that a decrease in brush height with decreasing salt concentration in the OB regime was observed even for strong polyelectrolytes, including NaPSS, by Chu et al. using ellipsometry and QCM-D.

(However, NaPSS studies in the surface forces apparatus by Balastre et al. a showed salt-independent brush height in the OB regime.) A Monte Carlo of Szleifer and coworkers[56] suggests that this decrease in brush height at low salt concentration for highly charged polyelectrolytes results from counterion condensation controlled by the Manning parameter.

In the SB regime, our results agree with the prediction by Israëls et al.[3] and Pincus[26] that the brush height H should depend on grafting density σ and chain length N as $H \sim N\sigma^{+1/3}$, which is also shown by numerous experiments.[25,51,52] While our findings of the dependencies of brush height and swelling on grafting densities partially disagree with scaling theory in the OB regime, we do find the predicted linear dependence of brush height on chain length N in both the OB and SB regimes.

The discrepancies between experimental results and theory explored here should motivate additional experimental work closer to conditions for which weak polyelectrolyte theory is most applicable, namely long chains, at lower grafting densities, and additional pH values near the pH at which the chain becomes neutral. In addition, computer simulations and self-consistent field theory should also explore a similarly wider range of conditions than has been carried out heretofore.

Note: This chapter in its entirety has been published as a peer-reviewed publication and permission has been granted from all authors as well as the publisher.

2.vi References

1 T. Wu, P. Gong, I. Szleifer, P. Vlček, V. Šubr and J. Genzer, *Macromolecules,* **2007**, 40, 8756–8764.

2 E. B. Zhulina, T. M. Birshtein and O. V. Borisov, *Macromolecules*, **1995**, 28, 1491–1499.

3 R. Israels, J. F. A. M. Leermakers, J. Fleer and E. B. Zhulina, *Macromolecules*, **1994**, 27, 3249–3261.

4 D. V. Andreeva and D. G. Shchukin, *Mater. Today*, **2008**, 11, 24–30.

5 N. Saleh, T. Sarbu, K. Sirk, G. V Lowry, K. Matyjaszewski and R. D. Tilton, *Langmuir*, **2005**, 21, 9873–9878.
6 N. Su and Na, *Polymers (Basel).*, **2015**, 7, 1599–1616.
7 G. Liu, M. Cai, X. Wang, F. Zhou and W. Liu, *ACS Appl. Mater. Interfaces,* **2014**, 6, 11625–11632.
8 S. P. Adiga and D. W. Brenner, *J. Funct. Biomater*., **2012**, 3, 239–56.
9 M. Motornov, K. Tam, M. Pita, I. Tokarev, E. Katz and S. Minko, *IOP Publ. Nanotechnol. Nanotechnol.,* **2009**, 20, 434006–434016.
10 J.-Y. Lin, C.-Y. Lin, J.-P. Hsu and S. Tseng, *Anal. Chem***., 2016**, 88, 1176–1187.
11 S. Das, M. Banik, G. Chen, S. Sinha and R. Mukherjee, *Soft Matter*, **2015**, 11, 8550–8583.
12 J. Klein, E. Kumacheva, D. Mahalu, D. Perahia and L. J. Fetters, *Nature*, **1994**, 370, 634–636.
13 A. Halperin and D. E. Leckband, *Comptes Rendus l'Académie des Sci. - Ser. IV - Phys.,* **2000**, 1, 1171–1178.
14 M. Krishnamoorthy, S. Hakobyan, M. Ramstedt and J. E. Gautrot, *Chem. Rev.,* **2014,** 114, 10976–11026.
15 O. Azzaroni, S. Moya, T. Farhan, A. A. Brown and W. T. S. Huck, *Macromolecules*, **2005,** 38, 10192–10199.
16 M. Chen, W. H. Briscoe, S. P. Armes, H. Cohen and J. Klein, *Eur. Polym. J*., **2011**, 47, 511–523.
17 A. Kusumo, L. Bombalski, Q. Lin, K. Matyjaszewski, J. W. Schneider and R. D. Tilton, *Langmuir,* **2007**, 23, 4448–4454.
18 G. Sudre, D. Hourdet, C. Creton, F. Cousin and Y. Tran, *Macromol. Chem. Phys.*, **2013**, 214, 2882–2890.
19 M. P. Weir and A. J. Parnell, *Polymers (Basel*)., **2011**, 3, 2107–2132.
20 E. S. Dehghani, V. V. Naik, J. Mandal, N. D. Spencer and E. M. Benetti, *Macromolecules,* **2017**, 50, 2495–2503.
21 X. Chu, J. Yang, G. Liu and J. Zhao, *Soft Matter*, **2014**, 10, 5568–5578.
22 Z. Zhang, M. Moxey, A. Alswieleh, A. J. Morse, A. L. Lewis, M. Geoghegan and G. J. Leggett, *Langmuir*, **2016**, 32, 5048–5057.
23 H. Sakata, M. Kobayashi, H. Otsuka and A. Takahara, *Polym. J.,* **2005**, 37, 767–775.
24 V. Mazzini, G. Liu and V. S. J. Craig, *J. Chem. Phys*., **2018**, 148, 222805.
25 F. Li, M. Balastre, P. Schorr, J.-F. Argillier, J. Yang, J. W. Mays and M. Tirrell, *Langmuir,* **2006**, 22, 4084–4091.
26 P. Pincus, *Macromolecules***, 1991**, 24, 2912–2919.
27 K. Sadman, C. G. Wiener, R. A. Weiss, C. C. White, K. R. Shull and B. D. Vogt, *Anal. Chem*., **2018,** 90, 4079−4088.
28 G. C. Denolf, L. F. Sturdy and K. R. Shull, *Langmuir,* **2014,** 30, 9731−9740.
29 J. T. O'Neal, E. Y. Dai, Y. Zhang, K. B. Clark, K. G. Wilcox, I. M. George, N. E. Ramasamy, D. Enriquez, P. Batys, M. Sammalkorpi and J. L. Lutkenhaus, *Langmuir*, **2018**, 34, 999–1009.
30 R. Kou, J. Zhang, T. Wang and G. Liu, *Langmuir*, **2015**, 31, 10461–10468.
31 P. Zhuang, A. Dirani, K. Glinel and A. M. Jonas, *Langmuir***, 2016**, 32, 3433–3444.
32 B. Almeida and A. Shukla*, J Biomed Mater Res Part A,* **2017**, 105A, 464–474.

33 E. Bittrich, K. B. Rodenhausen, K.-J. Eichhorn, T. Hofmann, M. Schubert, M. Stamm and P. Uhlmann, *Biointerphases*, **2010**, 5, 159–167.
34 H. G. Tompkins, *A User's Guide to Ellipsometry., Elsevier Science*, **1992.**
35 C. M. Herzinger, H. Yao, P. G. Snyder, F. G. Celii, Y. -C. Kao, B. Johs and J. A. Woollam, *J. Appl. Phys*., **1995,** 77, 4677–4687.
36 M. C. Dixon, *J. Biomol. Tech*., **2008**, 19, 151–8.
37 G. Liu and G. Zhang, in *QCM-D Studies on Polymer Behavior at Interfaces, Springer Science & Business Media***, 2013**, pp. 1–8.
38 A. Alassi, M. Benammar and D. Brett, *Sensors*, **2017**, 17, 2799.
39 V. M. Mecea, *Anal. Lett*., **2005**, 38, 753–767.
40 X. Zhang, S. S. Chu, J. R. Ho and C. P. Grigoropoulos, *Appl. Phys. A Mater. Sci. Process*., **1997**, 64, 545–552.
41 G. Sauerbrey, *Zeitschrift für Phys*., **1959**, 155, 206–222.
42 T. Zhou, H. Qi, L. Han, D. Barbash and C. Y. Li, *Nat. Commun*., **2016,** 7, 11119.
43 L. C. H. Moh, M. D. Losego and P. V. Braun, *Langmuir,* **2011**, 27, 3698–3702.
44 J. Genzer, K. Efimenko and D. A.Fischer, *Langmuir*, **2002,** 18, 9307–9311.
45 E. P. K. Currie, A. B. Sieval, G. J. Fleer and M. A. Cohen Stuart, *Langmuir*, **2000**, 16, 8324–8333.
46 M. Geoghegan, *Polymer (Guildf*)., **2017,** 112, 414–417.
47 J. D. Willott, T. J. Murdoch, F. A. M. Leermakers and W. M. de Vos, *Macromolecules,* **2018**, 51, 1198–1206.
48 J. A. V. Butler, B. E. Conway and D. W. F. James, *Trans. Faraday Soc.,* **1954**, 50, 612.
49 Z. Adamczyk, A. Bratek, B. Jachimska, T. Jasiński and P. Warszyński*, J. Phys. Chem. B,* **2006**, 110, 22426–22435.
50 J. Yu, J. Mao, G. Yuan, S. Satija, W. Chen and M. Tirrell, *Polymer (Guildf).,* **2016,** 98, 448–453.
51 M. Balastre, F. Li, P. Schorr, J. Yang, J. W. Mays and M. V. Tirrell, *Macromolecules,* **2002**, 35, 9480–9486.
52 T. Jiang, Z. Li and J. Wu, *Macromolecules,* **2007,** 40, 334–343.
53 J. D. Willott, B. A. Humphreys, G. B. Webber, E. J. Wanless and W. M. de Vos, *Langmuir,* **2019,** 35, 2709–2718.
54 R. J. Nap, M. Tagliazucchi and I. Szleifer, *J. Chem. Phys.*, **2014,** 140, 024910.
55 T. Jiang and J. Wu, *J. Phys. Chem. B*, **2008,** 112, 7713–7720.
56 O. J. Hehmeyer, G. Arya, A. Z. Panagiotopoulos and I. Szleifer, *J. Chem. Phys.*, **2007**, 126, 244902.
57 A. L. P. Fernandes, R. R. Martins, C. G. Da, T. Neto, M. R. Pereira and J. L. C. Fonseca, *J Appl Polym Sci,* **2003**, 89, 191–196.
58 H. Zhang and J. Rühe, *Macromolecules*, **2005**, 38, 4855–4860.
59 K. K. Kanazawa and J. G. Gordon, *Anal. Chem*., **1985**, 57, 1770–1771.

Appendix 2.a

2.A.i Quartz Crystal Microbalance with Dissipation (QCM-D) – Effect of Overlying Solvent

Appendix Figure 2.A(A) from our work shows that the change in dissipation at the third overtone (n=3, F_0 =5 MHz), $\Delta D(bare\ crystal)$, with salt concentration *for a blank crystal*, with no added brush, is almost identical to the results of Zhang et al., for a poly(zwitterionic) brush composed of poly(2-(methacryloyloxy)ethyl phophorylcholine), or PMPC, in the presence of $CaCl_2$ and LiCl.[22] Furthermore, $\Delta D(bare\ crystal)$ data are plotted on a linear scale (Figure 2.A (B)) instead of the semi-log axis published in their work,[22] a linear dependence on salt concentration is evident, and shows that this extends up to much higher salt concentration than covered by Zhang et al. The effect of salt on $\Delta D(polymer\ coated)$ in the presence of a PAA brush (with M_n=2,000 g/mol, at pH = 7 from our studies) at the highest grafting density (σ=2.15 chains/nm^2) is also shown in Figure 2.A (B) as filled symbols. It is evident that the QCM-D response in the presence of the PAA brush closely resembles that obtained for a poly(zwitterionic) brush by Zhang et al. in the case of $CaCl_2$, both of which are similar to the response of a bare substrate. It is thus apparent that much of the QCM-D response is merely due to the change in flow medium, and, moreover, is similar to the trend in solution mass density, as shown in Figure 2.A(C), as well as solution viscosity in accordance with concentration and the Hofmeister series as previously predicted theoretically by Kanazawa and Gordon.[59] The densities of all of the salt solutions tested were confirmed gravimetrically and are given in Figure 2.A (C), which shows the same trend with salt type and concentration as shown by the QCM-D response in Figure 2.A (B). Thus, $\Delta D(polymer\ coated)$ is not much different from $\Delta D(bare\ crystal)$, and reflects the influence of the density and viscosity of the salt solution more than it does the presence of the brush, at least for $CaCl_2$ and LiCl.

Figure 2.A (B) shows a greater difference between the response of the brush and a blank crystal for KCl and NaCl than for $CaCl_2$. Figure 2.a (D) enlarges these data for the influence of KCl for the short-chain PAA brush (M_n= 2,000 Da) and adds similar data at other grafting densities at neutral pH 7. From this plot, it is evident that the influence of KCl salt solution on the QCM-D response on the PAA brush is sufficiently distinct from its influence on the bare crystal to allow the influence of the PAA brush to be determined clearly by subtraction, i.e., by taking $\Delta D(polymer\ coated) - \Delta D(bare\ crystal)$. Thus, hereafter, we focus only on KCl. Thus, in the main text, $\Delta D_{Swelling} \equiv \Delta D(polymer\ coated) - \Delta D(bare\ crystal)$ is used to signify the relative change in ΔD from the dry brush in air to the wet brush using Equation 1). %Swelling from a dry brush in air was found under the same conditions, determined by from $\Delta F_{Swelling} \equiv F(polymer\ coated) - \Delta F(bare\ crystal)$, using QCM-D measurements on both blank and brush-coated surfaces, and converted to %Swelling, using Equations 2.2 and 2.3 to convert $\Delta F_{swelling}$ to $\Delta d_{swelling}$ and finally obtaining %Swelling from the ratio of $\Delta d_{swelling}$ to $d_{brush,dry}$ (Equation 2.5), using VASE measurements to determine the dry brush thickness.

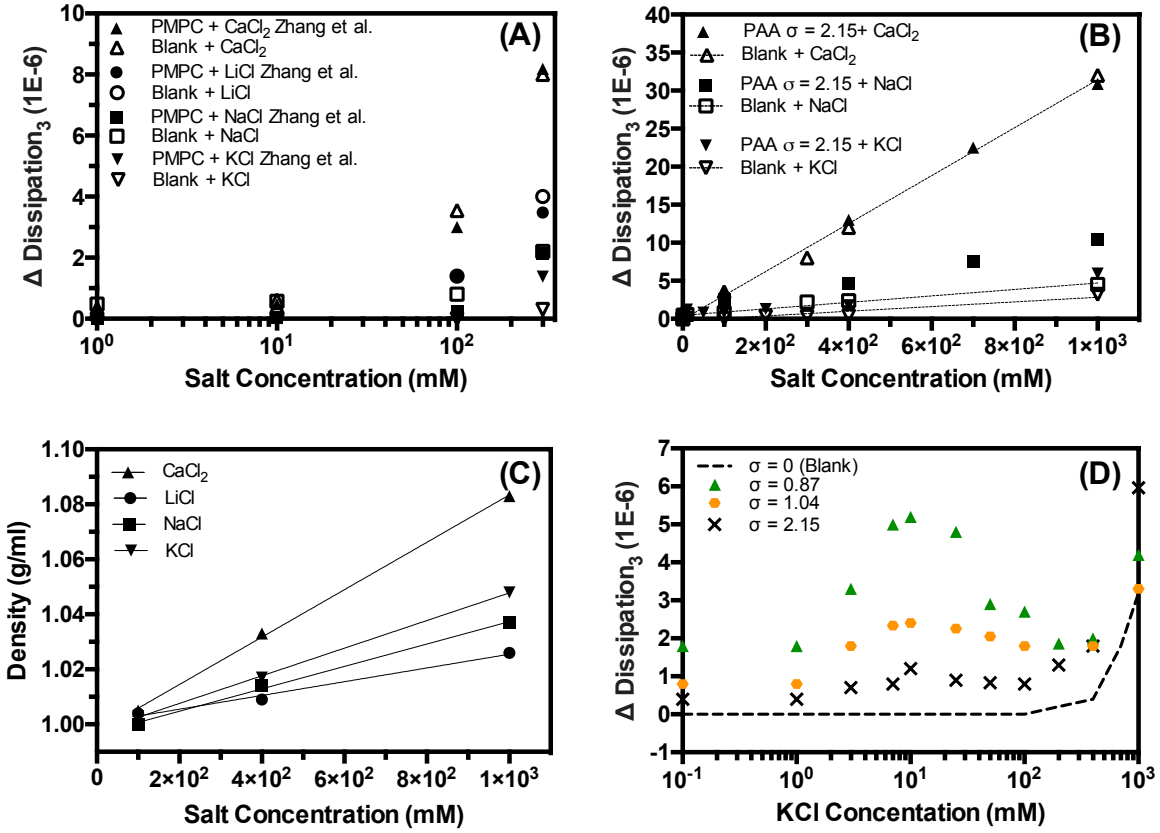

Figure 2.A (A-D). (A) Change in dissipation $\Delta D(bare\ crystal) = \Delta D_{Solvent}$ as a function of salt concentration for various salts on a blank gold crystal from our measurements and $\Delta D(polymer\ coated)$ on a PMPC-grafted brush on a gold crystal (the latter from Zhang et al.). Note that some data points are obscured by overlap, such as the open square covered by a filled square at the highest salt concentration. **(B)** Corresponding $\Delta D_{Solvent}$ data for a blank gold crystal, compared to $\Delta D(polymer\ coated)$ data from our study for the densely PAA-grafted surfaced (σ=2.15). Note the difference in scale on the x- and y-axes, relative to (A). **(C)** Densities of KCl solutions at pH 7 obtained gravimetrically. **(D)** Change in dissipation $\Delta D(bare\ crystal) = (\Delta D_{Solvent})$ as a function of salt concentration for a blank crystal and $\Delta D(polymer\ coated)$ for various grafting densities σ of PAA (Mn= 2,000 g/mol) at pH 7. Error bars are comparable in size to the symbols and are therefore not shown on these or following graphs.

Appendix 2.B

2.B.i Comparison to previous experimental work of Wu et al. – Replotting data as %Change in Swelling

As discussed in the main text, Wu et al.[1] defined a %Change in Swelling, which is here given by Equation B1, and plotted this against grafting density σ. In our main text, we instead plotted as %Swelling, and here we wish to compare our data, converted to %Change in Swelling, against that of Wu et al. Our %Swelling is the inferred thickness of the wet brush in salt water normalized by

that of the dry brush. The resulting dependence of this *relative* height increase determined by Wu et al. on grafting density in the OB regime is similar to that predicted theoretically for the *absolute height H* for weakly dissociating brushes by Zhulina et al.[2] We therefore recalculated our data at pH 7 in the OB regime in the way Wu et al. did as %Change in Swelling, and our results are shown below in Figure 2.B.i It can be seen that for this short-chain PAA brush, there is very little dependence of the grafting density on the %Change in Swelling at the lowest grafting densities, but this is followed by a steep decline for σ>1 chain/nm^2, at roughly at the same salt concentration at which the 0.31 power law dependence of height on grafting density switches to a power law closer to 0.20 (see Figure 2.vi(A) and (B)). Figure 2.B.i demonstrates that a power law exponent of -0.35, close to the value of -0.32 reported by Wu et al. at pH 5.8, can be obtained by extending the range over which a power law is fit to the data; however, this does not represent well the actual behavior.

$$\%\ \text{Change in Swelling} = \frac{d_{\text{brush,KCl}} - d_{\text{brush,pure water}}}{d_{\text{brush,pure water}}} x\ 100 \qquad [B1]$$

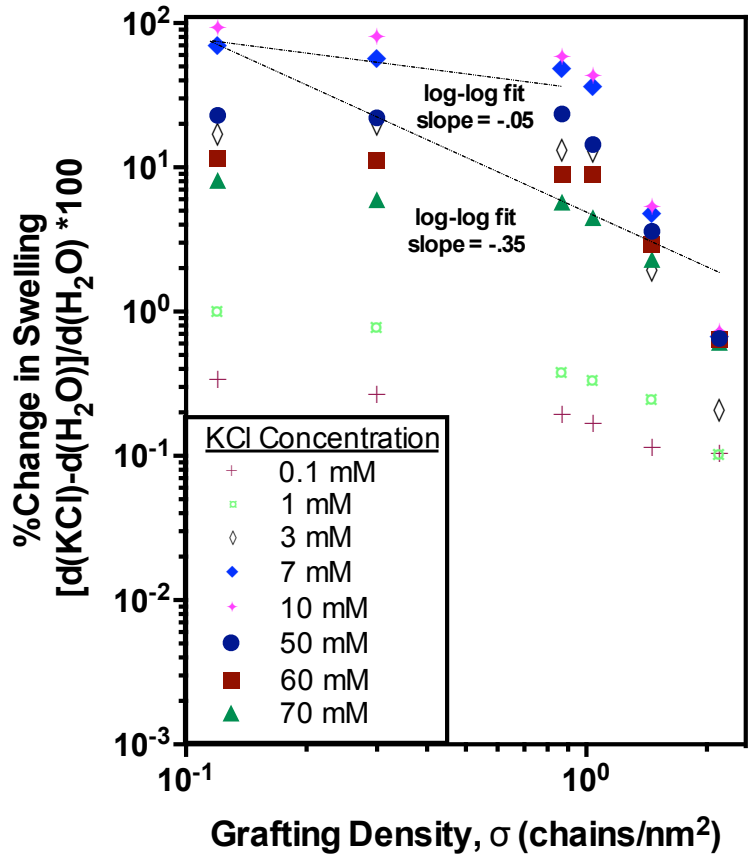

Figure 2.B.i %Change in Swelling (as defined by Wu et al.[1]) vs. grafting density for our short-chain (Mn= 2 kDa) PAA at various KCl concentrations in the OB regime at pH 7

To examine their data more closely we digitized the data of Wu et al. at pH 5.8. When replotted on log-log axes in Figure 2.B.ii as %Change in Swelling, their results show good agreement with our data. To plot the data in this way, the height at the lowest ionic strength (roughly 10^{-6} M) was taken to be the "zero-salt" value. We note that for a pH of 5.8, the minimum ionic strength, with no added salt, is $10^{-5.8}$ M in $[H^+]$ alone, which makes KCl concentration of 10^{-6} M, if indeed it can be accurately controlled to such a small value, roughly equivalent to zero salt. (In our study, the minimum KCl concentration is 0.1 mM, or 10^{-4} M.) In both our data and the data of Wu et al., we see two regimes; at low grafting densities, there is very little dependence of swelling on grafting density, but as σ approaches 1 chain/nm^2, the %Change in Swelling induced by salt decreases

drastically. It can also be seen from Figure 2.B.ii that if the data of Wu et al. are forced to fit to a power law over all grafted densities, then an exponent of -0.28 is obtained, which is similar to the exponent reported in their work of -0.32. However, the data are better represented by two regimes – with weak dependence of swelling on grafting density at low grafting densities, and a steep drop-off at higher densities. This transition to a steeper dependence seems to be magnified when the brush becomes more ionized: At pH 10 in the results of Wu et al., there is an almost negligible effect of grafting density on %Change in Swelling at lower grafting densities, followed by a dramatic decrease as σ approaches 1 chain/nm^2. This result from their work at pH 10 is similar to our results at pH 7, where we note that our brush is highly ionized at pH 7, as theirs is at pH 10. We cannot meaningfully compare our results at pH 7 with theirs at pH 5.8, since the pKa of a PAA brush is ~5, meaning that our brush is almost 16*x* more ionized than theirs.

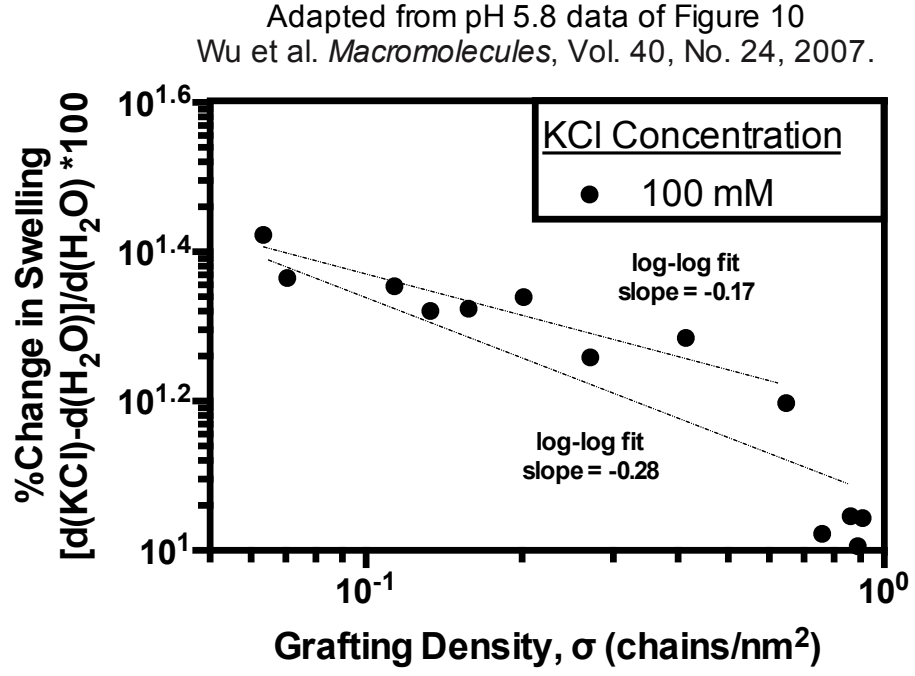

Figure 2.B.ii. Brush height data reported by Wu et al.[1] replotted as %Change in Swelling for a nominally 4 kDa PAA brush at pH 5.8.

Chapter 3

Swelling Hysteresis with Changes in pH or Salt Concentration in Weak Polyelectrolyte Brushes and Bilayer Films

3.i Abstract

We use a Quartz Crystal Microbalance with Dissipation (QCM-D) to investigate the swelling/de-swelling of brushes of weakly ionizable polyanion poly(acrylic acid) (PAA) either as a monolayer, or complexed into a bilayer by adsorption to the PAA brush of the polycation poly(ethylene imine) (PEI). In a cycle of stepped pH changes, at a low grafting density of 0.45 chains/nm^2 and a high PAA molecular weight of 39 kDa, we see hysteresis in swelling over timescales of many minutes. For higher grafting densities and shorter chains, we see little or no hysteresis, and, at intermediate chain length and grafting density, hysteresis is observed at short timescales but is greatly reduced at longer timescales. We also observe hysteresis in swelling upon changes of salt concentration. In addition, we also show that for a long enough PAA chain, at a pH value at which it is partially charged, in the low-salt "osmotic brush" regime, the brush height decreases with increased grafting density, in agreement with theoretical predictions, but not hitherto observed experimentally.

3.ii Introduction

Polyelectrolyte films, including adsorbed monolayers, or "brushes," as well as multilayers, made by Layer-by-Layer (LbL) assembly, have continued to gain popularity in recent years due to their applications in areas ranging from waterborne lubrication and colloidal stabilization to biomaterials.[1–4] Weak polyelectrolyte brushes are particularly desirable because their extent of

charge varies with pH, making them pH responsive. Layer-by-layer (LbL) films have also gained popularity because of their potential applications in electronics and drug delivery.[5–7] LbL multilayers are formed by the sequential adsorption of polyelectrolytes whose charge alternates in sign from one layer to the next, resulting in films ranging from nanometers to microns in thickness, with great flexibility in layer composition. This is especially useful in a field such as drug delivery, where individual film layers may be loaded with small molecule drugs to deliver a specific profile of release versus time.

While their possible applications are many, much is left to be understood about LbL self-assembly, including the ability to predict behavior such as the rate of approach to equilibrium during film growth. It is noteworthy that LbL film growth is an inherently non-equilibrium process, since it includes periodic washing of the deposit with a large excess of solvent that would, at equilibrium, dissolve the deposited LbL film. The lack of ability to predict how rapidly equilibrium is approached after changes in solution conditions presents a significant challenge to developing new LbL technologies. Molecular simulations have been carried out and theoretical models have been used to describe LbL films,[8–11] but these do not fully describe what has been demonstrated experimentally. In particular, hysteretic swelling with respect to changes in pH has been reported in experimental studies of both LbL films and standalone polyelectrolyte brushes.[12–15] While current theory suggests the possibility of hysteretic swelling in polyelectrolyte brushes with respect to changes in polyelectrolyte concentration or grafting density,[15] there is no theory to predict hysteresis with respect to pH. Moreover, experimentally, the dependence of this hysteretic response on film characteristics has not been thoroughly characterized. Note that LbL film growth relies on hysteresis with respect to polyelectroyte concentration in the film, since polyelectrolytes entering the film during a dipping step are not released during washing steps or subsequent dipping

steps. However, in practice, hysteretic swelling with respect to changes in pH is not always anticipated or desired. If polyelectrolyte brushes and LbL films are to be used in changing pH environments, as is often the case especially for biological or sensing applications, it is important that this hysteretic response be well-understood, so that production and use of these materials can be optimized. Ideally, this would involve understanding whether, and the extent to which, hysteresis with respect to pH might occur.

The Quartz Crystal Microbalance with Dissipation (QCM-D) is a well-known instrument for measuring subtle changes in adsorbed mass and viscoelasticity in both polyelectrolyte brushes and LbL films in real time, allowing the swelling dynamics to be carefully tracked.[16–18] Previously, we used QCM-D to measure the steady-state swelling of a weakly dissociating brush of poly(acrylic acid) (PAA), which, via a thiol-gold linkage, was self-assembled as a monolayer onto a gold-coated silica QCM-D crystal. The grafting density of the resultant brushes could be controlled reproducibly through use of a competitive adsorber and through variations in solution concentration.[19] Here, we again use QCM-D, this time to measure the swelling kinetics of PAA brushes, and to extend the work to include an LbL bilayer consisting of a PAA brush monolayer to which a complementary weak polycation, poly(ethylene imine) (PEI), is adsorbed. We investigate the time-dependent swelling responses of these brushes and bilayers to consecutive upward and downward changes in pH, to measure any hysteresis of the swelling, and its dependence on the grafting density and chain length of the polymers. The ability to measure the time-dependency of the swelling response is an advantage of using QCM-D, that heretofore has not been taken advantage of. Finally, we revisit the salt-dependent swelling of a long-chain brush of PAA at lower grafting densities and pH values close to the pKa of PAA in an effort to reconcile results with the brush-thickness scaling laws predicted in the theory of Zhulina et al. for weakly

charged polyelectrolyte brushes in the osmotic brush regime.[20] Our experiments demonstrate that the hysteresis is magnified at low brush grafting density and for long chains, which helps explain the disagreement between previous experimental findings and theoretical predictions.

3.iii Materials & Methods

3.iii.a. Materials

All brush samples were prepared as discussed in prior work.[19] Three α-thiol ω-bromo terminated poly(acrylic acid) (PAA-SH) samples (Short-chain: M_n=2,000 g/mol, M_w=2,600 g/mol, M_w/M_n: 1.3, -SH > 99%; Medium-chain: Mn=14,000 g/mol, Mw=18,200 g/mol, Mw/Mn: 1.27, -SH >99%; Long-chain: M_n= 39,000 g/mol, M_w=55,000 g/mol, M_w/M_n: 1.4, -SH > 99%) were obtained from Polymer Source Inc. (Quebec, Canada). Linear polyethyleneimines (PEI) (3 chain lengths: M_n=2,500 g/mol, M_n=10,000 g/mol, M_w=25,000 g/mol) were obtained from Polysciences, Inc. and Millipore Sigma USA. Potassium chloride (KCl) was obtained from Millipore Sigma USA and used as received. HPLC plus grade water (pH 7) (Millipore Sigma USA) was used to prepare all salt solutions, at concentrations between 0.1 and 1000 mM. Solutions of KCl were found to exhibit pH 7 upon mixing without buffer, while pH 1-9 solutions of KCl were obtained upon the addition of different concentrations of hydrochloric acid (HCl) (Sigma Aldrich USA) or potassium hydroxide (KOH) (Sigma Aldrich USA), respectively, all with concentrations < 3 mM. The pH and ionic strengths were confirmed using both a conductivity meter (CON 6+, Oakton) and a benchtop pH meter (Accumet AE150, Fisher scientific) calibrated against reference standards.

3.iii.b. Preparation of gold-coated QCM-D crystals

Gold-coated silicon wafers (QSX 301, AT-cut, F_0/n =5 MHz) were purchased from Q-

Sense by Biolin Scientific (New Jersey, USA). Prior to deposition of PAA, the sensors were cleaned via a TL-1 base cleaning solution, deionized water, absolute ethanol, and O_2- plasma as described previously.[19]

3.iii.c Preparation of PAA-SH brushes

Gold-coated silicon wafers were plasma treated before use. As described previously,[19] short-chain PAA-SH (M_n: 2,000 g/mol, M_w/M_n=1.3) was dissolved in absolute ethanol to a final concentration of 4 mM.[21] The 4 mM PAA solution was used both as is and after dilution in either absolute ethanol or a 10:1 (wt%) mixture of absolute ethanol to 2-mercaptoethanol, where the latter is a competitive adsorbant to compete with the PAA-SH in binding to the gold-coated QCM-D crystal, thereby controlling grafting density. Then, 40 μL of the PAA solution was deposited onto the crystal, incubated for 18 h, and rinsed repeatedly with absolute ethanol and dried, prior to QCM-D analysis. Preparation of medium-chain PAA-SH (M_n: 14,000 g/mol, M_w/M_n=1.27) was similar to that for short chains, except the incubation was for only 60 minutes, rather than the 18 h used for the short brush, since incubation longer than this led to the formation of a thick, heterogenous physical film due presumably to solvent evaporation. For the long-chain PAA-SH (M_n: 39,000 g/mol, M_w/M_n=1.4), incubation was for 20 minutes. Other details can be found in earlier work.[19]

3.iii.d Variable Angle Spectroscopic Ellipsometry (VASE)

The thickness of the dry PAA-SH brush on the gold-coated QCM-D crystal was obtained by Variable Angle Spectroscopic Ellipsometry (VASE) (Woollam M-2000 Spectroscopic Ellipsometer, J. A. Woollam, USA) as described previously,[19] using the parameters recommended for a PAA layer on bulk gold by Bittrich et al.[22] and the angles of incidence and fitting wavelengths used in our previous work.[19] The optical relative phase shift, Δ, and relative amplitude ratio, tan

(Ψ), measured by VASE, were modeled using two slabs, as described before,[19] taking the PAA layer to be transparent ($k_{film}(\lambda)=0$) and homogenous, and with index of refraction (n_{PAA}) of 1.522 at λ=631.5 nm. Its optical thicknesses was found from measured values of Δ and Ψ using conventional methods.[23,24] See previous work for details.[19]

3.iii.e Quartz Crystal Microbalance with Dissipation (QCM-D)

We used the same Q-Sense E4 system (Q-Sense AB, Gothenburg, Sweden) as previously.[19] Initially, fundamental frequency signals were established on the prepared sensors in air. Solutions were pumped through the device at a constant flow rate of 0.100 mL/min at room temperature (~22°C). In the case of the pH hysteresis experiments for a single brush layer, a baseline for each measurement was established by flowing ultra-pure water (pH 7) until a steady response was seen, followed by the appropriate KCl solution buffered in a succession of steps in pH (pH 7-4-1-4-7-9) with a pre-determined time interval at each pH, typically 4 minutes, although in some cases longer, as discussed in the Results section. For the experiments involving a PAA brush layer with an adsorbed overlayer (i.e., an LbL bilayer), the complementary polyelectrolyte PEI was introduced to the adsorbed PAA brush under flow until a steady-state was achieved, followed by a rinse step (with no polymer, at the appropriate pH and KCl concentration), again, allowing a steady-state to be reached. This bilayer steady-state baseline measurement was then subjected to the same pH steps as described previously for a brush layer alone, again with pre-determined time intervals at each pH. After each change in pH was introduced at the inlet, it took around six minutes for this change to be registered in a step-like response of the QCM-D signal. Once the response to the pH change was observed in the signal, the height was averaged over the entire time interval between the jumps in response, irrespective of any drift in the signal over this period. In some cases, most or all of the signal contained a draft, over which the signal was averaged, as

described in the Results & Discussion section. Experiments were performed in triplicate (N=3) and time averages over each run were then themselves averaged over the three runs and the standard deviation for these three is reported as the error bar.

Experiments investigating the scaling of brush height with respect to grafting density were conducted as previously described,[19] where for each grafting density, each result for a given salinity was obtained for a newly deposited brush, solvated with the desired buffer, rather than using step-wise changes in buffer conditions applied to the same brush, as done for the hysteresis studies. Again, experiments were performed in triplicate (N=3) and error bars represent standard deviation, which for these studies, are smaller than the symbols.

The change in frequency ΔF was used to calculate the change in mass using the Sauerbrey relation rather than a viscoelastic model for the reasons described previously.[19] Again, the work of DeNolf et al.[25] demonstrated that the Sauerbrey relation holds when the film is thin and/or rigid enough; specifically, d/λ_n , the ratio of the thickness of the film d to the shear wavelength of the material λ_n, must be no greater than 0.05, [25,26] a condition met in all of the brushes and bilayers studied here.

As mentioned previously, the Sauerbrey relation yields a quantitative measure of the adsorbed mass and swelling through the measurement of ΔF.[26] Details of the set-up of the QCM-D experiment are described in previous work.[19] Only one overtone (n=3) is used to interpret the Sauerbrey mass.[27] The mass change (Δm) calculated using Sauerbrey relation for rigid films is given by Equations 3.1 & 3.2.[28]

$$\Delta F = -\Delta m \left(\frac{2nF_0^2}{A\sqrt{\mu_q \rho_q}}\right) = -\frac{1}{C_f}\Delta m \qquad [3.1]$$

$$\Delta d = \frac{\Delta m}{\rho} \qquad [3.2]$$

The crystal parameter (C_f) is obtained from the following parameters given by the manufacturer: F_0 is the fundamental frequency (= 5 MHz), n is the overtone number (=3), Δm is the change in mass per unit area, ρ_q is the density of quartz (=2.648 g/cm^3), A is the crystal area (=1.54 cm^2), and μ_q is the shear modulus of quartz (= 2.947 x 10^{11} g·cm^{-1}·s^{-2}), respectively.[16,29,30] The Sauerbrey mass difference Δm is converted into a thickness increment Δd using the density ρ of the added-mass. A more negative ΔF indicates that more mass is adsorbed.

As before,[19] we obtain adsorbed brush mass by ellipsometry and use QCM-D to obtain changes in brush mass due to solvation of the brush. In our previous work, we demonstrated the importance of correcting QCM-D data obtained with a polymer brush by subtracting from these data the results obtained for a solvent-covered polymer-free crystal. This subtraction removes the effect of the density and viscosity of the solvent, which varies with salt concentration. To obtain our results, we assume the same additive relationship between the effects of the polymer brush described in previous work[19] and in great detail by Chu et al.[31]

3.iv Results

3.iv.a Variable Angle Spectroscopic Ellipsometry (VASE)

The dry thicknesses of PAA brushes and PAA/PEI bilayers were measured by variable angle spectroscopic ellipsometry (VASE). The grafting density σ in chains/nm^2 was calculated using the same method and formula as described in previous work.[19] These findings are summarized in Table 3.i.

Table 3.i: VASE results for the dry thicknesses of the PAA brushes and (PAA/PEI) bilayers investigated in this work

Type of Material	Chain Length PAA/PEI (kDa)	PAA Brush Grafting Density, σ (chains/nm^2)	Dry Thickness (nm)
(PAA/PEI) Bilayer	2/2.5	0.87	2.80 nm ± 0.21
PAA brush only	2	0.87	2.66 nm ± 0.13
(PAA/PEI) Bilayer	14/10	0.060	1.70 nm ± 0.19
PAA brush only	14	0.060	1.29 nm ± 0.11
(PAA/PEI) Bilayer	39/25	0.45	34.3 nm ± 1.13
PAA brush only	39	0.45	27.0 nm ± 2.04
(PAA/PEI) Bilayer	39/25	0.023	2.02 nm ± 0.22
PAA brush only	39	0.023	1.27 nm ± 0.17
PAA brush only	39	0.042	2.32 nm ± 0.24

3.iv.b Hysteresis Studies

Figure 3.i (A) shows a time-dependent swelling response, or Sauerbrey thickness in nm, of a short (2 kDa) PAA brush with a grafting density σ of 0.87 chains/nm^2 as pH is varied in steps, at fixed salt concentration. As in other figures below, the results shown are from one of three replicates of the same experiment, with all three showing nearly identical results in all cases, as shown by the small standard deviations given in the averaged results in Figure 3.i (b). This brush should be considered to be "dense,"[32] in that the chains are spaced at distances much closer than the free chain's radius of gyration, putting them in the "brush" rather than "mushroom" regime. In our previous work, it was demonstrated that this brush is quite extended, exhibiting a swelling/deswelling profile that disagrees with scaling theory for brushes that are low-to-moderately densely grafted.[19] The brushes collapse when the pH is decreased in agreement with what was seen by others including Yadav et al.,[13] presumably due to protonation of the chains, leading to the expulsion of salt counterions, and accompanying water, from the brush. Conversely, the brushes swell when pH is increased, in agreement with others,[13] as the chains are ionized and salt ions and water then enter the brush. It can be seen in Fig. 1(A) that in a pair of pH sweeps the

first of which drives PAA in three steps from ionized to neutral, and the second of which drives it in back to ionized, the Sauerbrey thicknesses in the first sweep are recovered in reverse order, as expected, in the second. In Figure 3.i (B), each of these average thicknesses (which are themselves averages over time – see the materials & methods section), is averaged across three triplicate runs, giving the average brush thickness versus pH with error bars representing the standard deviations. Averaged over three samples, there is minimal hysteresis, and the brush's swelling history is found to be highly reproducible.

Next, this brush was equilibrated with PEI of similar chain length to the PAA brush to form a (PAA/PEI) bilayer. It can be seen in Figure 3.i (C) that this bilayer, when subjected to identical pH downward/upward sweeps, also recovers its original Sauerbrey thicknesses during the second, upward, sweep in pH. Unlike the brush, which shrinks as pH is reduced, notably, the LbL bilayer swells as pH is lowered. LbL multilayers have been generally found to swell at reduced pH, as shown for example by Hiller and Rubner[33] for a multilayer of poly(allylamine) and poly(styrene sulfonate) and by Silva et al. [34] for an LbL multilayer of chitosan/alginate. The reason for this is unclear; however, it is hypothesized that this is potentially due to the incorporation of the polycation PEI, which in theory should possess the opposite swelling response to pH changes as that of a polyanion. Figure 3.i (D) demonstrates that this bilayer, averaged over 3 samples, also lacks hysteresis and the bilayer's history is reproducible.

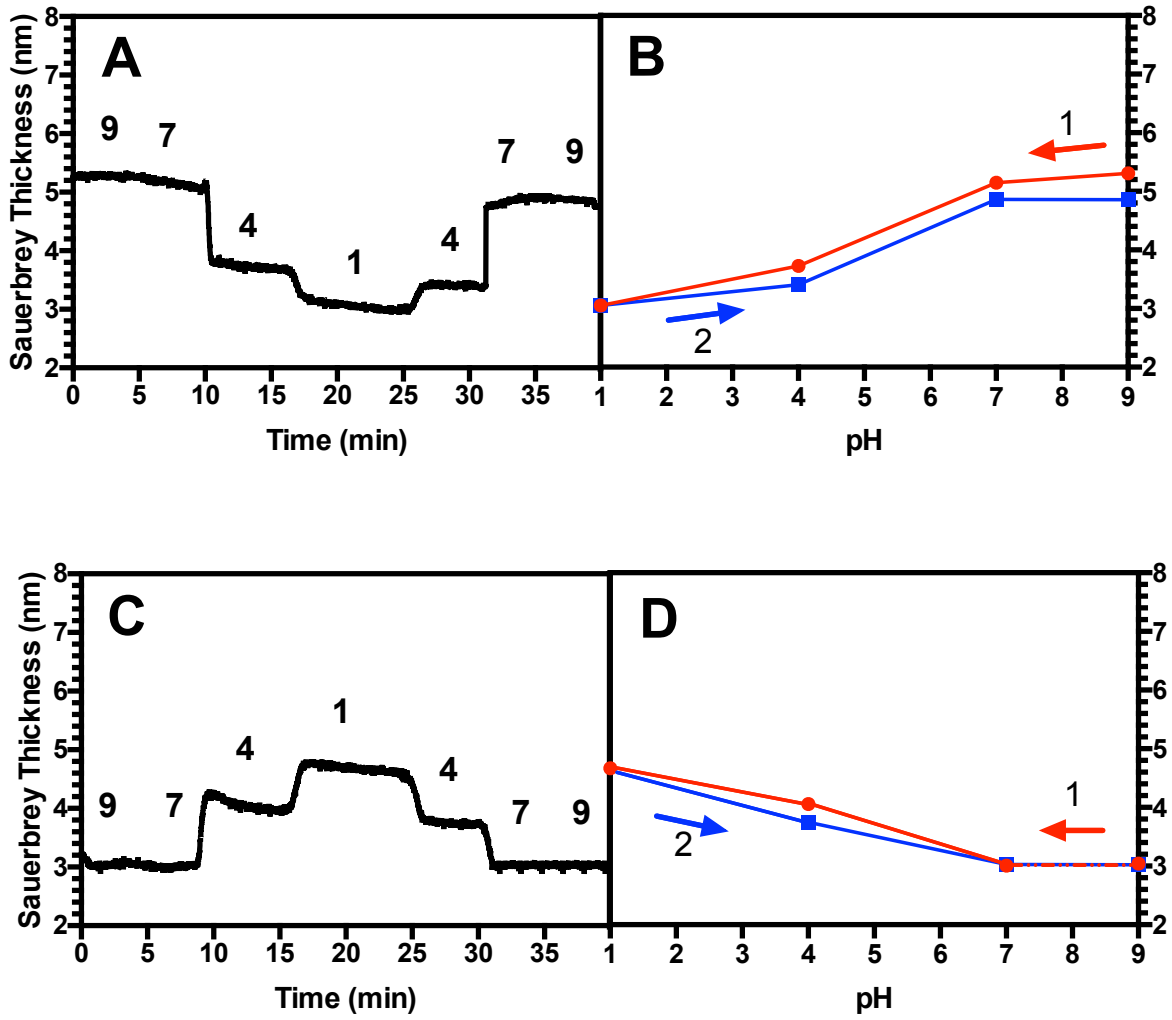

Figure 3.i(A-D): A) Representative thickness responses to pH changes for a 2 kDa PAA brush with no PEI adsorbed, grafting density σ =0.87 in 100 mM KCl with pH varied as shown, with effect of overlying solvent subtracted, as discussed at the end of the methods section. B) Time-averaged thickness response vs. pH obtained from A), with numbers indicating the order in which the pH scans occurred. Error bars in B) and D) represent the standard deviation for N=3, but are invisible since they are smaller than the symbols. C) Representative thickness response for a (PAA/PEI) bilayer with a 2 kDa PAA brush underlayer, grafting density σ =0.87 in 100 mM KCl and 2.5 kDa PEI adsorbed overlayer, with solvent subtracted. D) Time-averaged thickness response vs. pH obtained from C). The dashed line represents a connecting segment that falls on top of another segment.

Next, a long-chain (39 kDa) PAA brush was studied at a grafting density σ of 0.45 chains/nm^2, which is considered to be "high" for this chain length, since in previous work, this brush was shown to be highly extended, similarly as the 2 kDa brush whose behavior is described in Figure 3.i (A-B). Figure 3.ii (A) shows that the height of this long-chain PAA brush decreases at low pH as was seen in the dense short brush of Figure 3.ii (A-B) when subjected to a downward

pH sweep, and it regains its original height when the pH is thereafter stepped upwards. Figure 3.ii (B) shows that, averaged over 3 samples, there is negligible hysteresis, and the brush's swelling history is highly reproducible. Next, this brush was equilibrated with PEI of similar chain length (25 kDa) to form a (PAA/PEI) bilayer, which was then subjected to an identical pH sweep. Figure 3.ii (C) shows that the wet thickness at neutral pH of the bilayer is considerably greater than the thickness of the long brush alone, in Fig. 3.ii (A), unlike what was seen for the short dense brush in Figure 1. This suggests that this long PAA brush is able to incorporate more PEI of similar length to that of the brush, than the short brush can. The dry thickness of this long brush is 27 nm, where the dry thickness of the bilayer is 34 nm. The long-chain bilayer's response to the pH cyclic sweeps is found to be hysteretic, and it does not return to its original thickness when pH is increased again to pH 7. Figure 3.ii (D) averages this time response across three measurements and shows good reproducibility, demonstrating that while a bilayer of dense PAA underlayer exhibits hysteretic swelling, a dense, monolayer PAA brush, does not.

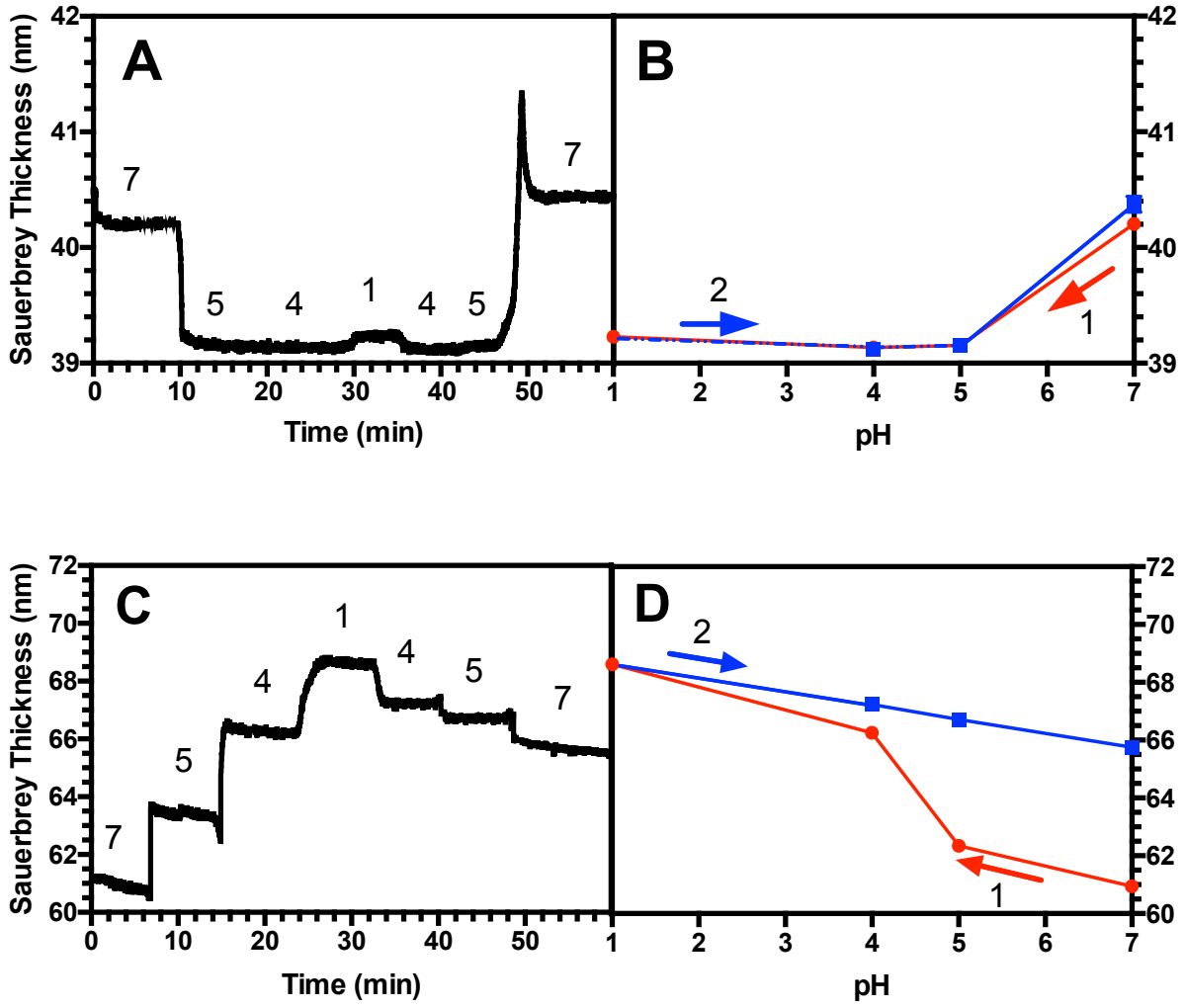

Figure 3.ii(A-D): The same as in Fig. 3.i except for a 39 kDa PAA brush, grafting density σ =0.45, again in 100 mM KCl and in C) and (D) the overlayer is a 25 kDa PEI. Error bars represent the standard deviation for N=3 and if they are not visible, they are smaller than the symbols. The dashed line represents a connecting segment that falls on top of another segment.

Next, this same long-chain (39 kDa) PAA brush was diluted to achieve a significantly less dense grafting density σ of 0.023 chains/nm^2, with a dry thickness of 1.27 nm. This is considerably more dilute than the brush of grafting density σ = 0.45 chains/nm^2 from Figure 3.ii, which possessed a dry thickness of 27.0 nm. Figure 3.iii (A) shows that the Sauerbrey thickness of this lower-density brush shrinks substantially in response to a decreasing pH. It should also be noted that the QCM-D data for this case do not reach as clear a steady state after each pH adjustment.

This more sluggish response may be due to chains having more room to reconfigure themselves in response to pH changes than in the densely grafted brushes of Figures 3.i-ii. The values in Figure 3.iii (B), averaged over three measurements, demonstrate the hysteresis clearly. The error bars, representing the standard deviation of these three measurements, are visible above the size of the symbols, reflecting the greater variability of this measurement across replicate samples than for the measurements in Figures 1 and 2. This is likely related to the lack of clear steady values at each pH in the sweep (see the materials & methods section for how the average values were obtained). After adsorbing PEI onto this brush, the PAA/PEI bilayer also swells hysteretically when subjected to a pH sweep, as shown in Figure 3.iii (C). However, the QCM-D time response shows less drift in time after each pH change than does the monolayer brush. Nevertheless, when averaged over three measurements in Figure 3.iii (D), it can be seen that the hysteresis of these films is pronounced.

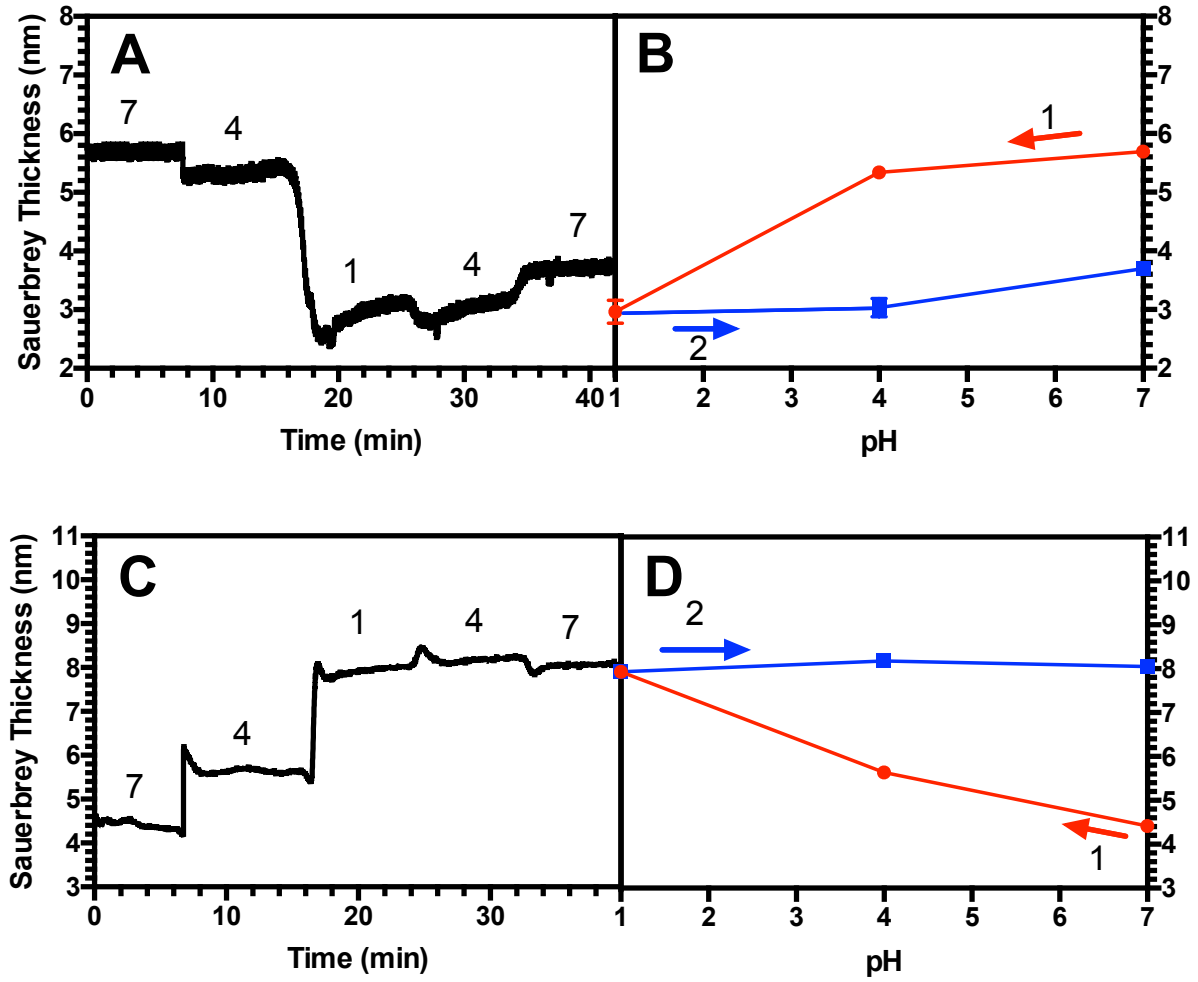

Figure 3.iii(A-D): The same as in Figure 3.ii, except for a grafting density σ =0.023 in 100 mM KCl.

Thus, a dilute-grafted long-chain PAA brush and its corresponding (PAA/PEI) bilayer show hysteresis, while for the densely grafted long-chain and short-chain brushes, and their (PAA/PEI) bilayers, show no hysteresis. To examine more precisely this transition to hysteretic behavior in long-chain, sparsely grafted brushes, we investigate a chain of intermediate length, 14 kDa, and grafting density, σ = 0.06 chains/nm^2. Figure 3.iv (A) shows that this brush, when subjected to a pH sweep, only slowly approaches a steady state, and as a result, only 3, rather than 3.iv, different pH values were investigated. Despite the slowness of equilibration, Figure 3.iv (B) shows that the brush de-swells with decreased pH as before, and when pH is increased again, does appear to approach its original height at each pH over an extended timescale. Figure 3.iv (B) shows

that, unlike the long-chain, dilute brush of Figure 3.iv (A-B), the intermediate-length brush at long times is not appreciably hysteretic; the error bars are comparable in size to the hysteretic gap in thicknesses. This medium-chain brush, when equilibrated with PEI of similar chain length to form a (PAA/PEI) bilayer, had a dry thickness of 1.70 nm compared to the 1.29 nm dry thickness of the PAA underlayer alone. In Figure 3.iv (C), it can be seen that the bilayer swelling is nearly, but not quite as, reversible when subjected to a reversing pH sweep, as the monolayer brush is, in Figure 3.iv (A). While the result in Figure 3.iv (D) suggests some hysteresis, again, it is difficult to be sure due to the limited size of our sample (N=3) and the magnitude of the error bars. Table 3.ii summarizes the hystereses for all PAA brushes and complementary bilayers.

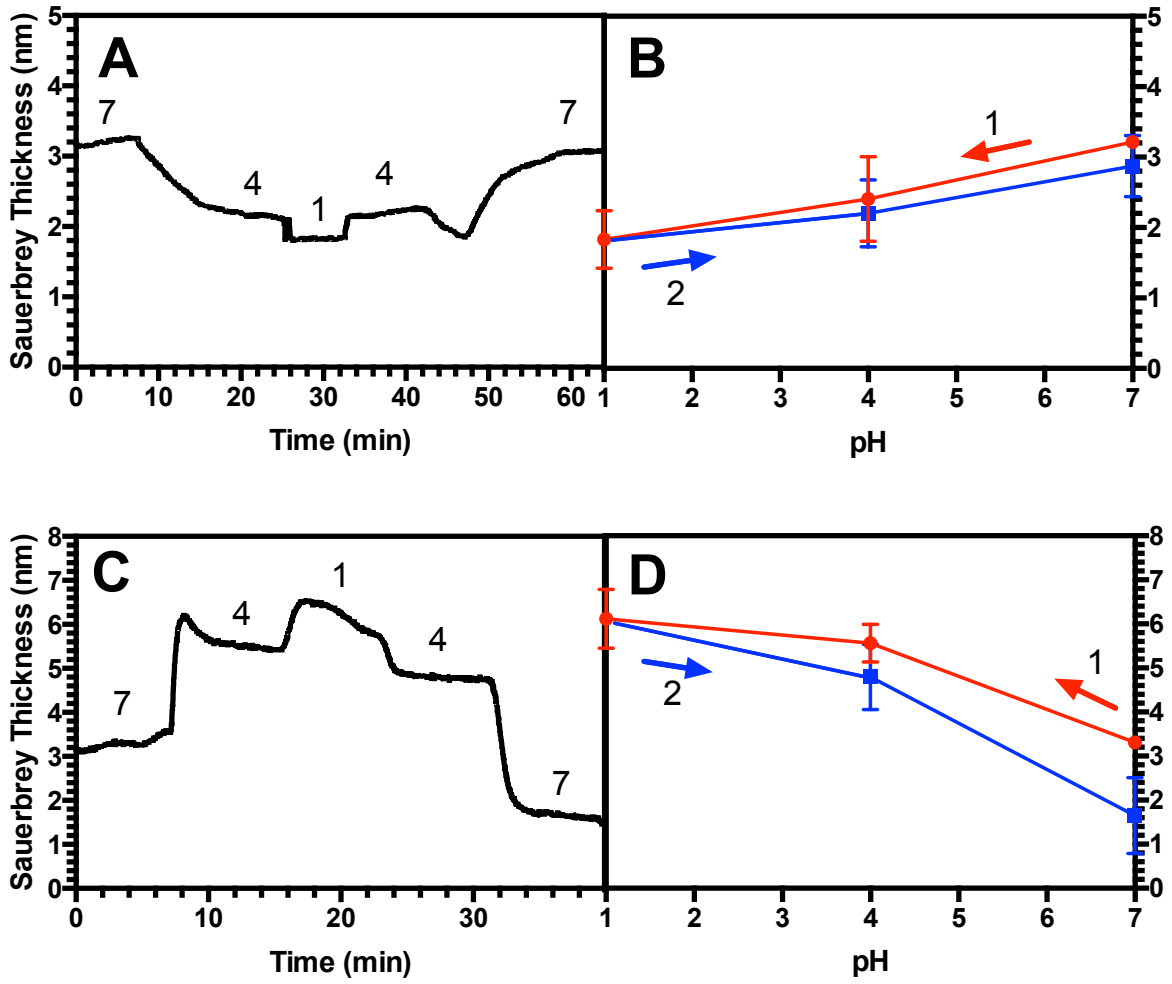

Figure 3.iv(A-D): The same as Figure 3.ii, except for a 14 kDa PAA brush, and 10 kDa PEI in C) and D) at grafting density σ =0.06 in 100 mM KCl. Error bars represent the standard deviation for N=3.

Table 3.ii: Summary of experimental findings for PAA brushes & LbL bilayers (PAA/PEI) for various chain lengths and grafting densities. ** and the yellow color indicate intermediate cases where slow approach to equilibrium suggests that hysteresis would be present at short times (a few minutes) but becomes small at longer times (many minutes).

Type of Material	PAA Brush Grafting Density, σ (chains/nm^2)	Chain Length (kDa) PAA, PEI	Hysteresis observed?
(PAA/PEI) Bilayer	0.87	2,2.5	No
PAA brush only	0.87	2	No
(PAA/PEI) Bilayer	0.06	14,10	**
PAA brush only	0.06	14	**
(PAA/PEI) Bilayer	0.45	39,25	Yes
PAA brush only	0.45	39	No
(PAA/PEI) Bilayer	0.023	39,25	Yes
PAA brush only	0.023	39	Yes

Since in these studies, the salt concentration is fixed (at 100 mM) and pH is varied; as a control, it was also important to confirm the past experimental work where it was shown that LbL films did not exhibit hysteretic swelling/de-swelling when the salt concentration was changed at fixed pH.[35] As shown in Figure 3.v, we find that for a short, dense standalone PAA brush (chain length= 2 kDa, grafting density σ = 0.87) (Figure 3.v(A-B)), there is no hysteresis; however, hysteresis is seen for a long-chain brush (chain length = 39 kDa) grafted at lower density than in our previous work (grafting density σ = 0.023) (Figure 3.v(C-D)). Reversible swelling with fixed pH and varied salt is consistent with the findings of Sikhorukov and colleagues, who observed reversibility in films of poly(styrene sulfonate) (PSS) and poly(allylamine hydrochloride) (PAH).[35]

Currently, no theory exists to predict the hysteresis of polyelectrolyte brushes or LbL films at fixed salt with changes in pH. We note that Yadav et al. found hysteresis with changes in pH in their materials that had polydispersity (M_w/M_n) of around 1.4, and found little hysteresis in their nearly monodisperse materials of similar average molecular weight. They therefore suggested that polydispersity is responsible for the hysteresis, but did not provide a mechanism for this. Here, we note that our materials posess dispersities of around 1.27, and if Yadav et al. are correct in their inference, the hysteresis in our materials may be related to their polydispersity.

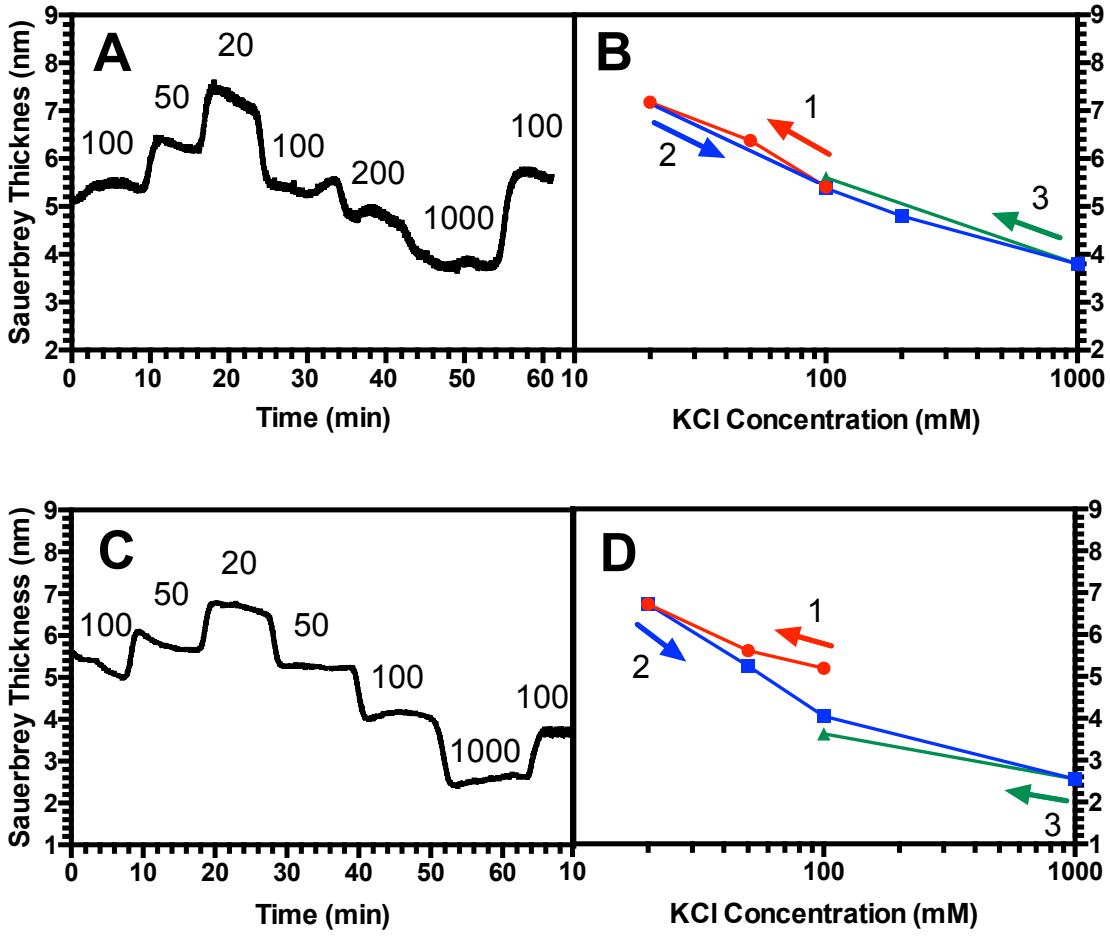

Figure 3.v(A-D): A) Representative swelling response for a 2 kDa PAA brush, grafting density σ =0.87 at fixed, neutral pH with varying KCl concentration in mM (values given in plots). B) Average swelling vs. KCl concentration. C) Representative swelling response for a 39 kDa PAA brush, grafting density σ =0.023 at fixed, neutral pH with varying KCl concentration in mM (values given in plots). D) Average swelling vs. KCl concentration. Note that in C) and D), that the first and final salt concentration are the same and lie near the middle of the x axis at 100 mM.

3.iv.c Revisiting scaling theory for monolayer PE brushes and comparison to previous findings

Zhulina et al. predict that in the osmotic brush (OB) regime corresponding to an extremely low external ionic strength, the height H of a weakly-dissociating polyelectrolyte brush should scale according to Equation 3.3[20] with respect to the number of monomers in the chain *N*, the grafting density σ , the ionic strength given as the sum of the external proton concentration *[H+],* and the total salt concentration (C_S). We include a coefficient of 2 in front of C_S in Eq. 3.3 to reflect that, as in previous work,[19] C_S refers to total salt concentration [KCl] and not ionic strength [K^+] + [Cl^-] as in Zhulina's original work.[20]

$$H \sim N\sigma^{-\frac{1}{3}}([H^+] + 2C_s)^{1/3} \quad [3.3]$$

Zhulina et al. also predict that in the salted brush (SB) regime corresponding to a higher external salt concentration above the critical value, the brush height H should scale according to Equation 3.4.[20]

$$H \sim N\sigma^{\frac{1}{3}}{C_s}^{-\frac{1}{3}} \quad [3.4]$$

Note that while the scaling of brush height with chain length is the same in the osmotic and salted brush regimes, the scaling with grafting density and salt concentration are inverted in the osmotic brush regime, relative to the salted brush regime. In our previous work, the same PAA brushes as used in this work were studied to test these scaling relationships at multiple fixed pH values at various grafting densities across a broad range of salt concentrations.[19] It was found that, as predicted by Eqs. 3.3 and 3.4, when ionized, the brushes initially swell at low external salt (<10 mM), corresponding to the low ionic strength "osmotic brush" regime, and de-swell at higher external salt concentrations, in the "salted brush" regime, giving very similar results at the two fixed pH values of 7 and 9. At pH 3, where the brushes are expected to be charge neutral, their

behavior was found to be drastically different; they no longer exhibit either of these swelling regimes and instead are nearly unaffected by external salt concentration.[19]

To explore more carefully the transition from the behavior at pH 7 and 9, and that at pH 3, it is of interest to examine their behavior at pH values below, but closer to, the pKa (~5). Such an investigation is especially of interest, since our previous findings for PAA brushes agreed with the scaling dependences on salt concentration predicted by Zhulina et al. in both osmotic and salted regime, but agreed with the predicted dependence on grafting density only in the salted brush regime.[19] In the osmotic brush regime, our earlier work showed a brush height roughly proportional to the +1/3 power of grafting density σ, similar to that in the salted brush regime, but disagreeing with Eq. 3.3. However, in our previous work the effect of grafting density was studied only at relatively high grafting density and only for the shortest brushes (2 kDa), which were highly stretched, deviating from the assumption of ideal Gaussian elasticity in the theory of Zhulina et al..[20] Our previous findings might therefore disagree with scaling predictions Zhulina et al. both because our chains were not weakly ionized at the pH values considered, and also because they were highly stretched and not close to the region of Gaussian elasticity.

In the present study, these limitations are rectified by using our long-chain PAA brush described in Figure 3.iii (A-B) which we diluted to a low grafting density σ of 0.023 chains/nm^2, significantly more sparsely grafted than in both Figure 3.ii (A-B) above, and our previous experimental work[19] (σ =0.45 chains/nm^2). Thus, our new, longer, more sparsely grafted chains are closer to the Gaussian regime. Figure 3.iii (A-B) demonstrates that for these chains the brush collapses partially at pH 4, while at pH 1 they can be considered to be fully charge neutral. Guided by this transition at around pH 4, Figure 3.vi demonstrates the swelling response of this same brush at fixed pH =4.2, where it is presumably partially ionized, with respect to variations in KCl

concentration. For this brush at this pH, the charge fraction is considerably lower than unity and the brush can be considered to be partially ionizable, rather than more nearly fully ionized, as expected at the pH values investigated previously (pH 7 & 9).[19] Furthermore, the brushes investigated are orders of magnitude more sparsely grafted than previously, since σ = 0.023 chains/nm^2 (red circles) and σ = 0.042 chains/nm^2 (green triangles), while for the previous brush, σ = 0.45 chains/nm^2. Also, the brush studied here contains much longer chains (39 kDa) than previously (=2 kDa). Both the sparser grafting and longer chain length result in chains that can be stretched much more easily than those studied previously.[19] For the more extensible chains studied here, it can be seen that the dependence on salt concentration, in the OB regime, shows a power-law exponent of around ~ +0.13 to +0.15, and in the SB regime, a ~ –.017 to –0.20 power-law exponent is seen (see log-log fit slopes for σ = 0.023 chains/nm^2 (red circles) and σ = 0.042 chains/nm^2 (green triangles). Although from Figure 3.vi it may appear that the height is relatively independent of grafting density in the OB regime below the maximum brush thickness at 10 mM KCl, it is apparent that at salt concentrations of 7-10 mM, there is a decrease of brush height with increased grafting density. This could be indicative of the OB regime with a weakly negative scaling dependency predicted by Zhulina et al.[20] However, we note the limitations of our system: the PAA brushes investigated here, while more elastic than those studied previously,[19] still possess finite extensibility which likely suppresses or weakens the inverse scaling of brush height with grafting density. We note that shorter chains, which are even more subject to the effects of finite extensibility, show a monotonic increase in brush height with grafting density at fixed salt concentration in the osmotic brush regime.[1] Thus, it appears that a PAA chain of 39 kDa is close to the minimum chain length capable of showing an inverse dependence of brush height on grafting

density, and that the OB scaling $H \sim \sigma^{-\frac{1}{3}}$ with exponent -1/3, of Zhulina et al., perhaps only applies for much longer chains than this.

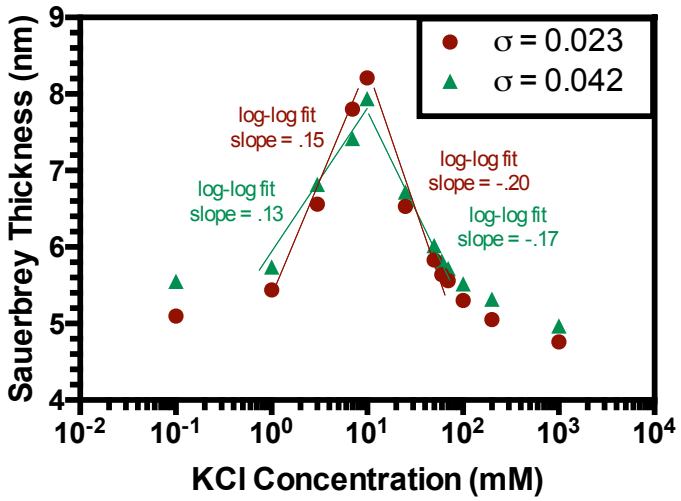

Figure 3.vi. Height (i.e. Sauerbrey thickness) at various salt concentrations for a 39 kDa PAA brush at grafting density σ = 0.023 chains/nm^2 (red circles) and σ = 0.042 chains/nm^2 (green triangles) at pH 4.2, below the pKa (~5). Log-log fits demonstrate the scaling exponents for the Osmotic Brush (OB) regime (left slope) and Salted Brush (SB) regimes (right slope).

3.v Discussion and Summary

3.v.a Hysteresis Studies

Here, we investigated the history-dependent swelling of a PAA brush as well as a (PAA/PEI) bilayer when pH or salt concentration is changed. We find that for a standalone PAA brush, when salt concentration is fixed, the brushes exhibit hysteresis in response to changes in pH when the chains are more elastic; namely, longer and less densely grafted (Fig. 3.iiiA-B). By contrast, two less elastic brushes were found not to be hysteretic, including a short, and therefore rigid, brush (Fig. 3.iA-B), as well as a long-chain brush at a high grafting density (Fig. 3.iiA-B). For the (PAA/PEI) bilayer with a PAA brush underlayer, we demonstrated that the PAA underlayer plays a significant role in the swelling reversibility, leading to similar behavior as a standalone

PAA brush. For a (PAA/PEI) bilayer with a short, rigid underlayer, no hysteresis is seen (Fig. 3.iC-D), while for a PAA/PEI bilayer with a longer, more elastic brush underlayer, hysteresis is observed (Fig. 3.iiiC-D). Hysteresis is also seen in the bilayer with a more densely grafted, longer-chain underlayer (Fig. 3.iiC-D). We also found that for moderate chain length and grafting density, both a standalone PAA brush and a (PAA/PEI) bilayer, show hysteresis at short times, but for longer times, the brushes have less hysteresis (Figure 3.iv). This work is the first experimental report of hysteresis in PAA and (PAA/PEI) brushes where the magnitude of the hysteresis is found to be a function of the brush properties. It is therefore a starting point for understanding the history dependence of the layer-by-layer (LbL) process, which depends crucially on hysteretic transport, wherein polyelectrolyte deposition during one dipping step is not reversed during the rinsing or subsequent dipping steps. We note that in their studies, Yadav et al. found sensitivity of hysteresis to polyelectrolyte polydispersity, for polydispersities similar to those in our PAA (i.e., M_w/M_n= 1.3 for 2 kDa; M_w/M_n=1.27 for 14 kDa, and M_w/M_n =1.4 for 39 kDa).

Intriguingly, we note that even an untethered polyelectrolyte in free solution, namely isotactic poly(methacrylic acid) (iPMA) in water, can show hysteresis in charge level upon change in pH.[36] Ghasemi and Larson[37] have suggested that this hysteresis is due to charge-conformation coupling in flexible weak polyelectrolytes. That is, a polyanion in a compact conformation resists deprotonation more strongly than does one in an extended conformation, because of the highly electrostatic repulsion in the former. Thus, a coiled chain will need a higher pH to achieve the same charge level than needed for an extended chain. Ghasemi and Larson suggested that this can lead to two conformation-charge states at the same pH, with at least one of the two being metastable. We hypothesize that, similarly, for tethered PAA chains, the resistance of monomers to deprotonation at a given pH depends on the chain stretch, producing two charge-conformation

states at the same pH (at least one being metastable). If the energy barrier between these two states is high at intermediate pH values, then the pH history will determine which state is accessed, leading to hysteresis.

3.v.b Comparison of scaling theory for monolayer PE brushes in the osmotic brush regime with new and previous findings

After finding an intermediate brush height at pH below the pKa, we revisited the major discrepancy between our previous experimental findings and the predictions of self-consistent field theory in the scaling of brush height with grafting density in the osmotic brush (OB) regime.[20] The theory of Zhulina et al.[20] predicts, seemingly paradoxically, that in the OB regime, higher grafting density σ leads to reduced brush height *H*, following the scaling law $H \sim \sigma^{-\frac{1}{3}}$ with exponent -1/3. Experiments in our previous work[19], and by Wu et al.[38], showed, however, a positive scaling exponent, between 0.18 and 0.31, for the dependence of *H* on σ . The theoretical result was derived, however, for Gaussian chains, while our previous work and that of Wu et al. with PAA brushes measured the grafting density dependence for short brushes only, namely 2 kDa for our brushes and 4.10 kDa reported for the brushes of Wu et al. Because of their shortness, these brushes are expected to show non-linear (or non-Gaussian) elasticity. This may be at least partly responsible for the failure of the scaling law $H \sim \sigma^{-\frac{1}{3}}$ for weak polyelectrolytes in the OB regime. By using the longer 39 kDa chains and lower grafting density, in Figure 6, the brushes are seen to swell slightly with decreased σ in the OB regime near the peak brush height, hinting at a possible transition for longer brushes towards the scaling law $H \sim \sigma^{-\frac{1}{3}}$ predicted by Zhulina et al. for the OB regime. Future experimental work should examine the behavior of still longer brushes. The theory could also be improved by accounting for the finite extensibility to confirm that this

suppresses the inverse dependence of brush height on grafting density. An interesting puzzle is that the OB scaling of brush height with the 1/3 power of ionic strength is observed even for short brushes, even though the prediction of the same theory for the dependence on grafting density fails, at least for the short brushes..

3.vi References

1 Pincus, P. Colloid stabilization with grafted polyelectrolytes. *Macromolecules* **1991**, *24*, 2912–2919 DOI: 10.1021/ma00010a043.

2 Weir, M. P.; Parnell, A. J. Water Soluble Responsive Polymer Brushes. *Polymers (Basel).* **2011**, *3*, 2107–2132 DOI: 10.3390/polym3042107.

3 Motornov, M.; Tam, K.; Pita, M.; Tokarev, I.; Katz, E.; Minko, S. Switchable selectivity for gating ion transport with mixed polyelectrolyte brushes: approaching "smart" drug delivery systems. *IOP Publ. Nanotechnol. Nanotechnol.* **2009**, *20*, 434006–434016 DOI: 10.1088/0957-4484/20/43/434006.

4 Yang, Z.; Tarabara, V. V.; Bruening, M. L. Adsorption of Anionic or Cationic Surfactants in Polyanionic Brushes and Its Effect on Brush Swelling and Fouling Resistance during Emulsion Filtration. *Langmuir* **2015**, *31*, 11790–11799 DOI: 10.1021/acs.langmuir.5b01938.

5 Wohl, B. M.; Engbersen, J. F. J. Responsive layer-by-layer materials for drug delivery. *Journal of Controlled Release*, 2012, *158*, 2–14.

6 Hammond, P. T. Engineering materials layer-by-layer: Challenges and opportunities in multilayer assembly. *AIChE Journal*, 2011, *57*, 2928–2940.

7 Fendler, J. H. Chemical self-assembly for electronic applications. *Chemistry of Materials*, 2001, *13*, 3196–3210.

8 Panchagnula, V.; Jeon, J.; Dobrynin, A. V. Molecular dynamics simulations of electrostatic layer-by-layer self-assembly. *Phys. Rev. Lett.* **2004**, *93*, 037801–1 DOI: 10.1103/PhysRevLett.93.037801.

9 van de Steeg, H. G. M.; Stuart, M. A. C.; de keizer, A.; Bijsterbosch, B. H. Polyelectrolyte Adsorption: A Subtle Balance of Forces. *Langmuir* **1992**, *8*, 2538–2546 DOI: 10.1021/la00046a030.

10 Patel, P. A.; Jeon, J.; Mather, P. T.; Dobrynin, A. V. Molecular Dynamics Simulations of Layer-by-Layer Assembly of Polyelectrolytes at Charged Surfaces: Effects of Chain Degree of Polymerization and Fraction of Charged Monomers. *Langmuir* **2005**, *21*, 6113–6122 DOI: 10.1021/la050432t.

11 Salehi, A.; Larson, R. G. A transport model and constitutive equation for oppositely charged polyelectrolyte mixtures with application to layer-by-layer assembly. *J. Chem. Phys.* **2018**, *149*, 194901 DOI: 10.1063/1.5051770.

12 Secrist, K. E.; Nolte, A. J. Humidity Swelling/Deswelling Hysteresis in a Polyelectrolyte Multilayer Film. **2019**, *16*, 51 DOI: 10.1021/ma101983s.

13 Yadav, V.; Harkin, A. V; Robertson, M. L.; Conrad, J. C. Hysteretic memory in pH-response of water contact angle on poly(acrylic acid) brushes †. *Soft Matter* **2016**, *12*, 3589 DOI: 10.1039/c5sm03134f

14 Aulich, D.; Hoy, O.; Luzinov, I.; Brücher, M.; Hergenröder, R.; Bittrich, E.; Eichhorn, K.-J.; Uhlmann, P.; Stamm, M.; Esser, N.; et al. In Situ Studies on the Switching Behavior of Ultrathin Poly(acrylic acid) Polyelectrolyte Brushes in Different Aqueous Environments. *Langmuir* **2010**, *26*, 12926–12932 DOI: 10.1021/la101762f.
15 Pryamitsyn, V. A.; Leermakers, F. A. M.; Fleer, G. J.; Zhulina, E. B. *Theory of the Collapse of the Polyelectrolyte Brush*; 1996.
16 Mecea, V. M. From Quartz Crystal Microbalance to Fundamental Principles of Mass Measurements. *Anal. Lett.* **2005**, *38*, 753–767 DOI: 10.1081/AL-200056171.
17 Höök, F.; Kasemo, B.; Nylander, T.; Fant, C.; Sott, K.; Elwing, H. Variations in coupled water, viscoelastic properties, and film thickness of a Mefp-1 protein film during adsorption and cross-linking: a quartz crystal microbalance with dissipation monitoring, ellipsometry, and surface plasmon resonance study. *Anal. Chem.* **2001**, *73*, 5796–5804.
18 Liu, G.; Zhang, G. Chapter 1: Basic Principles of QCM-D. In *QCM-D Studies on Polymer Behavior at Interfaces*; Springer Science & Business Media, 2013; pp 1–8.
19 Hollingsworth, N. R.; Wilkanowicz, S. I.; Larson, R. G. Salt- and pH-induced swelling of a poly(acrylic acid) brush via quartz crystal microbalance w/dissipation (QCM-D). *Soft Matter* **2019**, *15*, 7838–7851 DOI: 10.1039/C9SM01289C.
20 Zhulina, E. B.; Birshtein, T. M.; Borisov, O. V. Theory of Ionizable Polymer Brushes. *Macromolecules* **1995**, *28*, 1491–1499 DOI: 10.1021/ma00109a021.
21 Almeida, B.; Shukla, A. Degradation of alkanethiol self-assembled monolayers in mesenchymal stem cell culture. *J Biomed Mater Res Part A J Biomed Mater Res Part A* **2017**, *105A*, 464–474 DOI: 10.1002/jbm.a.35922.
22 Bittrich, E.; Rodenhausen, K. B.; Eichhorn, K.-J.; Hofmann, T.; Schubert, M.; Stamm, M.; Uhlmann, P. Protein adsorption on and swelling of polyelectrolyte brushes: A simultaneous ellipsometry-quartz crystal microbalance study. *Biointerphases* **2010**, *5*, 159–167 DOI: 10.1116/1.3530841.
23 Tompkins, H. G. *A User's Guide to Ellipsometry.*; Elsevier Science, 1992.
24 Herzinger, C. M.; Yao, H.; Snyder, P. G.; Celii, F. G.; Kao, Y. -C.; Johs, B.; Woollam, J. A. Determination of AlAs optical constants by variable angle spectroscopic ellipsometry and a multisample analysis. *J. Appl. Phys.* **1995**, *77*, 4677–4687 DOI: 10.1063/1.359435.
25 Denolf, G. C.; Sturdy, L. F.; Shull, K. R. High-Frequency Rheological Characterization of Homogeneous Polymer Films with the Quartz Crystal Microbalance. *Langmuir* **2014**, *30*, 9731−9740 DOI: 10.1021/la502090a.
26 Sadman, K.; Wiener, C. G.; Weiss, R. A.; White, C. C.; Shull, K. R.; Vogt, B. D. Quantitative Rheometry of Thin Soft Materials Using the Quartz Crystal Microbalance with Dissipation. *Anal. Chem.* **2018**, *90*, 4079−4088 DOI: 10.1021/acs.analchem.7b05423.
27 Dixon, M. C. Quartz crystal microbalance with dissipation monitoring: enabling real-time characterization of biological materials and their interactions. *J. Biomol. Tech.* **2008**, *19*, 151–158.
28 Alassi, A.; Benammar, M.; Brett, D. Quartz Crystal Microbalance Electronic Interfacing Systems: A Review. *Sensors* **2017**, *17*, 2799 DOI: 10.3390/s17122799.
29 Zhang, X.; Chu, S. S.; Ho, J. R.; Grigoropoulos, C. P. Excimer laser ablation of thin gold films on a quartz crystal microbalance at various argon background pressures. *Appl. Phys. A Mater. Sci. Process.* **1997**, *64*, 545–552 DOI: 10.1007/s003390050514.
30 Sauerbrey, G. Verwendung von Schwingquarzen zur Wägung dünner Schichten und zur Mikrowägung. *Zeitschrift für Phys.* **1959**, *155*, 206–222 DOI: 10.1007/BF01337937.

31 Chu, X.; Yang, J.; Liu, G.; Zhao, J. Swelling enhancement of polyelectrolyte brushes induced by external ions. *Soft Matter* **2014**, *10*, 5568–5578 DOI: 10.1039/c4sm00860j.
32 Zhou, T.; Qi, H.; Han, L.; Barbash, D.; Li, C. Y. Towards controlled polymer brushes via a self-assembly-assisted-grafting-to approach. *Nat. Commun.* **2016**, *7*, 11119 DOI: 10.1038/ncomms11119.
33 Hiller, A.; Rubner, M. F. Reversible Molecular Memory and pH-Switchable Swelling Transitions in Polyelectrolyte Multilayers. **2003** DOI: 10.1021/ma025837o.
34 Silva, J. M.; Caridade, S. G.; Costa, R. R.; Alves, N. M.; Groth, T.; Picart, C.; Reis, R. L.; Mano, J. F. PH Responsiveness of Multilayered Films and Membranes Made of Polysaccharides. *Langmuir* **2015**, *31*, 11318–11328 DOI: 10.1021/acs.langmuir.5b02478.
35 Sukhorukov, G. B.; Schmitt, J.; Decher, G. Reversible swelling of polyanion/polycation multilayer films in solutions of different ionic strength. *Berichte der Bunsengesellschaft für Phys. Chemie* **1996**, *100*, 948–953 DOI: 10.1002/bbpc.19961000642.
36 Leyte, J. C.; Arbouw-van Der Veen, H. M. R.; Zuiderweg, L. H. Irreversible potentiometric behavior of isotactic poly(methacrylic acid). *J. Phys. Chem.* **1972**, *76*, 2559–2561 DOI: 10.1021/j100662a014.
37 Ghasemi, M.; Larson, R. G. Role of Electrostatic Interactions in Charge Regulation of Weakly Dissociating Polyacids. *Submitted to Macromolecules* **2020**.
38 Wu, T.; Gong, P.; Szleifer, I.; Vlček, P.; Šubr, V.; Genzer, J. Behavior of Surface-Anchored Poly(acrylic acid) Brushes with Grafting Density Gradients on Solid Substrates: 1. Experiment. *Macromolecules* **2007**, *40*, 8756–8764 DOI: 10.1021/ma0710176.

Chapter 4

Immobilization of Calcium Oxide onto Polyacrylonitrile (PAN) Fibers as a Heterogeneous Catalyst for Biodiesel Production

In collaboration with Sabina Wilkanowicz, Asst. Professor, Civil Engineering, Mechanics and Petrochemistry, Warsaw University of Technology, Warsaw, Poland

4.i Abstract

We describe the design, creation, and usage of a CaO catalyst immobilized onto polymeric mats for environmentally-friendly biodiesel production. The polyacrylonitrile (PAN) fiber mats were prepared by electrohydrodynamic processing (EHD), commonly known as electrospinning or electrospraying, in which immobilized CaO particles were either physically entrapped on the fibers or chemically bound onto the fiber surface by a dopamine linkage. These two catalyst materials were later successfully used in the transesterification of fresh canola oil into biodiesel. Mechanically entrapped CaO particles in the PAN fibers were able to be re-used up to six times in the conversion of triglycerides into biodiesel, while the chemically immobilized catalyst was found impossible to reuse. The use of EHD processing allows us to create an easily separable, reusable catalyst that could be commonly used in transesterification reactions.

4.ii Introduction

While the first experiments with biodiesel date back to 1900, when Rudolf Diesel first tried to use vegetable oil as an engine fuel, a serious focus on biodiesel started at the beginning of 21st century, when scientists discovered transesterification of vegetable oils, oils extracted from microalgae or animals, like fish as an efficient source of fuel production.[1-3] Since then, scientists

focused on making biodiesel production more environmentally friendly by lowering the amount of waste water used in purifying the product from the catalyst, on finding new, effective but environmentally safe catalysts, and on making the process easier. Biodiesel – a mixture of fatty acid methyl esters (FAME) [4,5] – can now be produced from renewable sources with 40-90% larger energy yields than the energy invested in fuel production.[6.] Thanks to its chemical composition, biodiesel can be used in compression-ignition (diesel) engines, with little or no modifications, mixed with mineral diesel or used as a pure fuel. Biodiesel is regarded as an environmentally friendly fuel because of its decreased in emissions of SO_x, CO, unburnt hydrocarbons, and particulate matter during the combustion process.[7,8] Apart from that, biodiesel can be produced from waste vegetable oils, which is a great way to recycle used cooking oils.

Biodiesel, as a non-petroleum fuel, is produced via chemical reaction, where triglycerides present in fatty acids (mostly vegetable oils) are broken down. This reaction is commonly known as transesterification or esterification, depending on the whether the catalyst used is basic or acidic, respectively.[9-11] During the transesterification reaction, triglycerides in the oil are broken down via the exchange of alkyl groups between an ester and an alcohol used as a second reactant. It is important to use good quality oils in the transesterification reaction, or to carry out the esterification reaction before the conversion into a fuel, in case there are free fatty acids (FFA) present in the oil. Also to be avoided is water, which can affect the transesterification reaction and cause hydrolysis (saponification) which would result in many undesirable products, and microbial growth, which can plug engine filters.[12,13] One of the most important characteristics of biodiesel is its viscosity. This physical property affects the operation of fuel injection equipment, especially at lower temperatures, when viscosity increases.[14,15] The purpose of biodiesel production via transesterification is to decrease the viscosity of the oil and render its physical properties similar

to those of conventional diesel fuels. A high fuel viscosity can affect its atomization and degrade the performance of the engine.[16,17] The most popular alcohol used in biodiesel production is methanol, because of its low production cost and its chemical and physical properties – including high polarity and short length, as well as having a higher reaction rate than that of other alcohols.[18,19] Ethanol is also commonly used in biodiesel production because it is derived from agricultural products and is less undesirable in the environment than other alcohols.[14,20] Other alcohols used in the transesterification reaction are propanol, butanol, and amyl alcohol.

Biodiesel production can be catalysed by acid and alkali catalysts and by enzymes, such as lipase.[21-23] Acid catalysts - including sulphuric, phosphoric, hydrochloric or organic sulfonic acids - are not as popular as alkali catalysts – which can be homogenous, as is the case for NaOH, KOH, and other alkoxides or heterogenous, as is true of metal oxides. The lack of popularity of acid catalysts arises because their reactions require a higher alcohol-to-oil molar ratio, a higher reaction temperature, and a longer reaction time.[24] Also, if the reaction is carried out at a temperature above the boiling point of the reacting alcohol, the pressure must be elevated to keep alcohol in the liquid phase. This can cause an increase in production costs due to the need for more resistant reactors. On the other hand, homogenous alkali-catalysts require various purification steps in which water is used to separate the catalyst from the biodiesel. This results in a massive amount of wastewater which can easily contaminate the environment or require more biodiesel production steps, such as waste-water purification.[18,25,26] In addition to this, during the purification step the biodiesel is emulsified, which causes a loss of biodiesel, environmental contamination with fatty acid methyl esters, and an extended production process, which raises its costs.[27]

Many of the problems that result from homogenous basic catalysts can be resolved by using a heterogenous basic catalyst. These catalysts present a lot of advantages: they are noncorrosive,

environmentally benign, nontoxic, and present fewer disposal problems. Heterogenous catalysts are much more easily separated from the liquid products and present similar activity to homogenous catalysts. In addition to these, the biggest advantages of using heterogenous catalysts are the longer catalyst lifetime and the possibility of reusing them in the biodiesel production process.[28-30] Among the most popular heterogenous basic catalysts are group II metal oxides, which have basicity that follows the order: MgO < CaO < SrO < BaO. The catalytic activities of these oxides in the transesterification reaction are also consistent with this order, but are less than those of the most popular homogenous catalysts such as KOH, or NaOH. It is believed that basic sites in the catalyst are generated by the presence of M^{2+}-O^{2-} ion pairs in different coordinations.[31-34] CaO has been found to be a very attractive catalyst in the biodiesel production process, because of its low cost, very low toxicity and solubility in methanol. Moreover, CaO is an alkaline earth metal oxide, which forms an ionic crystal, and the Lewis acidity of its cation is very weak due to its small electronegativity. The oxygen anion in CaO also presents strong basic properties.[18,35] Apart from that, CaO activity can be accelerated in the presence of a small amount (less than 2.8% by weight of oil) of water, because this increases the concentration of methoxide ions, which are the catalytic agents for transesterification reactions.[2,24,36] The transesterification reaction catalysed by CaO can be performed in mild conditions, at a reaction temperature under 80°C, environmental pressure, and short reaction times, less than 24h. CaO can be removed from the biodiesel after the production process, by centrifuging reactants or filtering them, for later, repeated, reuse in future transesterification reactions.[37,38]

Electro-hydrodynamic processing (EHP), also called electrospinning (when producing fibres) or electrospraying (when producing beads or capsules) is a one-step nano-technological tool commonly used in food, pharma, and cosmetics applications, which permits the production of

polymer micro-, submicro-, or nano-structures.[39–41] This technology allows utilization of any synthetic or natural polymer in any kind of solvent to produce fibril or bead nano-structures in "natural atmospheric conditions", meaning without use of harsh temperature, pressure or relative humidity.[40,42,43] Ultra-small beads or ultrathin fibres can be formed when the solution viscosity for electrospinning (mainly determined by polymer molecular weight and concentration), drops below a threshold value.[44] The advantages of EHP are high encapsulation efficiency, sustained immobilization or release of entrapped material, and greater thermal, light and storage stability. Because of their extremely high surface area and trapping efficiency, electrospinning and electrospraying has been proposed for a huge range of applications[45] and provides a novel route of stabilization of immobilized material.[46,47]

Electro-hydrodynamic processing has also previously been a technique of interest for various steps in biodiesel production. Chang et al.[48] focused on utilization of electrospun polymeric nanofibers as a catalyst for an esterification reaction. In this reaction, acetic acid and ethanol were transformed to esters via a reaction catalysed by perfluorosulfonic acid (PFSA) and poly(vinyl alcohol) (PVA) nanofibers. Other researcher groups used solid acid catalysts containing 13 wt% of nanocomposite made from Nafion resin and highly porous SiO_2 in transesterification reactions.[49,50] This special composition and catalyst assembly increased the number of acid sites due to the high specific surface area of silica nanoparticles, thereby improving the activity of the catalyst. The improvement of utilization of enzymes in transesterification reactions has become the focus of many research groups, and electrospinning is one way of accomplishing this. For example, immobilization of *Pseudomonas cepacia* lipase onto polymeric electrospun nanofibers has been shown to improve the performance of transesterification reactions. A catalyst immobilized onto fibres is highly exposed and in constant contact with all reactants, due to the high surface area of

the polymeric mat, which leads to high catalytic activity. Sakai[51]successfully immobilized *Pseudomonas cepacia* lipase onto electrospun polyacrylonitrile (PAN) fibres and used it in the transesterification reaction of oil and n-butanol. This immobilized enzyme was active for 20 days. Sakai used this method also to immobilize *Pseudomonas cepacia* lipase onto PAN fibres for transesterification reaction in nonaqueous solvents. They were able to reuse this immobilized catalyst for 10 times until the enzyme lost its activity.[52] While Sakai's researcher group immobilized lipase on PAN nanofibers by physical adsorption, Li et al.[53] immobilized lipase on PAN spun nanofibers by covalent binding. When covalently linked to the fibres, the immobilized enzyme retained 79% of the activity of the free lipase, and was used for biodiesel production from soybean oil. The catalyst was reused up to 10 times in the reaction and suggested that lipase immobilization onto PAN membrane enhanced its stability.[52,54] To enhance activity and stability of the enzyme during the transesterification reaction, Liu et al.[55] immobilized *Pseudomonas fluorescens* lipase with LiCl onto polyurethane (PU) nanofibers. The enzyme immobilized on the PU mat with 5 wt% addition of LiCl was able to catalyse the conversion of soybean oil to biodiesel with 90% efficiency. Youran Li et al.[56] modified the surface of a PAN hollow membrane by using nitrile-click chemistry to later interact it with lipase. They immobilized the enzyme onto the PAN-PEI membrane and added sodium alginate and $CaCl_2$ to encapsulate the enzyme molecules and increase the amount of immobilized enzyme. The membrane with immobilized lipase for later used for biodiesel production. They were able to reuse this modified membrane up to 20 times for transesterification of soybean oil.

In this work we successfully immobilized CaO onto electro-hydrodynamically processed polyacrylonitrile nanofibers by both mechanical and chemical binding, and we compare the advantages and disadvantages of the two binding techniques. This is the first report of

immobilization of CaO onto PAN fibres for biodiesel production. As mentioned above, this polymer had been used before to immobilize lipase, but never for immobilizing heterogenous catalysts.[51,52,54,56] The immobilized catalyst was then used to transesterify Canola oil and methanol into biodiesel and the chemical composition of the resulting FAME was analysed by FTIR spectroscopy. We found that the biodiesel produced with CaO immobilized onto polymers presented similar physical properties to biodiesel made with KOH and free-flowing (not immobilized) CaO catalyst. The catalyst immobilized chemically with dopamine on PAN did not present as favourable properties as those obtained when the CaO was mechanically immobilized onto PAN. The former required additional immobilization steps during the process; its reaction was also slower than that of the mechanically immobilized catalyst and it produced a mat that could not be reused in additional transesterification reactions. The mechanically entrapped CaO-PAN mat, on the other hand, was able to be reused in transesterification reactions up to 6 times. Finally, the reaction time, efficiency and conditions were similar to ones applied in the transformation of Canola oil to biodiesel with free-flowing CaO.

4.iii Materials and Methods

4.iii.a Materials

Polyacrylonitryle (PAN, Mw ~ 150,000 g/mol) was received in free-flowing fine powder, from Sigma-Aldrich (USA). Dopamine hydrochloride (DOPA), dimethylformamide (DMF, ≥ 99%, molecular biology grade), Methanol (≥ 99.9%, HPLC grade) and ethanol (≥ 96%, HPLC grade) were purchased from Sigma-Aldrich (USA) and used as received. Cooking oil - Canola oil was purchased from a local grocery store (Kroger, USA). Calcium oxide (CaO, ≥ 97%, analytical grade) was purchased from Fisher Scientific (USA).

4.iii.b Preparation of polymer solutions

PAN polymer was dissolved in DMF, by stirring the solution at 80°C. The final concentration of PAN in DMF was 10% (w/v). PAN-CaO solution was prepared by dissolving PAN and suspending CaO in DMF while stirring the mixture at 80°C. Final concentrations of PAN and CaO in the solution were 10% (w/v) and 5% (w/v), respectively.

4.iii.c Preparation of polymeric mats via electrospinning

The electrospinning apparatus, equipped with a variable high-voltage 0-30kV power supply, was assembled in-house. The anode was connected to a stainless-steel needle (Ø 0.9 mm) connected directly to the 10 ml plastic syringe. The electrospinning process parameters for each solution are presented in Table 4.i. The disc-shaped copper ground electrode was connected to a stainless-steel plate, where all fiber mats were collected. The experimental setup was housed in a laminar flow safety cabinet.

4.iii.d Chemical immobilization of CaO on PAN nanofibers

After EHD processing, the polymeric fibrous mat was activated by Pinner reaction.[57-60] 4 grams of PAN mat was suspended in 200 g of 96 % of ethanol and 2 % of 0.2N HCl. The mixture was left for 24h under slow shaking in room conditions. After the activation reaction, the mat was washed 4 times with pure ethanol and suspended in 200 g of 96 % ethanol with 300 mg of dopamine (DOPA) and 2 g of previously sonicated CaO. The mixture was left under the same conditions, as in the activation step. When the reaction finished, the mat was washed 6 times with pure ethanol, until the washing solution was pure and clear from excess CaO used in the reaction.

It was then dried and weighed, to analyze how much of the CaO was bonded to the PAN mat by dopamine.

4.iii.e Amount of immobilized CaO analysis

The amount of catalyst mechanically and chemically immobilized to the PAN mats was determined using two methods, one by using an acid–base titration[61] and second one was calculated by known weights and proportions of used CaO and PAN.

In brief, a sample of a PAN mat with catalyst chemically or mechanically immobilized was weighed. The CaO in the polymer mat was dissolved in a 50 cm3 0.1 mol/L HCl solution. The mixture was shaken for 2 hours at room temperature to let reaction products to escape from the PAN fibers. The reaction of CaO with HCl created CaCl2 and H2O. The amount of original CaO was calculated from the amount of reacted HCl, which in turn was determined by titrating it against 0.05 mol/L NaOH using phenolphthalein as a reaction indicator.

The second method was used to determine a catalyst amount for mechanically immobilized CaO, made by electrospinning, the known amount and proportion of PAN and CaO used in the electrospinning mixture and the weighed mass of PAN-CaO mat made in the process allowed calculation of the amount of the catalyst.

In the case of PAN-DOPA-CaO, the PAN mat used to chemically immobilize CaO using the DOPA linker was weighed both before and after catalyst immobilization and the CaO amount was obtained by difference.

4.iii.f Scanning Electron Microscopy and Scanning Transmission Electron Microscopy

SEM and STEM were conducted on a Helios NanoLab 650 microscope (Thermo Fisher Scientific) with an accelerating voltage of 10 kV for SEM and 25-30 kV for STEM and a working distance of 40 mm. Analyzed samples were not sputtered with any conductive coating. Fiber diameters of all materials were measured by means of ImageJ software from the SEM micrographs in their original magnification.

4.iii.g Infrared spectroscopy

Fourier transform infrared spectra (FTIR) were collected by using the attenuated total reflection (ATR) attachment on a Nicolet iS50 FT-IR (Thermo Fisher Scientific) spectrometer. Single spectra were averaged over 16 scans at 4 cm-1 resolution in the wavelength range from 4000 to 400 cm-1. All experiments were performed in duplicate.

4.iii.h Transesterification reaction

Canola oil and methanol were mixed in a molar ratio 1:6, in a total volume of 50 cm3, placed into the flask equipped with a magnetic stirrer and thermometer and heated to 55°C. When 55°C was reached, 1 g of the catalyst was added to the mixture when free-flowing CaO and approximately 1 g of mechanically entrapped CaO (PAN-CaO) were used. On the other hand, approximately 0.5 g of the catalyst was added at this point in case of chemically bonded CaO (PAN-DOPA-CaO). It was impossible to use higher amount of CaO chemically immobilized to PAN fibers, because of extensively high mat volume, that would soak all the reactants and block the reaction. The highest possible CaO amount, chemically immobilized to the polymer was approximately 0.5 g. The transesterification time was optimized for all different reactions to obtain the best yields. The reaction was conducted for up to 4 hours, when free-flowing CaO was used as a catalyst, and up to 8 and 24 hours, when PAN-CaO and PAN-DOPA-CaO catalyst were used,

respectively. The transesterification reaction time was monitored by FTIR and kinematic viscosity analysis of the samples. After the reaction with CaO, the mixture was centrifuged for 15 minutes, at 5000 rpm and room temperature conditions, during which three phases appeared – a top layer of biodiesel, and lower layers of glycerol and CaO pellets. PAN-CaO and PAN-DOPA-CaO were removed from the reaction environment immediately after the reaction stopped. Biodiesel samples from the reaction conducted via immobilized CaO were left to separate, with no additional centrifugation. The biodiesel was collected for FTIR and analysis of physical properties. All catalysts were recycled for repeat transesterification reactions.

4.iii.i Physical properties analysis

All viscosity and density measurements were taken at 20℃ and atmospheric pressure. Dynamic viscosity measurements of polymer solutions were performed with the MCR 702 Rheometer (Anton Paar). The kinematic viscosities of the oil and all biodiesel samples were measured with AVS 350 Viscometer (Schott, Germany). The densities of oil and biodiesel samples were measured by pycnometry.

4.iii.j Quantification of CaO concentration in biodiesel after transesterification process

Analysis of CaO concentration in biodiesel was made using FTIR spectroscopy. First, a calibration curve was prepared. To do so, CaO powder was suspended in 1 cm3 of biodiesel made from the same Canola oil, as analyzed biodiesel samples, and KOH used as a transesterification catalyst. 200 mg, 100 mg, 50 mg, 25 mg, 12.5 mg, 6.25 mg and 3.125 mg of CaO was suspended, to obtain biodiesel samples with CaO concentrations: 20, 10, 5, 2.5, 1.25, 0.625 and 0.3125%. All samples were vortexed before taking each FTIR spectra on a Nicolet iS50 FT-IR (Thermo Fisher Scientific) spectrometer. Single spectra were averaged over 16 scans at 4 cm-1 resolution in the wavelength

range from 4000 to 400 cm-1. All experiments were performed in duplicate. After FTIR analysis, characteristic for CaO peak absorbance on the wavelength 3643 cm-1 was detected for all analyzed samples and a calibration curve was created. After preparing the calibration curve, the FTIR test was repeated for all biodiesel samples made using free flowing CaO, mechanically immobilized PAN-CaO, and PAN-DOPA-CaO. The absorbance on the wavelength 3643 cm-1 was detected and amount of leaching of CaO in each sample was calculated from the calibration curve.

4.iv Results and Discussion

The transesterification reaction of fatty acids with methanol has become a very popular procedure for the production of biodiesel, commonly used as a biofuel in diesel engines. Actually, it is more common to blend biodiesel with mineral diesel, rather than using 100% biodiesel as a fuel. The most common blend ratio is 20%, where 80% of the fuel comes from mineral diesel, and 20% comes from biodiesel obtained from transesterification of oil [62,63]. In the U.S.A. alone, biodiesel production has increased from 343 million gallons in 2010 to 1.278 billion gallons in 2014 – a 272% increase over just a five-year period [64]. This shows how important biodiesel production is and how important it is to reduce the cost of production of this fuel. One path to make biodiesel production more efficient and environmentally friendly is through the use of heterogenous, reusable, alkaline catalysts for transesterification reactions. As discussed above, calcium oxide has become a very popular basic heterogenous catalyst in biodiesel production. CaO can be derived from many natural sources, such as shells, rocks, and chitosan, making it a cheap and natural catalyst. Calcium oxide is also more environmentally friendly than homogenous catalysts, such as KOH or NaOH, because CaO doesn't produce waste water from the additional washing steps needed to purify the biodiesel from the catalyst after the transesterification reaction. Despite that, biodiesel production using a CaO catalyst nevertheless requires additional steps of

fuel purification, such as filtration or centrifugation to remove CaO from reactants. This step is not as harsh to the environment as fuel washing, but still increases biodiesel production costs – by requiring special expensive equipment. If not filtered or centrifuged out, the CaO can contaminate the fuel and affect its physio-chemical properties. An ideal solution to this problem is to immobilize CaO onto polymeric mats, which allow the catalyst to work, while also making the production process faster and cheaper by eliminating steps. In the work described here, electrohydrodynamic processing (EHD) was used to chemically and mechanically immobilize CaO particles onto and into non-degradable (polyacrylonitrile, PAN) polymer fibers.

4.iv.a Immobilization of calcium oxide onto polymeric fibers via electro-hydrodynamic processing

Polyacrylonitrile (PAN) fibers were used as the encapsulant material or as the immobilizing scaffold for CaO particles, for mechanical or chemical immobilization, respectively. To do so, 10% of PAN was dissolved in DMF and 5% of CaO particles were added to the polymeric solution to be processed to obtain nanofibers with CaO particles entrapped in the polymer via the EHD technique. A PAN solution without CaO was also processed, to compare the fiber composition of materials with and without immobilized catalyst, and to prepare a scaffold to immobilize the catalyst via a chemical method. In Table 4.i, all EHD process conditions for both electrospun polymeric solutions are presented.

Table 4.i. Electro-hydrodynamic processing parameters of polymeric solutions of PAN, PAN-CaO and their physical properties

Sample	Voltage [kV]	Flow rate [cm^3/h]	Distance injector-collector [cm]	Viscosity [Pa·s]
PAN	11	1	15	1.15
PAN-CaO	13	1	15	1.08

The chemical bonding of CaO onto PAN fibers required additional steps of preparation. First, a polymeric mat was activated via a Pinner reaction[57-60] to obtain imidoesters on PAN fibers. After activation of the fibers, the mat the second step of the procedure was performed – an amidination reaction, where DOPA-CaO can bind to previously activated PAN fibers. The procedure is presented in Figure 4.i.

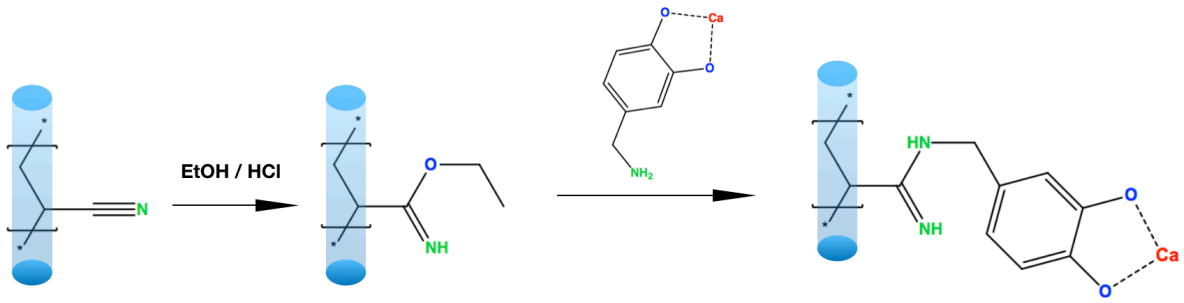

Figure 4.i. Chemical immobilization of CaO onto PAN fibers that had been previously activated with Pinner reaction.

The amount of bonded CaO was determined by weighing the mat before and after the immobilization process. The weight of the PAN fiber mat increased from 4 g before linking it with the catalyst to a dry weight of 4.5 g afterwards, implying that around 500 mg of CaO was immobilized onto the PAN fibers by a dopamine linkage. According to the titration measurements, the amount of CaO in the PAN-DOPA-CaO mat was approximately 0.92 g, which is close to the calculated from mat weight – 1 g. In case of PAN-DOPA-CaO, the mass of the catalyst calculated from titration method was 0.44 g, and 0.5 g calculated from the weights of CaO and PAN mat. The

accuracy of the procedure was also determined by scanning transmission electron microscopy and FTIR analysis.

The electron micrographs in Figure 4.ii reveal the nanofibrous structure of PAN with and without CaO particles immobilized onto them. All fibers made from PAN with or without CaO particles are homogenous (Figure 4.ii, A(i), B(i), C(i)). For PAN fibers inside of which CaO is mechanically entrapped, here called "PAN-CaO," it is possible in Figure 4.ii B(i) to observe some small beads – i.e., tiny grains, representing CaO particles, indicated on the micrograph with arrows. For PAN fibers with chemically bonded CaO, here called "PAN-DOPA-CaO," it is very difficult to observe in Figure 4.iiC(i) the presence of the catalyst particles on the PAN fibers at this magnification, although some very tiny beads stuck to the fiber surface are marked on the figure with arrows.

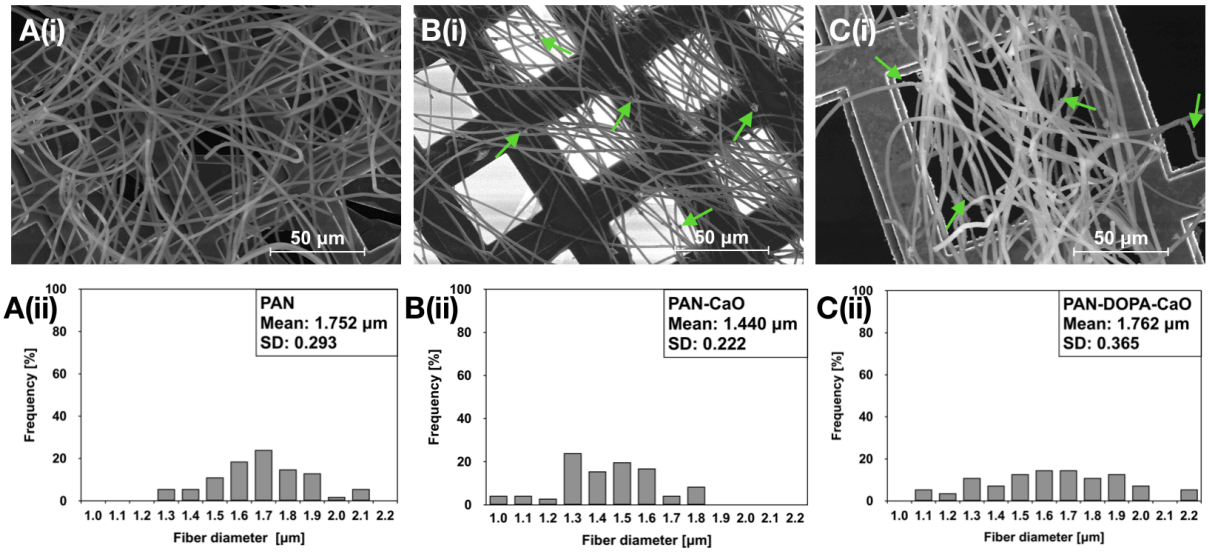

Figure 4.ii (A-C)(i&ii). Top: Scanning Electron Microscopy of PAN nanofibers (A(i)), PAN fibers with CaO mechanically immobilized onto them (B(i)) and PAN fibers with chemically immobilized CaO catalyst onto the fibers (C(i)). Green arrows indicate CaO beads presence along the PAN fibers in both materials, where the catalyst was immobilized. Bottom: Fiber size diameter distribution of PAN, PAN with CaO mechanically immobilized onto the fibers and PAN with CaO particles chemically immobilized on the fibers (A(ii), B(ii) and C(ii) respectively).

It was possible to observe the real surface morphology of this material only at the larger magnification presented in Figure 4.iii. The fiber diameter did not change much when CaO

particles were entrapped in the polymer or immobilized onto them, as can be seen by comparison of the fibers in Figure 4.ii, B(i) and C(i) to those of the pure PAN mat in Figure 4.ii, A(i). The average fiber size diameter of pure PAN was 1.752 μm (Figure 4.ii, A(ii)), of PAN-CaO was 1.440 μm (Figure 4.ii, B(ii)) and was 1.762 μm for PAN-DOPA-CaO (Figure 4.ii, C(ii)). The reason for this change in fiber diameter (albeit rather small) for PAN-CaO might be the addition of CaO to the PAN solution before processing it via EHD. Adding any conductive agent to the spinning solution can affect surface tension, conductivity and viscosity of the polymeric solution and possibly make the polymer stretch more resulting in thinner fibers.

All materials were characterized using scanning and transmission electron microscopy (SEM and STEM, respectively) to determine the positions of the CaO particles bonded to the PAN fibers, either mechanically or chemically. Pure PAN fibers didn't show any particles inside or outside the material (Figure 4.iii, A(i) and (ii) for SEM and STEM respectively). PAN-CaO fibers made by spinning the solution of PAN with CaO particles suspended in it had particles encapsulated within and/or attached outside the fibers (Figure 4.iii, B (i) and (ii)). Red arrows on the micrographs indicate a few of the many beads and particles of the catalyst along the PAN fibers, but in many cases do not clearly show whether the particles are inside or outside of the fiber. CaO particles smaller than the fiber diameter could be entrapped without affecting the fiber structure, suggesting that a fraction of the CaO powder might become encased within the fibers during EHD processing. But particles bigger than the fiber diameter are quite clearly attached to the outside of the PAN fiber. For PAN-DOPA-CaO, the CaO particles were chemically immobilized onto the PAN fibers, mostly on the outside (Figure 4.iii, C(i) and (ii), with red arrows indicating CaO particles). We suppose, however, that some fraction of CaO might react with activated PAN and bond even inside the fibers.

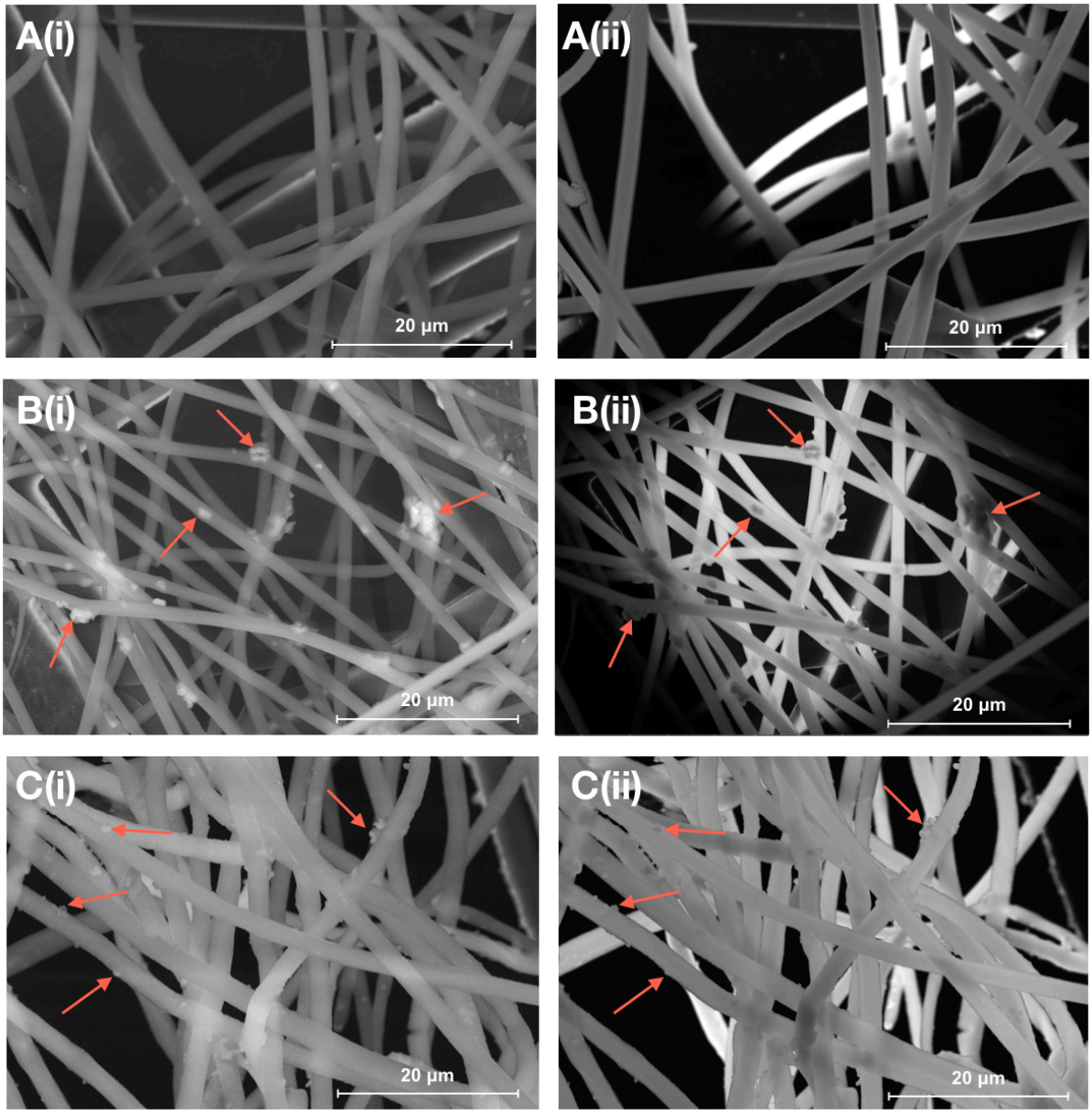

Figure 4.iii(A-C)(i&ii). Scanning Electron Microscopy (i) and Scanning Transmission Electron Microscopy (ii) of PAN nanofibers (A), PAN fibers with CaO mechanically immobilized onto them (B) and PAN fibers with CaO catalyst chemically immobilized onto the fibers (C). Red arrows indicate CaO particles.

PAN fibers with CaO particles immobilized both chemically and mechanically were also analyzed after reusing the mats 7 times for PAN-CaO and a single time for PAN-DOPA-CaO (Figure 4.iv, A and B, respectively), in transesterification reactions. The fiber structures and diameters of mats of both PAN-CaO and PAN-DOPA-CaO were left nearly unchanged by transesterification

reactions. For both, CaO particles (indicated by red arrows in Figure 4.iv), were still bonded to the material, suggesting that all materials studied in this paper were able to retain immobilized catalyst on the polymeric mat even after reuse.

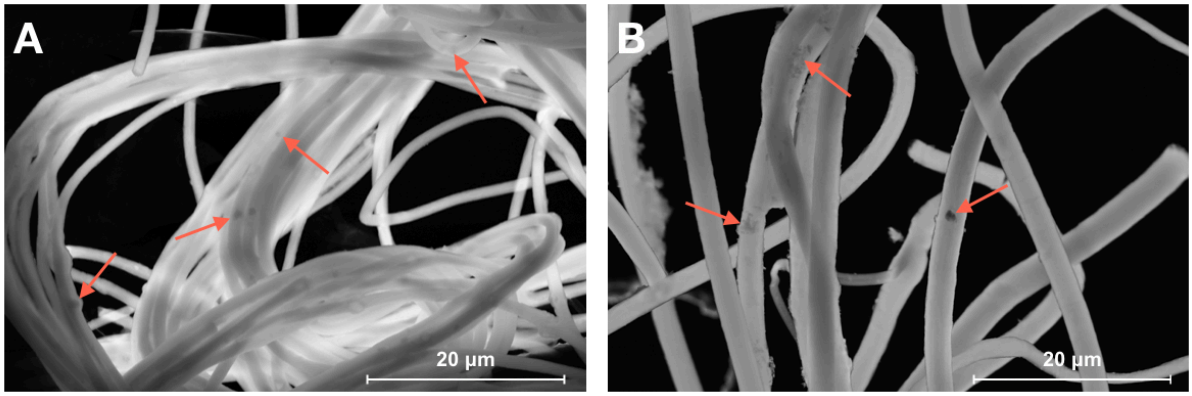

Figure 4.iv(A&B). Scanning Transmission Electron Microscopy (STEM) of PAN fibers with CaO mechanically immobilized (A) and chemically immobilized (B) after have been used in biodiesel production. Red arrows indicate CaO particles still stuck to the PAN fibers after a transesterification reaction repeated 8 (A) and 2 (B) times.

After morphological analysis via electron microscopy, all materials made from PAN with and without immobilized CaO, as well as the pure CaO catalyst powder, were characterized using FTIR spectroscopy, giving the spectra shown in Figure 4.v. Two characteristic peaks for CaO were observed at wavelengths 874 and 3634 cm^{-1} (Figure 4.v, B), representing catalyst particles. The FTIR spectra of pure PAN fiber mats were the same as that of pure PAN FTIR data in the literature [65] and were of course missing the characteristic CaO peaks at wavelengths 874 and 3634 cm^{-1} (Figure 4.v, A). After chemical and mechanical immobilization of CaO onto polymeric PAN fibers via EHD processing, these two peaks also appeared in the spectra for PAN-CaO and PAN-DOPA-CaO materials (Figure 4.v, C and D, respectively), proving proper immobilization of the catalyst. After the above chemical composition and physical structure characterizations, both materials were used in the transesterification reaction of cooking oil, to analyze their utility in the biodiesel production process.

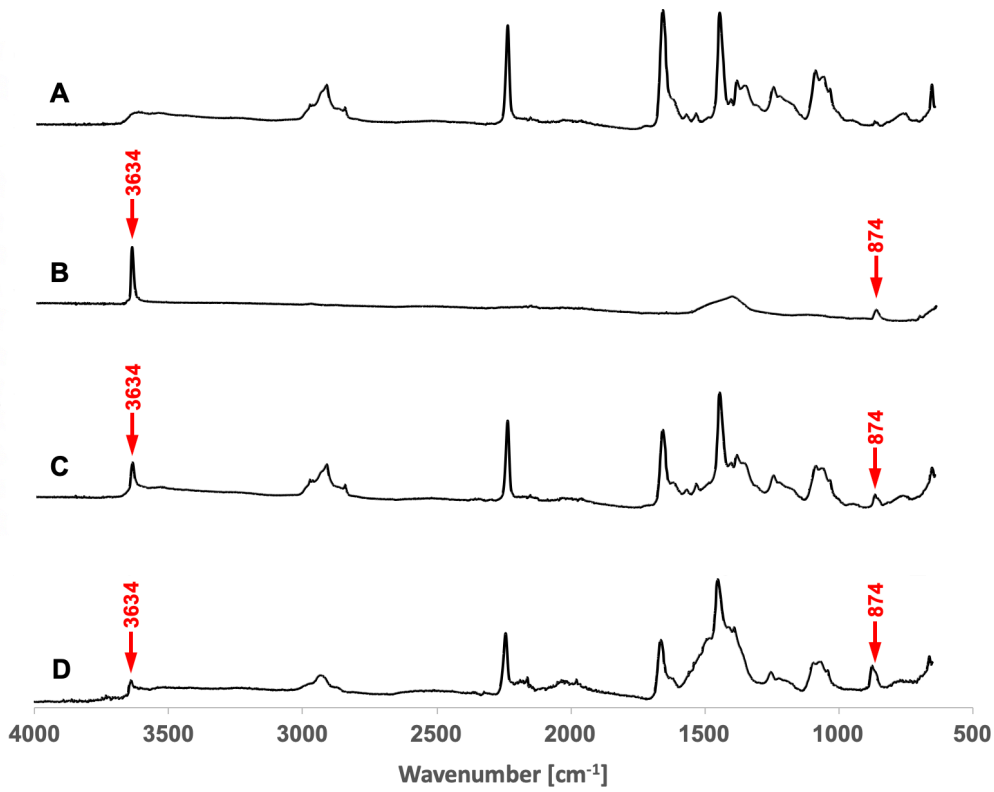

Figure 4.v (A-D). FTIR spectra of CaO powder (A), PAN nanofibers (B), PAN nanofibers with mechanically immobilized CaO – PAN-CaO (C) and PAN nanofibers with chemically immobilized CaO – PAN-DOPA-CaO (D).

4.iv.a Transesterification reaction of Canola oil by CaO immobilized onto polymeric fibers

To transesterify Canola oil and methanol into biodiesel, four different catalysts were used, namely KOH, as a typical catalyst used commonly in transesterification of oils, CaO in powder form, and CaO immobilized into two PAN polymeric mats. Thanks to immobilization, samples of biodiesel made via reaction catalyzed by chemically and mechanically immobilized CaO could be compared to samples made using not-immobilized CaO and KOH. All reactions were performed under the same conditions, at 55°C and atmospheric pressure, with stirring at around 700 rpm. The weight of catalyst per mass of fiber and the molar ratio of reactants (1:6 oil:methanol) were also the same for each reaction. Only for PAN-DOPA-CaO was the catalyst weight lower (by two-fold), evidently because of less efficient chemical binding of CaO onto the PAN mat. The reaction

time varied for each sample to produce the highest yield for each reaction. Production of biodiesel via catalysis by KOH lasted 3 hours. When free-flowing CaO was used, the reaction stopped after 4 hours, while twice as much time (i.e., 8 hours) was required for catalysis by PAN-CaO. In each case, when the reaction finished, the samples with KOH used as a catalyst were left to phase separate for 12 hours, at room conditions, producing an upper phase of biodiesel and a lower one of glycerol. The sample for which free-flowing CaO powder was used was centrifuged for 15 minutes at 5000 rpm and room temperature. After centrifugation, the sample was separated from the catalyst and left to phase separate, just as with the previous sample. The samples that used immobilized CaO were separated from the catalyst by simply removing the polymeric mats from reaction flask. The phase separation of biodiesel from glycerol was allowed to occur over time, just as when KOH was used as a catalyst. After separation, all biodiesel samples were collected into new flasks to analyze reaction yield and the samples' kinematic viscosity and density. Reaction yield was measured by weight of used-in-reaction Canola oil and obtained biodiesel, and is presented by Equation 4.1.[26]

$$E = \frac{m_B}{m_O} \cdot 100\% \qquad [4.1]$$

Here E is the reaction yield, m_B is the mass of biodiesel obtained in the transesterification process, and m_O the mass of Canola oil used in the reaction. The yield of the transesterification catalyzed with KOH was 92% while those from the free CaO powder and PAN-CaO were both 89%. The reaction catalyzed with PAN-DOPA-CaO had the lowest yield of 75%, which was probably the result of usage of a lower amount of the catalyst.

Table 4.ii presents the physical properties and reaction times for all biodiesel samples produced with various catalysts – KOH, free-flowing CaO, and chemically and CaO mechanically

immobilized onto PAN fibers. The viscosities and densities of all analyzed biodiesel samples were compared to those for Canola oil and to a biodiesel sample, whose reaction was catalyzed with KOH. The viscosity and density of the samples match closely the literature values for biodiesel samples, measured at 20℃.[66,67]

Table 4.ii. Process production and biodiesel physical properties of samples made using KOH, CaO, PAN-CaO and PAN-DOPA-CaO catalysts. All measurements were taken at 20℃. Literature data for kinematic viscosity and density measured at 20℃ are: 74.2 mm^2/s and 0.9145 kg/dm^3 for Canola oil and 3.5-8.2 mm^2/s and 0.82-0.9 kg/dm^3 for biodiesel

Sample	Reaction yield [%]	Reaction time [h]	Viscosity [mm^2/s]	Density [kg/dm^3]
Canola oil	N/A	N/A	72.52	0.888
KOH	92	3	5.27	0.849
CaO	89	4	5.63	0.831
PAN-CaO	89	8	5.33	0.835
PAN-DOPA-CaO	75	24	5.81	0.841

After analysis of the physical properties of biodiesel samples, their chemical composition was also analyzed, using FTIR spectroscopy. Figure 4.vi contains the FTIR spectra of Canola oil and all biodiesel samples obtained from different catalysts – KOH, CaO powder, labelled "CaO", and CaO immobilized mechanically and chemically onto PAN fiber mats, labelled in Figure 4.vi "PAN-CaO" and "PAN-DOPA-CaO." The most evident changes between Canola oil and biodiesel spectra appear in the spectral wavenumbers between 800 and 1600 cm^{-1}. The FTIR spectra of all biodiesel samples synthesized here show similar chemical composition to each other and to other biodiesel samples in the literature.[68]

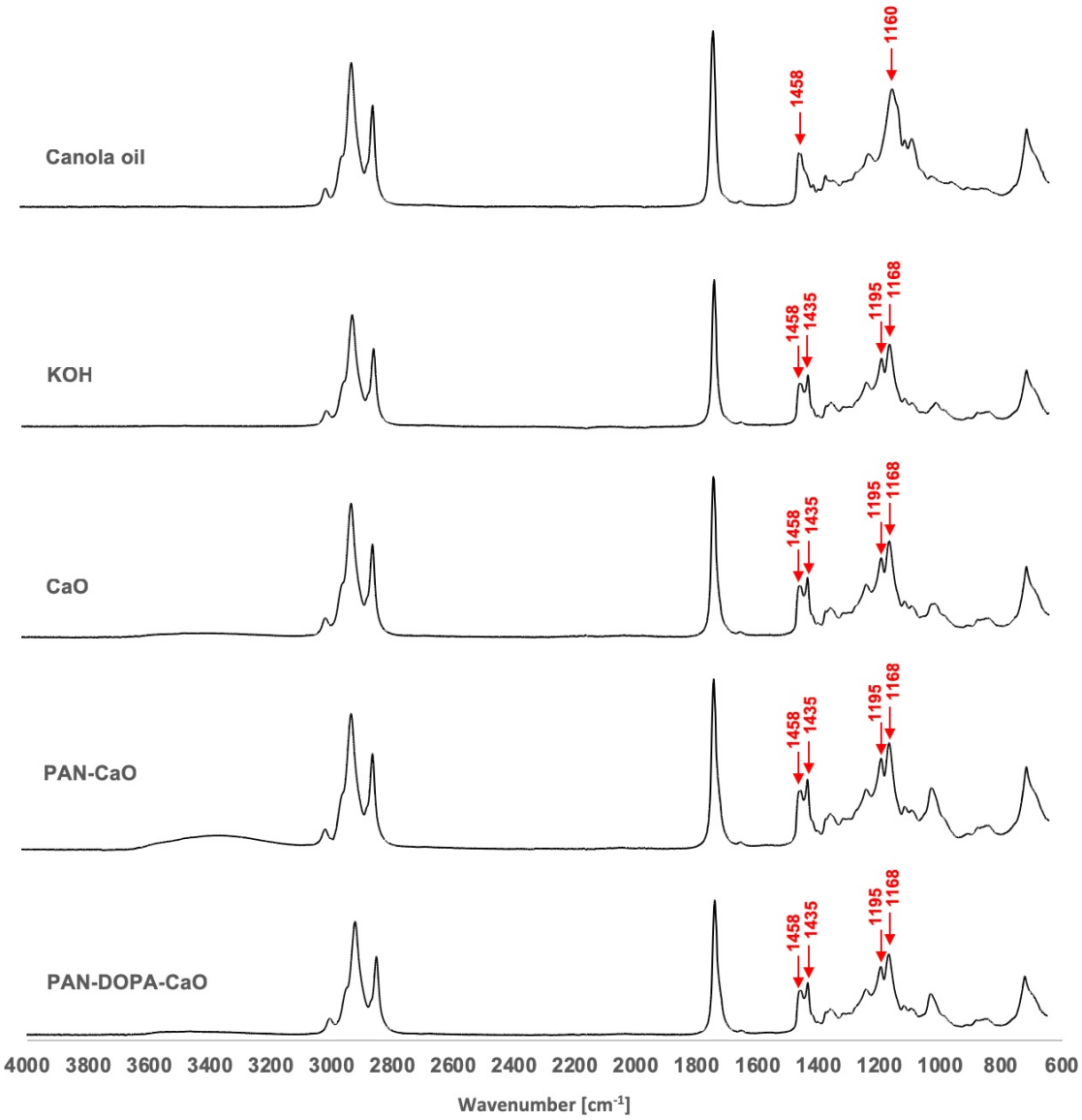

Figure 4.vi. FTIR spectra of Canola oil, standard sample of FAME and biodiesel samples made using of different catalysts: KOH, CaO, PAN-CaO and PAN-DOPA-CaO, the first of which was dissolved in the reaction mixture and the second one was free flowing. Arrows highlight peak changes in samples before and after transesterification reaction.

One of the most characteristic differences between the spectrum of Canola oil and those of biodiesel samples is the appearance of a new signal at 1435 cm^{-1}, which corresponds to the vibration of the methyl ester group. This signal is present in the FTIR spectra of all biodiesel samples, produced by the transesterification reaction catalyzed by KOH, CaO powder and CaO immobilized onto PAN fiber mats (Figure 4.vi). Interestingly, after Canola oil transformation, a

strong, broad signal at 1160 cm^{-1} in the oil separated into two sharper signals at 1168 and 1195 cm^{-1} for all biodiesel samples, which correspond to C-O-C group-stretching vibrations.

The transesterification reaction rates of biodiesel samples in which CaO was used as a catalyst (in all forms – free-flowing, chemically and mechanically immobilized) were measured to determine biodiesel conversion with time. Before starting the reaction, both the kinematic viscosity and FTIR of each sample were measured. During transesterification of canola oil with the three different forms of the CaO catalysts, samples were collected and their FTIR spectra (between 1050 and 1500 cm^{-1}) determined for each biodiesel sample, as shown in Figure 4.vii. For free-flowing CaO, after 2 hours of transesterification, clear peaks at wavelengths 1168, 1195 and 1435 cm^{-1} became evident, and further changes in the spectrum ceased after 4 hours as shown by the identical spectra at 4 and 6 hours of the reaction (Figure 4.vii, "CaO").

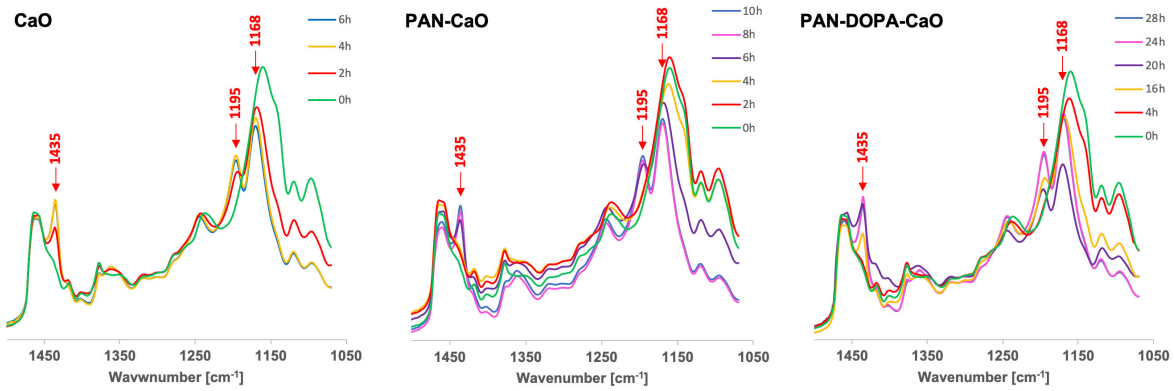

Figure 4.vii. Enlarged versions of important region of FTIR spectra of biodiesel samples made with different CaO catalyst linkages, including free-flowing CaO at different times after start of the reaction.

The reaction kinetics measured with FTIR spectrophotometry was also confirmed by the decreasing kinematic viscosity of the sample (Figure 4.viii) over time, implying an increase in fatty acid methyl esters – biodiesel compounds, and a decrease in triglycerides, from Canola oil. During the reaction conducted with free-flowing CaO, the kinematic viscosity of the mixture

decreased rapidly until, after 4 hours of the process, it stopped changing, meaning that conversion of Canola oil into biodiesel had come to completion (Figure 4.viii, solid line).

Biodiesel production with PAN-CaO took twice as long as the reaction with free-flowing CaO. After 6 hours of reaction, the characteristic FTIR biodiesel peaks appeared (Figure 4.vii, "PAN-CaO"). After 8 hours, when the reaction had been completed, all peaks reached their typical steady-state intensities. The reaction time was confirmed by analysis of the kinematic viscosity of the samples collected over time (Figure 4.viii, dashed line). After 6 hours of transesterification conducted by the PAN-CaO catalyst, the kinematic viscosity was low, and after 8 hours, remained constant up to 10 hours, meaning that the transesterification reaction was completed by 8 hours.

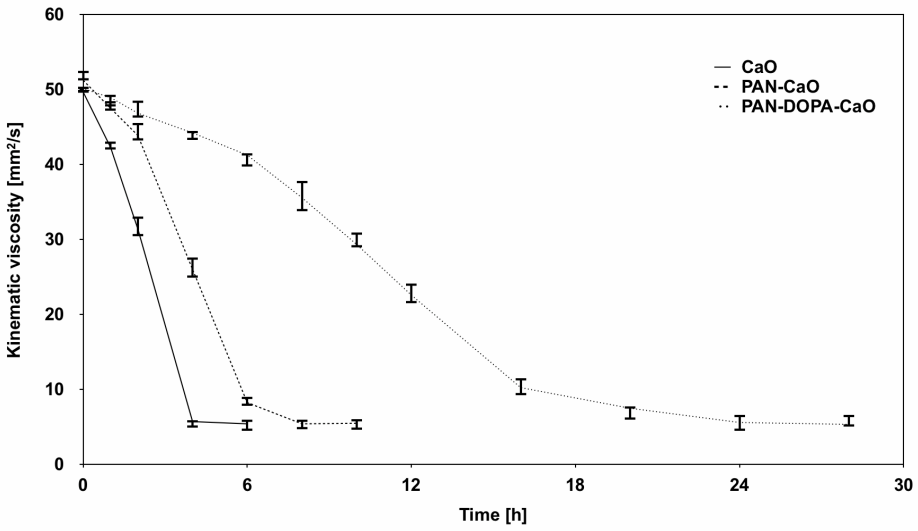

Figure 4.viii. Kinematic viscosity during biodiesel conversion as a function of time of samples made by using CaO catalyst (CaO, solid line), CaO catalyst immobilized mechanically in PAN nanofibers (PAN-CaO, dashed line) and CaO catalyst immobilized chemically in PAN nanofiber (PAN-DOPA-CaO, dotted line).

The transesterification reaction via PAN-DOPA-CaO was the slowest, and took around 20 hours to transform Canola oil almost completely into biodiesel (Figure 4.vii, "PAN-DOPA-CaO"). The sample's kinematic viscosity and chemical composition, analyzed via FTIR (Figure 4.viii), dotted line), was acceptable for biodiesel. After 24 hours of the reaction conducted by PAN-DOPA-CaO, the FTIR spectrum of the sample presented peaks characteristic for biodiesel, and the

kinematic viscosity remained stable – meaning the Canola oil was completely processed into the fuel. This difference in reaction times between samples of biodiesel made with mechanically and chemically immobilized CaO (PAN-CaO and PAN-DOPA-CaO, respectively) and one conducted with free-flowing CaO is probably the result of impeded contact of reactants (triglycerides and methanol) when the catalyst is entrapped inside the PAN fibers or bonded to them by dopamine linkages, making access of the catalysts by the reactants more difficult. EHD processing is commonly used as a technique of encapsulating bioactives (e.g. catalysts, enzymes) to protect them from the external environment. This can explain the slower reaction times for biodiesel production with immobilized CaO catalyst.[40,43] However, chemically immobilized CaO with a dopamine linkage to PAN fibers (PAN-DOPA-CaO), only allowed half of the mass of catalyst used in other transesterification reactions conducted with CaO powder or PAN-CaO to be bonded. And since the area of the PAN-DOPA-CaO mat is fixed, it was impossible to use the same amount of CaO during the reaction, and hence the lower density of catalyst in the PAN-DOPA-CaO mat, compared to the others, probably accounts for its slower reaction rate.

As a result of biodiesel synthesis, CaO may appear in the biodiesel samples, and we quantified the amount in samples made via transesterification of Canola oil using the different catalysts – namely CaO powder, and CaO mechanically and chemically immobilized onto PAN. To do so by FTIR spectroscopy, a calibration curve was created by deliberately adding 200mg, 100mg, 50mg, 25mg, 12.5mg, 6.25mg and 3.125mg of CaO powder per 1 ml of biodiesel sample to yield final CaO concentrations in the biodiesel samples of: 20%, 10%, 5%, 2.5%, 1.25%, 0.625%, 0.3125%, and mixing well, using a vortex shaker. The spectral peak at wavelength 3643 cm^{-1}, which is characteristic for CaO, was chosen for FTIR characterization of CaO concentrations.

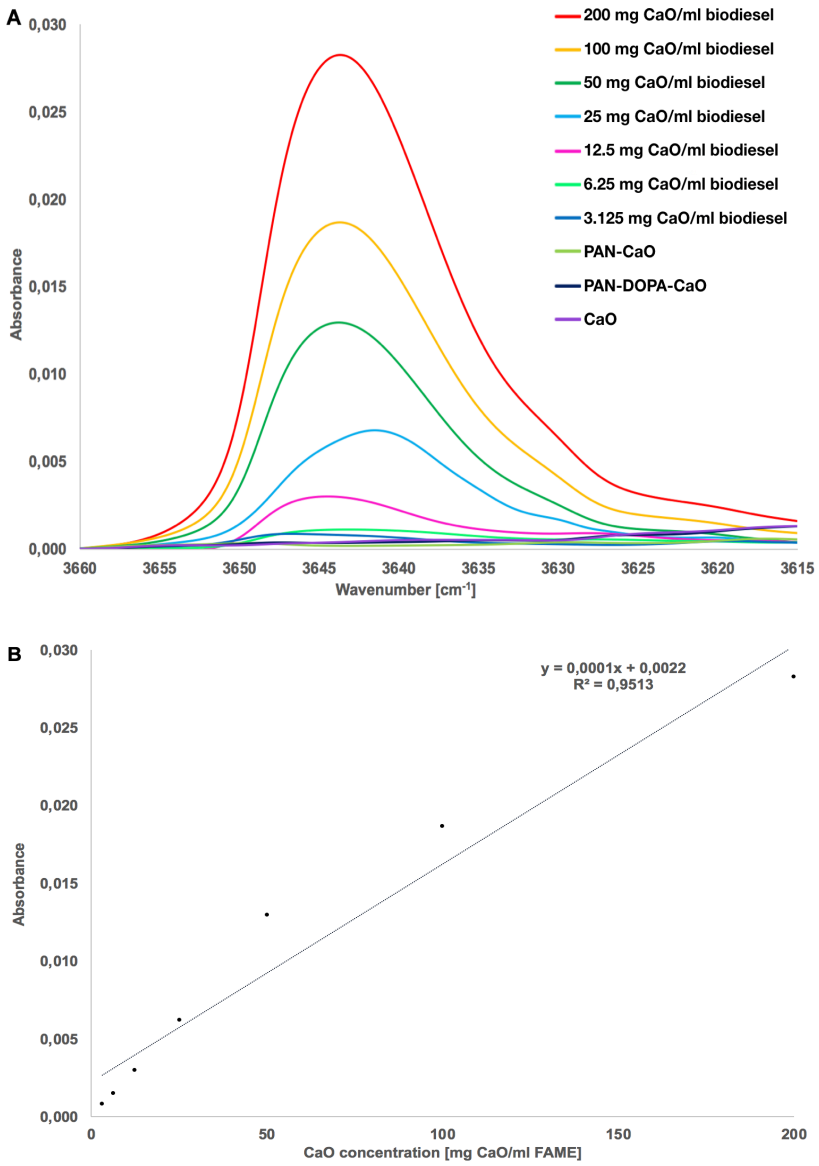

Figure 4.ix (A&B). Left: FTIR spectra of peak at 3643 cm-1 for biodiesel samples with different CaO concentrations (from 200 mg to 3.125mg in 1 ml of FAME sample) and biodiesel samples made with different forms of CaO, namely – unbound CaO (CaO), CaO mechanically immobilized on PAN nanofibers (PAN-CaO) and CaO chemically immobilized onto PAN fibers with DOPA link (PAN-DOPA-CaO). Right: peaks of maximum absorbances from curves on the left as a function of CaO concentration in biodiesel samples.

In Figure 4.ix(A), the sample absorbances near the selected wavelength peak are presented for the above selected CaO concentrations in the biodiesel samples, and the peak absorbances at 3643 cm^{-1} were used to create the calibration curve in Figure 4.ix(B). Then, original samples of biodiesel made via transesterification of oil using the three forms of CaO mentioned above were analyzed by FTIR and the calibration curve in Figure 4.ix(B) was used to find that for all three

biodiesel forms, the amount of leaching of CaO was around 2.2mg per 1 dm^3 of the fuel, corresponding to around 2 ppm of leaching of CaO into the biodiesel samples. This is below the maximum allowable CaO concentration of 5 ppm for useable biodiesel fuels according to standards PN-EN 590 and PN-EN 14214. Thus, centrifugation removed most of the CaO from fuel produced by free-flowing catalyst, while little CaO was released into fuel produced by PAN-CaO and PAN-DOPA-CaO mats, as indicated by the electron micrographs showing retention of catalyst to the fibers after diesel production (Figure 4.iv).

Thus, our analysis of the physio-chemical properties of biodiesel samples, made via transesterification reaction with different catalysts, showed the synthesis of fuel of suitable quality. The polymeric mats made via EDH processing fulfilled their function – biofuel samples with good physio-chemical properties were obtained and CaO catalyst was easily separated from the reaction product. We also analyzed whether entrapped CaO catalysts (PAN-CaO and PAN-DOPA-CaO, respectively) were reusable for biodiesel production by repeating the transesterification of Canola oil using the same catalysts – PAN-CaO and PAN-DOPA-CaO – and comparing the data to that from the same analysis performed using free-flowing CaO. Table 3 gives the kinematic viscosities of the biodiesel samples after transesterification reactions were repeated for each of the three different CaO catalysts. When transesterification of Canola oil into biodiesel was catalyzed by CaO powder, the catalyst was reusable 6 times, i.e., it could be used 7 times altogether. The last reuse of this catalyst in the transesterification process, listed as Reaction 8, did not catalyze the reaction completely - unreacted Canola oil was still left in the mixture, and its viscosity was higher than the acceptable range for biodiesel (3.5-8.2 mm^2/s).[66,67] For reactions catalyzed with PAN-CaO, biodiesel samples yielded similar results as those conducted and repeated with the free-flowing CaO; see Table 4.iii.

Table 4.iii. Kinematic viscosity of biodiesel samples made via Canola oil transesterification with different means of deploying of the catalyst: unbound CaO (CaO), CaO immobilized mechanically on PAN fibers (PAN-CaO) and CaO immobilized chemically on PAN fibers (PAN-DOPA-CaO). Reactions were repeated up to 8 times using the same catalyst

Sample	Biodiesel viscosity after reactions repeated with the same catalyst [mm^2/s]							
	Reaction 1	Reaction 2	Reaction 3	Reaction 4	Reaction 5	Reaction 6	Reaction 7	Reaction 8
CaO	5.63	5.49	5.82	5.88	6.02	7.38	7.79	13.42
PAN-CaO	5.33	5.36	5.41	5.39	5.73	6.48	8.12	12.57
PAN-DOPA-CaO	5.81	31.57	40.98					

In the reaction conducted with PAN-DOPA-CaO, it was impossible to reuse the mat in even one additional transesterification of Canola oil, since after the first re-use reaction, some parts of triglycerides were still unconverted and mixed with biodiesel. Additionally, the mixture viscosity was unacceptably high.

4.v Conclusions and Perspective

The combustion of fossil fuels for transportation is the second largest source of carbon dioxide (CO_2) emissions in the world. Biodiesel fuels are an alternative to fossil fuels that reduce the overall carbon footprint of transportation. In 2017, United States used 390 million gallons of gasoline every day, and only used 700 million gallons of biodiesel per year.[69] Some of the hindrances to increased biodiesel production and use include the harsh chemical processing required, the expensive bioreactor machinery, and the multiple purification steps required to remove catalysts that are harmful to car engines.

Here, we presented an alternative method of biodiesel production, that uses electrohydrodynamic processing combined with catalyst immobilization. Thanks to the ease of immobilization, a heterogenous, basic catalyst, CaO, was entrapped in a polymeric fibrous mat made from polyacrylonitrile (PAN) and used in the conversion of Canola oil into biodiesel. We proposed and

compared two different techniques of immobilization of CaO: one mechanical and the other chemical. In the mechanical immobilization, we mixed the polymeric solution with CaO powder and electrospun the mixture. The chemical method required more steps: First, an electrospun polymeric PAN mat was activated by a Pinner reaction and later used to immobilize a CaO catalyst onto PAN, by bonding CaO particles with a dopamine linkage. The structure and morphology of all materials were analyzed via scanning transmission electron microscopy. The resulting PAN fibers were homogenous and uniform, and the CaO catalyst particles were successfully entrapped inside or bonded to the fiber surface. The presence of CaO particles immobilized within the PAN mats was analyzed by FTIR spectroscopy, which confirmed that the CaO was incorporated properly. Catalysts immobilized by both schemes were later successfully used in the transesterification reaction of fresh Canola oil into biodiesel. For both immobilized catalysts, the transesterification process was slower than when free-flowing CaO or dissolved KOH were used as catalysts. But the immobilization carries the benefit that the transesterification reaction doesn't require separating the catalyst from the reaction environment, for example by centrifugation or washing with water. The slower reaction process we observed relative to free-flowing CaO was probably caused by mass transfer resistances for the transport of reactants to CaO particles immobilized in PAN fibers. To overcome this limitation, it would be interesting to see if a combination of different heterogenous catalysts, like MgO of Al_2O_3 with CaO could improve the reaction time and reusability of the catalyst. Another possibility is to accelerate the reaction by physical methods such as ultrasound. This idea would need to be carefully optimized, not only to improve transesterification time, and to possibly increase yield, but most importantly, to do so without damaging the catalyst carrier – PAN mat. It would also be interesting to compare results with those obtained on a different polymer used as a support for the transesterification catalyst.

Switching the polymer to one that could display less reactants swelling from the one hand, and more diffusion of methanol to the catalyst from the other hand, could improve the biofuel production process. Furthermore, it would be worth seeing if an environmentally more "friendly," degradable polymer, such as photodegradable polyethersulphone, could improve, or at least not worsen, biodiesel production.

By measuring CaO concentration via FTIR spectroscopy we showed that the CaO in all biodiesel samples recovered from the mats was almost undetectable, which means that the catalyst was immobilized properly. Electron microscopy confirmed that particles of CaO were still present inside or on the polymer fiber surface of the mat samples after their use in the reactions. The catalyst PAN-CaO could be reused to produce biodiesel by transesterification up to six times after the initial reaction. This means that our catalyst construct fulfills all known requirements, especially catalyst reusability and efficiency along with easy catalyst removal from the reaction environment. EHD processing allowed us to create this easily separable, reusable, catalyst that could be commonly used in transesterification reactions. Despite all great advantages of using EHD processing it is still important to carry out more analysis to determine if this technology could be efficient enough to be used in the industry.

Economic analysis should be based on checking if the PAN-CaO mat could be also used in transesterification of other vegetable oils and especially of used cooking oils (UCO). On the one hand, biodiesel production of UCO is more difficult and sometimes requires more steps than for processing pure oils, including purification of UCO (filtration and water removal) and also requires an esterification step of the oil before the proper transesterification reaction. On the other hand, it is very desirable to transform used oil into the fuel rather than using fresh oils, that could be otherwise used in food industry. If the PAN-CaO mat could be as efficient in the transesterification

of UCO as it is with Canola oil, this would motivate its use in industry, even if mat production increases some costs but, at the same time, decreases the costs of catalyst separation and purification after the reaction. Future steps should include an analysis of PAN-CaO usage in the transformation of UCO into a biofuel.

Note: This chapter in its entirety has been published as a peer-reviewed publication and permission has been granted from all authors as well as the publisher.

4.vi References

1 R. Shomal, H. Hisham, A. Mlhem, R. Hassan, S. Al-Zuhair, Simultaneous extraction–reaction process for biodiesel production from microalgae, Energy Reports. 5 (2019) 37–40. doi:10.1016/j.egyr.2018.11.003.

2 D. Papargyriou, E. Broumidis, M. de Vere-Tucker, S. Gavrielides, P. Hilditch, J.T.S. Irvine, A.D. Bonaccorso, Investigation of solid base catalysts for biodiesel production from fish oil, Renew. Energy. 139 (2019) 661–669. doi:10.1016/j.renene.2019.02.124.

3 A. Gholami, F. Pourfayaz, A. Hajinezhad, M. Mohadesi, Biodiesel production from Norouzak (Salvia leriifolia) oil using choline hydroxide catalyst in a microchannel reactor, Renew. Energy. 136 (2019) 993–1001. doi:10.1016/j.renene.2019.01.057.

4 I.N. Martyanov, A. Sayari, Comparative study of triglyceride transesterification in the presence of catalytic amounts of sodium, magnesium, and calcium methoxides, Appl. Catal. A Gen. 339 (2008) 45–52. doi:10.1016/j.apcata.2008.01.007.

5 X. Liang, G. Gong, H. Wu, J. Yang, Highly efficient procedure for the synthesis of biodiesel from soybean oil using chloroaluminate ionic liquid as catalyst, Fuel. 88 (2009) 613–616. doi:10.1016/j.fuel.2008.09.024.

6 C.S. Cordeiro, F.R. da Silva, F. Wypych, L.P. Ramos, Heterogeneous Catalysts for Biodiesel Production, Quim. Nova. 34 (2011) 477–486.

7 T. Valliyappan, N.N. Bakhshi, A.K. Dalai, Pyrolysis of glycerol for the production of hydrogen or syn gas, Bioresour. Technol. 99 (2008) 4476–4483. doi:10.1016/j.biortech.2007.08.069.

8 S. Dooley, H.J. Curran, J.M. Simmie, Autoignition measurements and a validated kinetic model for the biodiesel surrogate, methyl butanoate, Combust. Flame. 153 (2008) 2–32. doi:10.1016/j.combustflame.2008.01.005.

9 K. Colombo, L. Ender, A.A.C. Barros, The study of biodiesel production using CaO as a heterogeneous catalytic reaction, Egypt. J. Pet. 26 (2017) 341–349. doi:10.1016/j.ejpe.2016.05.006.

10 G. Nahar, K. Kendall, Biodiesel formulations as fuel for internally reforming solid oxide fuel cell, Fuel Process. Technol. 92 (2011) 1345–1354. doi:10.1016/j.fuproc.2011.02.015.

11 Y. Feng, B. He, Y. Cao, J. Li, M. Liu, F. Yan, X. Liang, Biodiesel production using cation-exchange resin as heterogeneous catalyst, Bioresour. Technol. 101 (2010) 1518–

1521. doi:10.1016/j.biortech.2009.07.084.
12 J. Boro, A.J. Thakur, D. Deka, Solid oxide derived from waste shells of Turbonilla striatula as a renewable catalyst for biodiesel production, Fuel Process. Technol. 92 (2011) 2061–2067. doi:10.1016/j.fuproc.2011.06.008.
13 M.J. Ramos, A. Casas, L. Rodríguez, R. Romero, Á. Pérez, Transesterification of sunflower oil over zeolites using different metal loading: A case of leaching and agglomeration studies, Appl. Catal. A Gen. 346 (2008) 79–85. doi:10.1016/j.apcata.2008.05.008.
14 A. Demirbas, Biodiesel from sunflower oil in supercritical methanol with calcium oxide, Energy Convers. Manag. 48 (2007) 937–941. doi:10.1016/j.enconman.2006.08.004.
15 M.E. Borges, L. Díaz, Recent developments on heterogeneous catalysts for biodiesel production by oil esterification and transesterification reactions: A review, Renew. Sustain. Energy Rev. 16 (2012) 2839–2849. doi:10.1016/j.rser.2012.01.071.
16 D. Kusdiana, S. Saka, Kinetics of transesterification in rapeseed oil to biodiesel fuel as treated in supercritical methanol, Fuel. 80 (2001) 693–698. doi:10.1016/S0016-2361(00)00140-X.
17 S. Saka, D. Kusdiana, Biodiesel fuel from rapeseed oil as prepared in supercritical methanol, Fuel. 80 (2001) 225–231. doi:10.1016/S0016-2361(00)00083-1.
18 M. Kouzu, J.S. Hidaka, Transesterification of vegetable oil into biodiesel catalyzed by CaO: A review, Fuel. 93 (2012) 1–12. doi:10.1016/j.fuel.2011.09.015.
19 W. Xie, Z. Yang, Ba-ZnO catalysts for soybean oil transesterification, Catal. Letters. 117 (2007) 159–165. doi:10.1007/s10562-007-9129-2.
20 S. Hama, H. Yamaji, M. Kaieda, M. Oda, A. Kondo, H. Fukuda, Effect of fatty acid membrane composition on whole-cell biocatalysts for biodiesel-fuel production, Biochem. Eng. J. 21 (2004) 155–160. doi:10.1016/j.bej.2004.05.009.
21 E. Séverac, O. Galy, F. Turon, P. Monsan, A. Marty, Continuous lipase-catalyzed production of esters from crude high-oleic sunflower oil, Bioresour. Technol. 102 (2011) 4954–4961. doi:10.1016/j.biortech.2011.01.041.
22 J. Calero, D. Luna, C. Luna, F.M. Bautista, B. Hurtado, A.A. Romero, A. Posadillo, R. Estevez, Rhizomucor miehei lipase supported on inorganic solids, as biocatalyst for the synthesis of biofuels: Improving the experimental conditions by response surface methodology, Energies. 12 (2019) 1–15. doi:10.3390/en12050831.
23 M. Aghababaie, M. Beheshti, A. Razmjou, A.K. Bordbar, Two phase enzymatic membrane reactor for the production of biodiesel from crude Eruca sativa oil, Renew. Energy. 140 (2019) 104–110. doi:10.1016/j.renene.2019.03.069.
24 X. Liu, H. He, Y. Wang, S. Zhu, X. Piao, Transesterification of soybean oil to biodiesel using CaO as a solid base catalyst, Fuel. 87 (2008) 216–221. doi:10.1016/j.fuel.2007.04.013.
25 H. Fukuda, A. Kondo, H. Noda, Fukuda-H._2001_Biodiesel-fuel-production-by-transesterification-of-oils.pdf, J. Biosci. Bioeng. 92 (2001) 405–416.
26 W. Widayat, T. Darmawan, H. Hadiyanto, R.A. Rosyid, Preparation of Heterogeneous CaO Catalysts for Biodiesel Production, J. Phys. Conf. Ser. 877 (2017) 1–8. doi:10.1088/1742-6596/877/1/012018.
27 T. Ebiura, T. Echizen, A. Ishikawa, K. Murai, T. Baba, Selective transesterification of triolein with methanol to methyl oleate and glycerol using alumina loaded with alkali metal salt as a solid-base catalyst, Appl. Catal. A Gen. 283 (2005) 111–116.

doi:10.1016/j.apcata.2004.12.041.
28 S. Gryglewicz, Rapeseed oil methyl esters preparation using heterogeneous catalysts, Bioresour. Technol. 70 (1999) 249–253.
29 K. Tanabe, W.F. Hölderich, Industrial application of solid acid-base catalysts, Appl. Catal. A Gen. 181 (1999) 399–434. doi:10.1016/S0926-860X(98)00397-4.
30 A. Al-Ani, N.E. Mordvinova, O.I. Lebedev, A.Y. Khodakov, V. Zholobenko, Ion-exchanged zeolite P as a nanostructured catalyst for biodiesel production, Energy Reports. 5 (2019) 357–363. doi:10.1016/j.egyr.2019.03.003.
31 S. Yan, C. Dimaggio, S. Mohan, M. Kim, S.O. Salley, K.Y.S. Ng, Advancements in heterogeneous catalysis for biodiesel synthesis, Top. Catal. 53 (2010) 721–736. doi:10.1007/s11244-010-9460-5.
32 A. D'Cruz, M.G. Kulkarni, L.C. Meher, A.K. Dalai, Synthesis of biodiesel from canola oil using heterogeneous base catalyst, JAOCS, J. Am. Oil Chem. Soc. 84 (2007) 937–943. doi:10.1007/s11746-007-1121-x.
33 R.S. Watkins, A.F. Lee, K. Wilson, Li-CaO catalysed tri-glyceride transesterification for biodiesel applications, Green Chem. 6 (2004) 335–340. doi:10.1039/b404883k.
34 G.P. Benedictto, M.S. Legnoverde, J.C. Tara, R.M. Sotelo, E.I. Basaldella, Synthesis of K + /MgO heterogeneous catalysts derived from MgCO 3 for biodiesel production, Mater. Lett. 246 (2019) 199–202. doi:10.1016/j.matlet.2019.03.081.
35 T. Iizuka, H. Hattori, Y. Ohno, J. Sohma, K. Tanabe, Basic sites and reducing sites of calcium oxide and their catalytic activities, J. Catal. 22 (1971) 130–139. doi:10.1016/0021-9517(71)90273-9.
36 Z. Helwani, M.R. Othman, N. Aziz, J. Kim, W.J.N. Fernando, Solid heterogeneous catalysts for transesterification of triglycerides with methanol: A review, Appl. Catal. A Gen. 363 (2009) 1–10. doi:10.1016/j.apcata.2009.05.021.
37 C. Reddy, V. Reddy, R. Oshel, J.G. Verkade, Room-temperature conversion of soybean oil and poultry fat to biodiesel catalyzed by nanocrystalline calcium oxides, Energy and Fuels. 20 (2006) 1310–1314. doi:10.1021/ef050435d.
38 Y. Ono, Solid base catalysts for the synthesis of fine chemicals, J. Catal. 216 (2003) 406–415. doi:10.1016/S0021-9517(02)00120-3.
39 S. Torres-Giner, A. Martinez-Abad, M.J. Ocio, J.M. Lagaron, Stabilization of a nutraceutical omega-3 fatty acid by encapsulation in ultrathin electrosprayed zein prolamine, J. Food Sci. 75 (2010) 69–79. doi:10.1111/j.1750-3841.2010.01678.x.
40 A. López-Rubio, E. Sanchez, S. Wilkanowicz, Y. Sanz, J.M. Lagaron, Electrospinning as a useful technique for the encapsulation of living bifidobacteria in food hydrocolloids, Food Hydrocoll. 28 (2012) 159–167. doi:10.1016/j.foodhyd.2011.12.008.
41 R. Pérez-Masiá, R. López-Nicolás, M.J. Periago, G. Ros, J.M. Lagaron, A. López-Rubio, Encapsulation of folic acid in food hydrocolloids through nanospray drying and electrospraying for nutraceutical applications, Food Chem. 168 (2015) 124–133. doi:10.1016/j.foodchem.2014.07.051.
42 N.A.A. Shukry, K.A. Sekak, M.R. Ahmad, T.J.B. Effendi, Characteristics of Electrospun PVA-Aloe vera Nanofibres Produced via Electrospinning, Proc. Int. Xolloquium Text. Eng. (2014) 7–11. doi:10.1007/978-981-287-011-7.
43 S. Torres-Giner, S. Wilkanowicz, B. Melendez-Rodriguez, J.M. Lagaron, Nanoencapsulation of Aloe vera in Synthetic and Naturally Occurring Polymers by Electrohydrodynamic Processing of Interest in Food Technology and Bioactive

Packaging, J. Agric. Food Chem. 65 (2017) 4439–4448. doi:10.1021/acs.jafc.7b01393.
44 S. Torres-Giner, M.J. Ocio, J.M. Lagaron, Development of active antimicrobial fiber based chitosan polysaccharide nanostructures using electrospinning, Eng. Life Sci. 8 (2008) 303–314. doi:10.1002/elsc.200700066.
45 Y. Qin, Alginate fibers: an overwiew of the production processes and applications in wound management, Polym. Int. 57 (2008) 171–180. doi:10.1002/pi.
46 A. Fernandez, S. Torres-Giner, J.M. Lagaron, Novel route to stabilization of bioactive antioxidants by encapsulation in electrospun fibers of zein prolamine, Food Hydrocoll. 23 (2009) 1427–1432. doi:10.1016/j.foodhyd.2008.10.011.
47 J. Anu Bhushani, C. Anandharamakrishnan, Electrospinning and electrospraying techniques: Potential food based applications, Trends Food Sci. Technol. 38 (2014) 21–33. doi:10.1016/j.tifs.2014.03.004.
48 C. Xuefei, H. Yang, X. Zhen-Liang, Poly(vinyl alcohol)-perfluorinated sulfonic acid nanofiber mats prepared via electrospinning as catalyst, Mater. Lett. 65 (2011) 1719–1722. doi:10.1016/j.matlet.2011.02.063.
49 M.A. Harmer, W.E. Farneth, Q. Sun, High surface area nafion resin/silica nanocomposites: A new class of solid acid catalyst, J. Am. Chem. Soc. 118 (1996) 7708–7715. doi:10.1021/ja9541950.
50 W. Shi, H. Li, R. Zhou, X. Qin, H. Zhang, Y. Su, Q. Du, Preparation and characterization of phosphotungstic acid/PVA nanofiber composite catalytic membranes via electrospinning for biodiesel production, Fuel. 180 (2016) 759–766. doi:10.1016/j.fuel.2016.04.066.
51 S. Sakai, Y. Liu, T. Yamaguchi, R. Watanabe, M. Kawabe, K. Kawakami, Production of butyl-biodiesel using lipase physically-adsorbed onto electrospun polyacrylonitrile fibers, Bioresour. Technol. 101 (2010) 7344–7349. doi:10.1016/j.biortech.2010.04.036.
52 S. Sakai, Y. Liu, T. Yamaguchi, R. Watanabe, M. Kawabe, K. Kawakami, Immobilization of Pseudomonas cepacia lipase onto electrospun polyacrylonitrile fibers through physical adsorption and application to transesterification in nonaqueous solvent, Biotechnol. Lett. 32 (2010) 1059–1062. doi:10.1007/s10529-010-0279-8.
53 S.F. Li, Y.H. Fan, J.F. Hu, Y.S. Huang, W.T. Wu, Immobilization of Pseudomonas cepacia lipase onto the electrospun PAN nanofibrous membranes for transesterification reaction, J. Mol. Catal. B Enzym. 73 (2011) 98–103. doi:10.1016/j.molcatb.2011.08.005.
54 S.F. Li, Y.H. Fan, R.F. Hu, W.T. Wu, Pseudomonas cepacia lipase immobilized onto the electrospun PAN nanofibrous membranes for biodiesel production from soybean oil, J. Mol. Catal. B Enzym. 72 (2011) 40–45. doi:10.1016/j.molcatb.2011.04.022.
55 C.X. Liu, S.P. Zhang, Z.G. Su, P. Wang, LiCl-induced improvement of multilayer nanofibrous lipase for biodiesel synthesis, Bioresour. Technol. 103 (2012) 266–272. doi:10.1016/j.biortech.2011.09.089.
56 Y. Li, H. Wang, J. Lu, A. Chu, L. Zhang, Z. Ding, S. Xu, Z. Gu, G. Shi, Preparation of immobilized lipase by modified polyacrylonitrile hollow membrane using nitrile-click chemistry, Bioresour. Technol. 274 (2019) 9–17. doi:10.1016/j.biortech.2018.11.075.
57 S. Caron, L. Wei, J. Douville, A. Ghosh, Preparation and utility of trihaloethyl imidates: Useful reagents for the synthesis of amidines, J. Org. Chem. 75 (2010) 945–947. doi:10.1021/jo902159z.
58 T. Handa, A. Hirose, S. Yoshida, H. Tsuchiya, The Effect of Methylacrylate, Biotechnol. Bioeng. 24 (1982) 1639–1652.

59 B. Pabin-Szafko, E. Wiśniewska, J. Szafko, Azowe inicjatory funkcyjne - Synteza i charakterystyka molekularna, Polimery/Polymers. 50 (2005) 1–7.
60 P.R. Adiyala, D. Chandrasekhar, J.S. Kapure, C.N. Reddy, R.A. Maurya, Synthesis of α-amino amidines through molecular iodine-catalyzed three-component coupling of isocyanides, aldehydes and amines, Beilstein J. Org. Chem. 10 (2014) 2065–2070. doi:10.3762/bjoc.10.214.
61 C.C. Fu, T.C. Hung, C.H. Su, D. Suryani, W.T. Wu, W.C. Dai, Y.T. Yeh, Immobilization of calcium oxide onto chitosan beads as a heterogeneous catalyst for biodiesel production, Polym. Int. 60 (2011) 957–962. doi:10.1002/pi.3031.
62 M.K. Y. Zhang, M.A. Dubé, D.D. McLean, Biodiesel production from waste cooking oil, Process Des. Technol. Assessment, Bioresour. Technol. 99 (2008) 1131–1140. doi:10.5772/25313.
63 A. Arbelaez, R. Marcela, Diseño Conceptual De Un Proceso Para La Obtención De Biodiesel a Partir De Algunos Aceites Vegetales Colombianos, Eng. Thesis. 1 (2007) 1–119.
64 I. S., Recent Trends in the Profitability of Biodiesel Production, Farm Doc Dly. (2014) 2011–2014.
65 R. Farsani, S. Raissi, A. Shokuhfar, A. Sedghi, FT-IR study of stabilized PAN fibers for fabrication of carbon fibers, Int. J. Mech. Mechatronics Eng. 3 (2009) 319–322.
66 S.N. Sahasrabudhe, V. Rodriguez-Martinez, M. O'Meara, B.E. Farkas, Density, viscosity, and surface tension of five vegetable oils at elevated temperatures: Measurement and modeling, Int. J. Food Prop. 20 (2017) 1965–1981. doi:10.1080/10942912.2017.1360905.
67 B. Esteban, J.R. Riba, G. Baquero, A. Rius, R. Puig, Temperature dependence of density and viscosity of vegetable oils, Biomass and Bioenergy. 42 (2012) 164–171. doi:10.1016/j.biombioe.2012.03.007.
68 N. application. SHIMADZU, Infrered Spectroscopy differences between biodiesel prepared from rapeseed and the edible rapeseed oil., (n.d.) 1–2.
69 USDA, Monthly Biodiesel Production Report - Energy Information Administration, (2019). doi:10.1111/j.1466-7657.2008.00671.x.

Chapter 5

Conclusions

5.i Overview

In this thesis, we investigated and engineered polymer interfaces, including both polymer thin films—in the morphologies of brushes and LbL bilayers—and polymer membranes. Polymer thin films remain attractive since they can be used in a variety of technologies. Polymer membranes are also of interest for a variety of applications. Because of this interest, this work aimed to provide deeper insight into the fundamental behavior of these materials as well as to develop novel applied materials to advance both the knowledge and state of the art in the field.

5.ii Polymer Thin Films

5.ii.a Polyelectrolyte brushes

In the area of polymer thin films, this work focuses on the understanding of ionizable polymer—or polyelectrolyte—brushes and multilayers. Polyelectrolyte brushes are used in applications such as waterborne lubrication and gas separation.[1] However, their fundamental swelling/de-swelling is still not well-understood. To address this, this work investigates the swelling/de-swelling behavior of brushes of varied chain lengths of the weakly ionizable polyelectrolyte, poly(acrylic acid) (PAA), in the presence of salt at various pH values and varied grafting densities using Quartz Crystal Microbalance with Dissipation (QCM-D). After correcting for the brush-free solvent effect on the underlying crystal, we compared our experimental findings to those predicted by scaling theory.[2] At pH 7, where the brushes are ionized, at low and moderate

grafting densities, our results in the high-salt "salted brush" (SB) regime (C_s > 10 mM salt) agree with the predicted scaling $H \sim N\sigma^{+1/3}C_s^{-1/3}$ of brush height H, [2] while in the low-salt "osmotic brush" (OB) regime (C_s <10 mM salt), we find $H \sim N\sigma^{+1/3}C_s^{+0.28-0.38}$.[2] Here, the dependence on C_s agrees with scaling theory but the dependence on σ does not. The predicted scaling with respect to N is also confirmed.[2] We hypothesize that the disagreement in scaling of height with respect to grafting density σ is likely due to the fact that our brushes are short and quite densely-grafted at all grafting densities investigated, and thus inelastic, where the scaling theory[2] ultimately describes Gaussian brush. Ultimately, this work became the most complete study of polyelectrolyte brushes with respect to varied external conditions can be used to better inform numerical theory and researchers developing novel applied materials. These findings were published in *Soft Matter*.[3]

5.ii.b Polyelectrolyte bilayers

Next, these brushes are complexed with a polyelectrolyte of the opposite charge poly(ethylene imine) (PEI) to form a PAA/PEI LbL bilayer with a PAA brush underlayer for investigation by QCM-D. LbL self-assembly is extremely exciting for its ease of manufacture and versatility in a variety of different industries from sensing to drug delivery.[4] It was found that both brush and bilayer structures may or may not exhibit history-dependent swelling/de-swelling with respect to a pH cycle at fixed salt concentration depending on their chain length and grafting density. It is important that this hysteretic response, if any, is well-characterized, so that the nonequilibrium foundational to LbL film assembly can be well-understood and LbL films can be used in dynamic environments. When salt concentration is fixed and pH is varied, at a low grafting density of 0.45 chains/nm^2 and a high PAA molecular weight of 39 kDa, we see hysteresis in swelling over timescales of many minutes. For higher grafting densities and shorter chains, we see

little or no hysteresis. Finally, at intermediate chain length and grafting densities, hysteresis is observed at short timescales but is greatly reduced at longer timescales, which agrees with our expectation and suggests that we are perhaps able to find an intermediate case and "arrest" the onset of hysteresis. When we fix pH and vary the salt concentration, we observe hysteresis in swelling upon changes of salt concentration with the same dependence on grafting density and chain length as for fixed salt/varied pH. Finally, we revisited the discrepancies in scaling between our findings and scaling prediction[2,3] with height with respect to grafting density for a PAA brush, where we show that for a long enough PAA chain, at a pH value at which it is partially charged, in the OB regime, the brush height decreases with increased grafting density, in agreement with theoretical predictions. This has not yet been demonstrated experimentally.

Ultimately, this work confirms and extends previous experimental findings and provides a comprehensive data set for testing theories and for comparison against other polyelectrolyte brushes and multilayers, and is truly the first reporting of hysteresis with varying extents of hysteresis with fixed salt and varied pH, or with fixed pH and varied salt, both with respect to chain length and grafting density. We also presented a potential mechanism for this hysteresis by comparing to simulation data from our group and suggest that hysteresis can be due to charge-conformation coupling.[5] This work was recently submitted for publication.[6]

5.iii Polymer Membranes

5.iii.a Catalytic Polymer Membrane for Biodiesel Production

In the area of polymer membranes, this work highlighted a major advancement in the area of catalysis for sustainable fuel processing via an innovative electrospun polyacrylonitrile membrane featuring novel chemistry to immobilize heterogenous basic catalyst onto the

membrane fibers using dopamine-catalyst coordination. This membrane was found to successfully process biodiesel (when compared to industrial standards) from crude canola oil.

There are pros and cons to using homogenous (acidic) or heterogenous (basic) catalysts in biodiesel processing. Homogenous acidic catalysts often involve high temperatures and demanding reaction conditions. To circumvent this, these membranes use a basic catalyst, which allows the use of mild reaction conditions, and which are less damaging to the engine if residual catalyst remains. A traditional draw of using a heterogenous catalysts are that they must be physically separated from the resultant biodiesel, requiring time consuming filtration. Additionally, alkaline catalysts are extremely toxic to the environment and often end up in the environmental waste stream from leaching out of the membrane.[7] To circumvent this, in this work, we chemically immobilize the heterogenous base catalyst CaO to a membrane of electrospun fibers of poly(acrylonitrile) (PAN) via dopamine-metal coordination. In doing so, the membranes can now also be wrung out after use to then be re-used multiple times. For these important reasons and their ease of manufacture and use, these membranes hold extreme promise for future catalysis applications.

Ultimately, in this chapter, we develop a novel immobilization chemistry for an electrospun PAN membrane to successfully immobilize a heterogenous basic catalyst CaO, thus avoiding engine damage and dangerous reactor conditions, while being safer for the environment. Through Scanning Electron Microscope (SEM) and Fourier Transform Infrared Spectroscopy (FT-IR) analysis, we were able to demonstrate that we achieved uniform fibers of uniform thickness, with catalyst present in the appropriate groups. We also demonstrate that we are successful in the conversion of biomass to biodiesel when compared to FAME standard. Of course, the catalytic membrane featured longer reaction times and lower yields than the positive controls of catalyst

alone and a membrane with physically incorporated catalyst. This was largely due to the fact that the catalytic membrane featured less catalyst, as the amount of catalyst tethered is limited by the stoichiometry of available functional groups for linkage. Future work could be to develop chemistry to increase the number of dopamine linkages to improve CaO efficiency as a catalyst to yield shorter reaction times. Additionally, alternative immobilization chemistries could be explored. Dopamine may also be used to immobilize other heteroatoms in other less efficient metal oxide catalysts such as Fe_3O_4. Ultimately, this membrane features a relatively simple chemistry and provides a good foundation upon which more efficient, less expensive membranes can be manufactured at scale to provide even higher quality biodiesel. With the advantages of biodiesel and an emphasis on sustainability in industry moving forward, this will be exciting work. This chapter was published in *Fuel Processing Technology.*[8]

5.iv References

1 Das, S.; Banik, M.; Chen, G.; Sinha, S.; Mukherjee, R. Polyelectrolyte brushes: theory, modelling, synthesis and applications. *Soft Matter* **2015**, *11*, 8550–8583 DOI: 10.1039/C5SM01962A.

2 Zhulina, E. B.; Birshtein, T. M.; Borisov, O. V. Theory of Ionizable Polymer Brushes. *Macromolecules* **1995**, *28*, 1491–1499 DOI: 10.1021/ma00109a021.

3 Hollingsworth, N. R.; Wilkanowicz, S. I.; Larson, R. G. Salt- and pH-induced swelling of a poly(acrylic acid) brush via quartz crystal microbalance w/dissipation (QCM-D). *Soft Matter* **2019**, *15*, 7838–7851 DOI: 10.1039/C9SM01289C.

4 Hammond, P. T. Engineering Materials Layer-by-Layer: Challenges and Opportunities in Multilayer Assembly. **2011** DOI: 10.1002/aic.12769.

5 Ghasemi, M.; Larson, R. G. Role of Electrostatic Interactions in Charge Regulation of Weakly Dissociating Polyacids. *Submitted to Macromolecules* **2020**.

6 Hollingsworth, N. R.; Larson, R. G. Swelling hysteresis with changes in pH or salt concentration in weak polyelectrolyte brushes and bilayer films. *Submitted to Macromolecules* **2020**.

7 Jothiramalingam, R.; Wang, M. K. Review of recent developments in solid acid, base, and enzyme catalysts (heterogeneous) for biodiesel production via transesterification. *Industrial and Engineering Chemistry Research*, **2009**, *48*, 6162–6172.

8 Wilkanowicz, S. I.; Hollingsworth, N. R.; Saud, K.; Kadiyala, U.; Larson, R. G. Immobilization of calcium oxide onto polyacrylonitrile (PAN) fibers as a heterogeneous catalyst for biodiesel production. *Fuel Process. Technol.* **2020**, *197*, 106214 DOI: 10.1016/J.FUPROC.2019.106214.